جامعة البحرين
المكتبة
LIBRARY
University of Bahrain

UNIVERSITY OF BAHRAIN

College of Engineering

Department of Electrical and Electronics Engineering

Smart Controller Design For Unified Power Flow Controller (UPFC) Using Evolutionary Optimization Algorithms

A Thesis Submitted in Partial Fulfillment of the Requirements for the Master Degree in Electrical and Electronics Engineering

Submitted by

Sayed Ahmed Ali Makki Alqallaf

University Number: 20037139

Supervised by

Dr. S. Ali Al-Mawsawi

Associate Professor

Dr. Anwar Haider

Assistant Professor

University of Bahrain

Kingdom of Bahrain

January, 2015

LIBRARY
University of Bahrain

DECLARATION

I declare that this work is the result of my own investigation and that it has not already been accepted in substance for any degree, not is it being currently submitted for any degree.

Signed : _____ Date : 11/01/2015

S. Ahmed Ali (candidate)

The Thesis defense committee considers the thesis titled:

"SMART CONTROLLER DESIGN FOR UNIFIED POWER FLOW CONTROLLER (UPFC) USING EVOLUTIONARY ALGORITHMS"

Submitted by S. Ahmed Ali to the Department of Electrical and Electronics Engineering satisfactory and acceptable for the Master of Science degree in Electrical Engineering.

Thesis Defense Committee:

Dr. S.A. Al-Mawsawi	Department of Electrical and Electronics Engineering
Supervisor	University of Bahrain
Dr. Anwar Haider	Department of Mechanical Engineering
Supervisor	University of Bahrain
Prof. Dr. K. M. El-Naggar	Department of Electrical Engineering
Member	College of Technological Studies
Dr. M. Taleb	Department of Electrical and Electronics
Member	University of Bahrain

Abstract

In the past few decades the power systems have witnessed an increase in size due to rapid and growing demand of power. This imposed a problem due to the limited resources and the strict environmental constraints that caused the system to be operated near to the stability limit and to have area interconnection. This led several problems, such as system low frequency oscillations that may lead to loss of synchronism. Flexible AC transmission system (FACTS) devices introduced by Electric Power Research Institute (EPRI) offer a solution to such problems.

In this study a design of a smart controller for the Unified Power Flow Controller (UPFC) based on evolutionary algorithms is carried. The UPFC is a FACTS device that is capable of controlling all the power system parameters. Therefore, it became the most versatile system among all FACTS devices.

This thesis is contains six chapters, the first chapter will be an introduction of FACTS controllers, where the devices are categorized based on technology used to control the system parameters. It then introduces the UPFC controller configuration and its modes of operation.

The second chapter discusses the modeling of the UPFC. It begins with a review of the UPFC load flow models that were introduced in literature. Based on the review the UPFC decoupled load flow model is chosen. The model is then investigated in order to realize different control strategies of the UPFC, then a study of the impact of installation location of the UPFC on the control parameters is discussed. The second part of the chapter discusses UPFC dynamic modeling, it compares two models that have been introduced in literature. Based on the comparison, the PWM UPFC model is chosen in this study.

The third chapter introduces two evolutionary algorithms, the Biogeography Based Optimization (BBO) and Particle Swarm Optimization (PSO) algorithms. After which, a discussion of the UPFC capability to damp interarea oscillation is presented. By using these algorithms a robust power oscillation damping (POD) controller is designed by using two different objective functions. The resulting controller from each case is compared.

The fourth chapter discusses the multifunction control capability of the UPFC, where a power flow controller, DC voltage regulator, bus voltage regulator, and POD controller are tuned simultaneously using the prior mentioned algorithms.

At the fifth chapter, a result analysis of the designed controllers is introduced for several types of system disturbances and system uncertainties in order to evaluate the robustness and the performance of the controllers.

The last chapter, presents the conclusion withdrawn from the study and the ability to enhance it more in the future.

Dedication

To my parents for their endless prayers, and for my wife for her support and patience, and for my best friend Zakariya.

Acknowledgments

I would like to thank my supervisors , Dr. S. A. Al-Mawsawi and Dr. A. Haider for their invaluable guidance,patience and inspiration that they provided during the course of this work.

An extended thanks to the chairperson and the faculty members of the Electrical and Electronics Engineering Department at University of Bahrain for their useful discussion and encouragement during my research work.

Contents

Title	Page
Declaration	**i**
Abstract	**ii**
Dedication	**iii**
Acknowledgments	**iv**
Content	**v**
List of Tables	**viii**
List of Figures	**x**
List of Appendices	**xvii**
List of Abbreviations	**xviii**
Chapter 1 Introduction	
1.1 Overview	**2**
1.2 FACTS Controllers	**4**
1.2.1 Thyristor Based FACTS Controllers	4
1.2.2 Voltage Source Converters Based FACTS Controllers	9
1.3 Unified Power Flow Controller (UPFC)	**15**
1.3.1 Construction of the UPFC	15
1.3.2 Modes of Operation	15
1.4 Motivation and Objective	**17**
1.5 Publications	**18**
1.6 Outline of The Thesis	**19**
Chapter 2 Unified Power Flow Controller Modeling	
2.1 Overview	**21**
2.2 Unified Power Flow Controller Load Flow Modeling	**21**
2.2.1 UPFC Decoupled Load Flow Mode	25
2.3 Investigation of Installation location and Impact on control parameter	**30**
2.3.1 Case 1: PQ - PV bus configuration	30
2.3.2 Case 2: PV - PQ Bus Configuration	35
2.4 Unified Power Flow Controller Dynamic Modeling	**39**
2.4.1 Fundamental Frequency Based Dynamic Modeling	40

2.4.2 Pulse Width Modulation Based Dynamic Modeling	49
2.5 Study System	**54**
2.6 Summary	**57**
Chapter 3 **Evolutionary Optimization Based Controller**	
3.1 Overview	**60**
3.2 Biogeography Based Optimization	**60**
3.2.1 Biogeography	60
3.2.2 Biogeography-Based Optimization	65
3.3 Particle Swarm Optimization	**72**
3.3.1 Particle Swarm Optimization Algorithm	73
3.4 Introduction to FACTS based Power System Stabilizers	**78**
3.5 UPFC Based Damping Controller	**79**
3.5.1 System Linearized Model	81
3.5.2 Objective Function	82
3.6 Controller Design	**84**
3.6.1 Robust Eigenvalue Based Damping Controller Design	84
3.6.2 Robust Time-value Based Damping Controller	86
3.7 Simulation Result	**87**
Chapter 4 **Unified Power Flow Controller Mult-Input Multi-Output Controller Design**	
4.1 Overview	**93**
4.2 UPFC MIMO control system	**94**
4.3 Control System Design	**95**
4.4 Simulation Results	**99**
Chapter 5 **Control System Performance Analysis**	
5.1 Overview	**108**
5.2 Response Analysis for Power Oscillation Damping (POD) Controller	**109**
5.2.1 Response Analysis under System Uncertainties	109
5.2.2 Analysis of Fine tuned system response	121
5.3 Response Analysis for Multi-Input Multi-Output (MIMO) UPFC Control System	134
5.3.1 Setpoint Variation	135
5.3.2 System Disturbance Rejection	141
5.3.3 Damping Power System Oscillations	143

Chapter 6 Conclusion and Future Work	
6.1 Conclusion	158
6.2 Suggestions for Future Work	160
References	161
Appendices	
Arabic Abstract	

List of Tables

No.	Table	Page
3.1	System eigenvalues under nominal loading condition without POD controller	81
3.2	Optimization constraints for the POD controller design	84
3.3	Damping Controller Parameters Using BBO and PSO for eigenvalue based objective function	85
3.4	Damping Controller Parameters Using BBO and PSO for time-value based objective function	86
3.5	System eigenvalues with stabilizer installed	90
3.6	Damping controllers settling time and response attained peaks	91
4.1	Optimization problem constraints	97
4.2	UPFC MIMO controllers parameters using BBO and PSO	98
4.3	System eigenvalues for UPFC MIMO control system	103
5.1	System operating points and its uncertainties	110
5.2	System performance under light loading conditions in the presence of uncertainty for POD controllers	112
5.3	System performance under nominal loading conditions in the presence of uncertainty for POD controllers	115
5.4	System performance under heavy loading conditions in the presence of uncertainty for POD controllers	118
5.5	System performance under leading power factor loading conditions in the presence of uncertainty for POD controllers	121
5.6	System performance before and after fine tuning under light	124

	loading conditions for POD controllers	
5.7	System performance before and after fine tuning under nominal loading conditions for POD controllers	127
5.8	System performance before and after fine under heavy loading conditions for POD controllers	130
5.9	System performance before and after fine tuning under leading power factor loading conditions for POD controllers	133
5.10	System eigenvalues and EM damping ratios at light loaded conditions for MIMO controllers	146
5.11	System eigenvalues and EM damping ratios at heavy loaded conditions for MIMO controllers	152
5.12	System eigenvalues and EM damping ratios at leading power factor loading conditions for MIMO controllers	155

List of Figures

No.	Figure	Page
1.1	Static Var Compensator (SVC)	5
1.2	V-I characteristics curve for SVC	5
1.3	Power curve for different degrees of compensation using TCSC	7
1.4	TCSC: Thyristor Switched Capacitors (TSC)	7
1.5	TCSC: Fixed Capacitor in Parallel with Thyristor Controlled Reactor	7
1.6	Thyristor Controlled Phase Shifters (TCPS)	8
1.7	TCPS Operation: Phasor Diagram	9
1.8	STATCOM schematic representation	10
1.9	STATCOM Operation	11
1.10	Static Synchronous Series Compensator (SSSC)	12
1.11	SSSC Operation: Phasor Diagram	13
1.12	Interline Power Flow Controller (IPFC)	14
1.13	Unified Power Flow Controller (UPFC)	15
1.14	UPFC Control Capabilities	17
2.1	Unified Power Flow Controller Schematic Diagram	22
2.2	Steady State UPFC Model	22
2.3	UPFC Power Injection Model	24
2.4	UPFC Equivalent Bus Representation	26
2.5	UPFC Decoupled Model Different Control Schemes	27
2.6	Flow Chart of Newton-Raphson Algorithm for the UPFC Decoupled Load Flow Model	29
2.7	Single machine infinite bus system with double transmission line circuit	30
2.8	Variation of series injected voltage V_B with active power setpoint and location variation	31
2.9	Variation of shunt injected voltage V_E with active power setpoint and location variation	32
2.10	Variation of series injected voltage V_B with reactive power Q_{Et} setpoint and location variation	33
2.11	Variation of shunt injected voltage V_E with reactive power Q_{Et} setpoint and location variation	34

2.12	Variation of series injected voltage V_B with receiving end voltage V_{Bt} setpoint and location variation	35
2.13	Variation of shunt injected voltage V_E with receiving end voltage V_{Bt} setpoint and location variation	36
2.14	Variation of series injected voltage V_B with reactive power Q_{Bt} setpoint and location variation	36
2.15	Variation of shunt injected voltage V_E with reactive power Q_{Bt} setpoint and location variation	37
2.16	Variation of series injected voltage V_B with sending end voltage V_{Et} setpoint and location variation	38
2.17	Variation of shunt injected voltage V_E with sending end voltage V_{Et} setpoint and location variation	38
2.18	UPFC with associated DC and AC currents	41
2.19	Detailed Fundamental Frequency UPFC Model	42
2.20	Shunt Converter Block Diagram Representation	44
2.21	Series Converter Block Diagram Representation	44
2.22	Fundamental frequency based control strategy	49
2.23	UPFC Three Phase Schematic Diagram	50
2.24	PWM based control strategy	53
2.25	SMIB system equipped with UPFC	54
3.1	Species migration model of an island, based on [MacArthur and Wilson,1967]	62
3.2	BBO individual species count curve with $E = I$	67
3.3	Biogeography-Based Optimization Flowchart	71
3.4	Schematic Representation of the motion of particles in PSO, moving towards the global best x_{gbest} and the current best x_{pbest} for each particle	73
3.5	Particle Swarm Optimization Flowchart	77
3.6	UPFC Based Damping Controller	80
3.7	UPFC Based Damping Controller Using δ_E Input channel	81
3.8	Convergence characteristic for Eigenvalue based objective function for BBO algorithm and PSO algorithm	85
3.9	Convergence characteristic for time-value based objective function for BBO algorithm and PSO algorithm	86
3.10	Rotor Angle δ variation	87
3.11	Deviation in rotor angular velocity $\Delta\omega$	88
3.12	Generator Electrical Power P_e	88
3.13	UPFC DC link voltage v_{dc}	89

3.14	Damping control signal δ_E	89
4.1	UPFC MIMO control system structure	94
4.2	Multiloop controllers for UPFC	95
4.3	Convergence characteristics for BBO and PSO for tuning MIMO controller using ITAE objective function	97
4.4	Dynamic response of UPFC MIMO control system - Generator rotor angle δ	99
4.5	Dynamic response of UPFC MIMO control system - Generator angular speed $\Delta\omega$	100
4.6	Dynamic response of UPFC MIMO control system - Deviation in regulated power flow ΔP_{e2}	100
4.7	Dynamic response of UPFC MIMO control system - Deviation in UPFC DC link voltage v_{dc}	101
4.8	Dynamic response of UPFC MIMO control system - Deviation in AC bus regulated voltage ΔV_{Et}	101
4.9	Dynamic response of UPFC MIMO control system - Excitation converter modulation index m_E	102
4.10	Dynamic response of UPFC MIMO control system - Boosting converter modulation index m_B	102
4.11	Line power flow P_{e2}	104
4.12	Generator angular speed deviation	104
4.13	Generator rotor angle	105
4.14	Deviation in UPFC DC link voltage Δv_{dc}	105
4.15	Deviation in AC bus voltage ΔV_{Et}	106
5.1	System uncertainty - Dynamic response of POD controller tuned with BBO algorithm for ζ-objective function under light loading condition	110
5.2	System uncertainty - Dynamic response of POD controller tuned with PSO algorithm for ζ-objective function under light loading condition	111
5.3	System uncertainty - Dynamic response of POD controller tuned with BBO algorithm for ITAE-objective function under light loading condition	111
5.4	System uncertainty - Dynamic response of POD controller tuned with PSO algorithm for ITAE-objective function under light loading condition	112
5.5	System uncertainty - Dynamic response of POD controller tuned with BBO algorithm for ζ-objective function under	113

	nominal loading condition	
5.6	System uncertainty - Dynamic response of POD controller tuned with PSO algorithm for ζ-objective function under nominal loading condition	114
5.7	System uncertainty - Dynamic response of POD controller tuned with BBO algorithm for ITAE-objective function under nominal loading condition	114
5.8	System uncertainty - Dynamic response of POD controller tuned with PSO algorithm for ITAE-objective function under nominal loading condition	115
5.9	System uncertainty - Dynamic response of POD controller tuned with BBO algorithm for ζ-objective function under heavy loading condition	116
5.10	System uncertainty - Dynamic response of POD controller tuned with PSO algorithm for ζ-objective function under heavy loading condition	117
5.11	System uncertainty - Dynamic response of POD controller tuned with BBO algorithm for ITAE-objective function under heavy loading condition	117
5.12	System uncertainty - Dynamic response of POD controller tuned with PSO algorithm for ITAE-objective function under heavy loading condition	118
5.13	System uncertainty - Dynamic response of POD controller tuned with BBO algorithm for ζ-objective function under leading power factor loading condition	119
5.14	System uncertainty - Dynamic response of POD controller tuned with PSO algorithm for ζ-objective function under leading power factor loading condition	120
5.15	System uncertainty - Dynamic response of POD controller tuned with BBO algorithm for ITAE-objective function under leading power factor loading condition	120
5.16	System uncertainty - Dynamic response of POD controller tuned with PSO algorithm for ITAE-objective function under leading power factor loading condition	121
5.17	Fine tuning - Dynamic response of POD controller tuned with BBO algorithm for ζ-objective function under light loading condition	122
5.18	Fine tuning - Dynamic response of POD controller tuned	123

	with PSO algorithm for ζ-objective function under light loading condition	
5.19	Fine tuning - Dynamic response of POD controller tuned with BBO algorithm for ITAE-objective function under light loading condition	123
5.20	Fine tuning - Dynamic response of POD controller tuned with PSO algorithm for ITAE-objective function under light loading condition	124
5.21	Fine tuning - Dynamic response of POD controller tuned with BBO algorithm for ζ-objective function under nominal loading condition	125
5.22	Fine tuning - Dynamic response of POD controller tuned with PSO algorithm for ζ-objective function under nominal loading condition	126
5.23	Fine tuning - Dynamic response of POD controller tuned with BBO algorithm for ITAE-objective function under nominal loading condition	126
5.24	Fine tuning - Dynamic response of POD controller tuned with PSO algorithm for ITAE-objective function under nominal loading condition	127
5.25	Fine tuning - Dynamic response of POD controller tuned with BBO algorithm for ζ-objective function under heavy loading condition	128
5.26	Fine tuning - Dynamic response of POD controller tuned with PSO algorithm for ζ-objective function under heavy loading condition	129
5.27	Fine tuning - Dynamic response of POD controller tuned with BBO algorithm for ITAE-objective function under heavy loading condition	129
5.28	Fine tuning - Dynamic response of POD controller tuned with PSO algorithm for ITAE-objective function under heavy loading condition	130
5.29	Fine tuning - Dynamic response of POD controller tuned with BBO algorithm for ζ-objective function under leading power factor loading condition	131
5.30	Fine tuning - Dynamic response of POD controller tuned with PSO algorithm for ζ-objective function under leading power factor loading condition	132

5.31	Fine tuning - Dynamic response of POD controller tuned with BBO algorithm for ITAE-objective function under leading power factor loading conditions	132
5.32	Fine tuning - Dynamic response of POD controller tuned with PSO algorithm for ITAE-objective function under leading power factor loading condition	133
5.33	Dynamic response - Generator angular speed deviation $\Delta\omega$ for BBO tuned MIMO control system under variation of power flow setpoint	135
5.34	Dynamic response - Line power flow $P_{e\,2}$ for BBO tuned MIMO control system under variation of power flow setpoint	136
5.35	Dynamic response - Deviation in line power flow ΔP_e BBO tuned MIMO control system under variation of power flow setpoint	136
5.36	Dynamic response - Deviation in UPFC DC link voltage Δv_{dc} for BBO tuned MIMO control system under variation of power flow setpoint	137
5.37	Dynamic response - Deviation in AC bus voltage ΔV_{Et} for BBO tuned MIMO control system under variation of power flow setpoint	137
5.38	Dynamic response - Generator angular speed deviation $\Delta\omega$ for PSO tuned MIMO control system under variation of power flow setpoint	138
5.39	Dynamic response - Line power flow $P_{e\,2}$ for PSO tuned MIMO control system under variation of power flow setpoint	139
5.40	Dynamic response - Deviation in line power flow $\Delta P_{e\,2}$ PSO tuned MIMO control system under variation of power flow setpoint	139
5.41	Dynamic response - Deviation in UPFC DC link voltage Δv_{dc} for PSO tuned MIMO control system under variation of power flow setpoint	140
5.42	Dynamic response - Deviation in AC bus voltage ΔV_{Et} for PSO tuned MIMO control system under variation of power flow setpoint	140
5.43	Dynamic response - Line power flow $P_{e\,2}$ after load disturbance in line 2	141
5.44	Dynamic Response - Generator angular speed Deviation $\Delta\omega$ after load disturbance in line 2	142

5.45	Dynamic response - Deviation in UPFC DC line voltage Δv_{dc} after load disturbance in line 2	142
5.46	Dynamic response - Deviation in AC bus voltage ΔV_{Et} after load disturbance in line 2	143
5.47	Dynamic response - Generator angular speed deviation $\Delta\omega$ after three six cycle fault for light loading condition	144
5.48	Dynamic response - Line power flow deviation $\Delta P_{e\,2}$ after three six cycle fault for light loading condition	144
5.49	Dynamic response - UPFC DC link voltage deviation Δv_{dc} after three six cycle fault for light loading condition	145
5.50	Dynamic response - AC bus voltage deviation ΔV_{Et} after three six cycle fault for light loading condition	145
5.51	Dynamic response - Generator angular speed deviation $\Delta\omega$ after three six cycle fault for Nominal loading condition	147
5.52	Dynamic response - Line power flow deviation $\Delta P_{e\,2}$ after three six cycle fault for nominal loading condition	147
5.53	Dynamic response - UPFC DC link voltage deviation Δv_{dc} after three six cycle fault for nominal loading condition	148
5.54	Dynamic response - AC bus voltage deviation ΔV_{Et} after three six cycle fault for nominal loading condition	148
5.55	Dynamic response - Generator angular speed deviation $\Delta\omega$ after three six cycle fault for heavy loading condition	149
5.56	Dynamic response - Line power flow deviation $\Delta P_{e\,2}$ after three six cycle fault for heavy loading condition	150
5.57	Dynamic response - UPFC DC link voltage deviation Δv_{dc} after three six cycle fault for heavy loading condition	150
5.58	Dynamic response - AC bus voltage deviation ΔV_{Et} after three six cycle fault for heavy loading condition	151
5.59	Dynamic response - Generator angular speed deviation $\Delta\omega$ after three six cycle fault for leading power factor condition	153
5.60	Dynamic response - Line power flow deviation $\Delta P_{e\,2}$ after three six cycle fault for leading power factor condition	154
5.61	Dynamic response - UPFC DC link voltage deviation Δv_{dc} after three six cycle fault for leading power factor condition	154
5.62	Dynamic response - AC bus voltage deviation ΔV_{Et} after three six cycle fault for leading power factor condition	155

List of Appendices

No.	Appendices
A	System Data
B	Single Machine Infinite Bus with UPFC

List of Abbreviations

Abbreviations	Description
BBO	Biogeography Based Optimization
CSC	Controllable Series Compensator
EA	Evolutionary Algorithm
EPRI	Electrical Power Research Institute
FACTS	Flexible AC Transmission Systems
GA	Genetic Algorithm
HSI	Habitat Suitability Index
IPFC	Interline Power Flow Controller
ITAE	Integral Time Absolute Error
MIMO	Multi-Input Multi-Output
POD	Power Oscillation Damping
PS	Phase Shifter
PSO	Particle Swarm Optimization
PSS	Power System Stabilizer
PWM	Pulse Width Modulation
SIV	Suitability Index Variable
SMIB	Single Machine Infinite Bus
SSSC	Static Synchronous Series Compensator
STATCOM	STATic COMpensator
SVC	Static Var Compensator

SVD	Singular Value Decomposition

Chapter 1
Introduction

- 1.1 Overview
- 1.2 FACTS Controllers
- 1.3 Unified Power Flow Controller (UPFC)
- 1.4 Motivation and Objective
- 1.5 Publications
- 1.6 Outline of The Thesis

Chapter 1
Introduction

1.1 Overview

Due to the increasing demand on power, and with the economical and environmental constraints on building new generating plants and installing new

Due to the increasing demand on power, and with the economical and environmental constraints on building new generating plants and installing new transmission lines, interconnection of the transmission system appeared as an option in order to cover the need for power. This also meant that the system is to be operated and utilized to its limits. Since the transmission system is governed by two limits namely, electrical stability limit, and thermal limit, and by operating outside the permissible range of stability, the system security is compromised. An innovative solution to such a problem was with the introduction of flexible AC transmission system (FACTS). FACTS controllers were introduced by Electrical Power Research Institute (EPRI) in 1980. The idea behind FACTS was to increase controllability and optimize the existing power system capacity through the use of power electronic devices. With such devices the transmission system is to be operated near to its thermal limits without compromising the system security and reliability. Since then, the use of FACTS controllers has been popular to solve different problems faced in power systems such as power flow control, voltage support, and even oscillation damping. FACTS installations increase the system operating range, security, and reliability and also provide more functionality over mechanical devic transmission lines, interconnection of the transmission system appeared as an option in order to cover the need for power. This also meant that the system is to be operated and utilized to its limits. Since the transmission system is governed by two limits namely, electrical stability limit, and thermal limit, and by operating outside the permissible range of stability, the system security is compromised. An innovative solu-

tion to such a problem was with the introduction of flexible AC transmission system (FACTS). FACTS controllers were introduced by Electrical Power Research Institute (EPRI) in 1980. The idea behind FACTS was to increase controllability and optimize the existing power system capacity through the use of power electronic devices. With such devices the transmission system is to be operated near to its thermal limits without compromising the system security and reliability. Since then, the use of FACTS controllers has been popular to solve different problems faced in power systems such as power flow control, voltage support, and even oscillation damping. FACTS installations increase the system operating range, security, and reliability and also provide more functionality over mechanical devices installed in the system.

FACTS controllers can be categorized by two different approaches. The first categorization of FACTS controllers is based on the connection of the device into the system:

1. Series Controllers
2. Shunt Controllers
3. Hybrid Controllers

The second approach is based on the technology of the FACTS controllers:

1. Thyristor based FACTS controllers
2. Voltage Source Converter (VSC) based FACTS controllers

It is safe to consider them as the first and second generations of FACTS controllers.

1.2 FACTS Controllers

1.2.1 Thyristor Based FACTS Controllers

This category of FACTS controllers employ conventional thyristors in their circuits. They include FACTS devices such as: Static Var Compensator (SVC), Thyristor Controlled Series Compensator (TCSC), and Thyristor Controlled Phase Shifter (TCPS). Each device of this family of FACTS devices can only control one of the three parameters of power system (impedance, bus voltage and phase angle).

1.2.1.1 Static Var Compensator (SVC)

SVC is a shunt connected controller, which is intended to act as a variable impedance where the current through a reactance of a transmission line is controlled using a back to back connected thyristors. Figure (1.1), shows the a schematic diagram for single phase SVC. It is composed of thyristor switched capacitors (TSC) and thyristor switched reactors (TSR). The SVC is operated to maintain the voltage at the bus at which it is connected to. Ideally, the best practice is to connect the SVC at the midpoint of the transmission line K. Padiyar (2007). The SVC V-I characteristics curve is shown in figure (1.2) . Its illustrating that voltage regulation can be achieved in normal operating range defined by the maximum inductive and capacitive currents. The capability to enhance the power system stability using SVC has been investigated in Noroozian (1998).

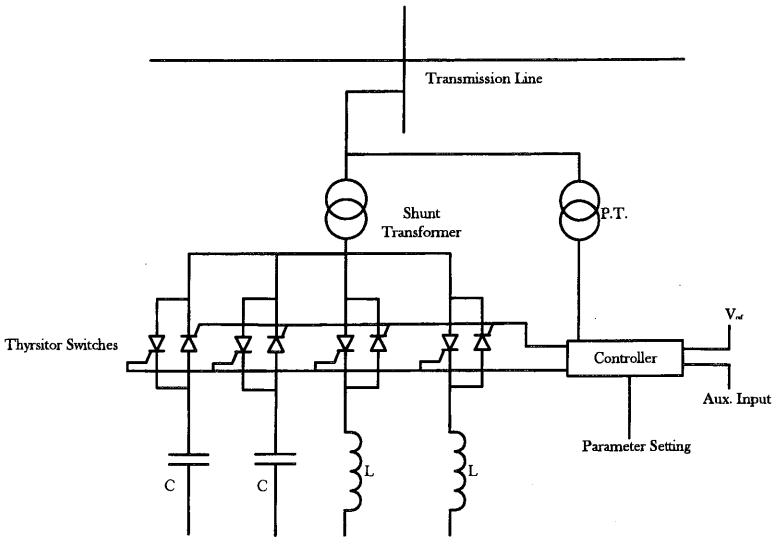


Figure (1.1)
Static Var Compensator (SVC)

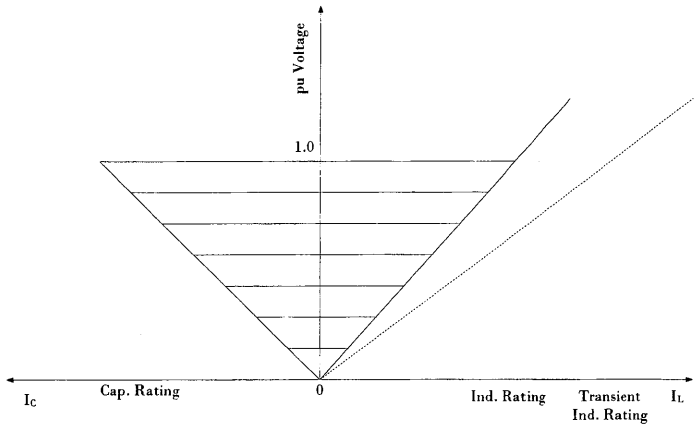


Figure (1.2)
V-I characteristics curve for SVC

1.2.1.2 Thyristor Controlled Series Compensator (TCSC)

Thyristor Controlled Series Compensator (TCSC), is used to control the power flow through a transmission line through impedance compensation. With different degrees of transmission compensation, variation in power transmitted can be achieved as it is shown in figure (1.3) . TCSC has two forms:

1. Thyristor Switched Capacitors (TSC): In this case the impedance of the transmission line is varied as the number of the capacitor banks connected to the system varies. This is done through the control of the firing angle of the corresponding thyristor pair connecting the respective capacitor bank. Figure (1.4) presents schematic diagram of TSC.

2. Fixed capacitor is parallel with thyristor controlled reactor (TCR). In this scheme, the impedance control is achieved by controlling the conduction period of the thyristor connecting the reactor. Hence maximum compensation is reached when TCR is off. Figure (1.5) shows a double fixed capacitor in parallel with TCR.

TCSC capability to damp power system oscillation has widely been addressed in literature. It has been in use for many years to increase line power transfer as well as enhancing system stabilityPanda & Padhy (2007).

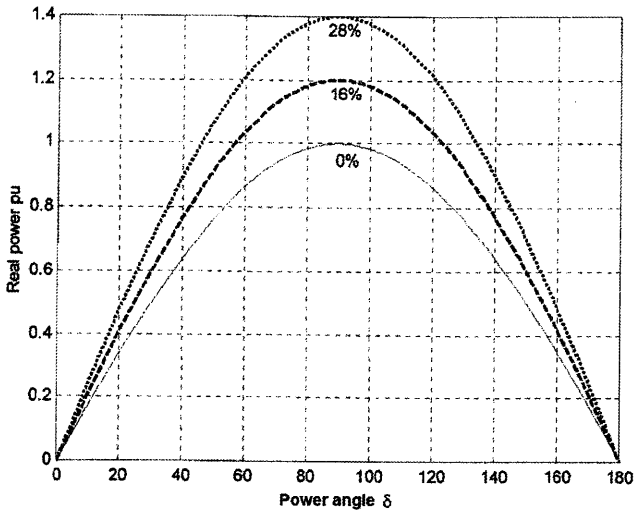


Figure (1.3)
Power curve for different degrees of compensation using TCSC

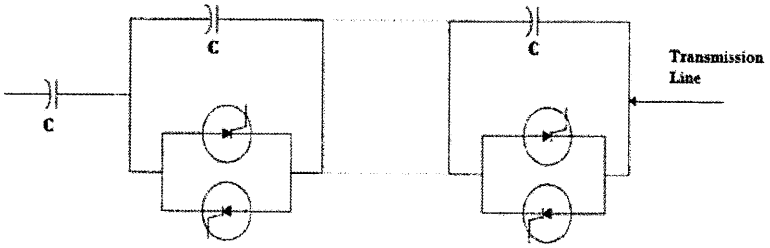


Figure (1.4)
TCSC: Thyristor Switched Capacitors (TSC)

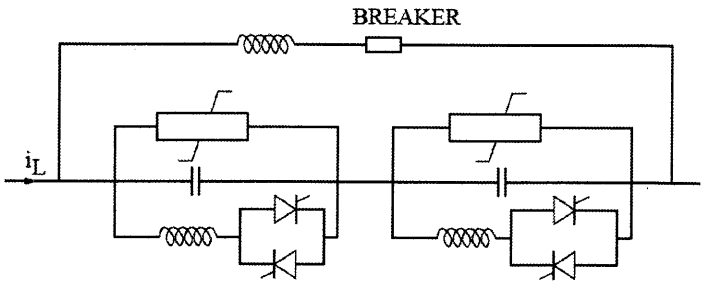


Figure (1.5)
TCSC: Fixed Capacitor in Parallel with Thyristor Controlled Reactor

1.2.1.3 Thyristor Controlled Phase Shifters (TCPS)

Thyristor Controlled Phase Shifters (TCPS), controls the transmission angle through the injection of series voltage that is quadrature to the original angle. This is done in order to control power flow in multiple transmission corridors, or to control it so as to increase the transient and dynamic stability of a transmission system Fang & Macdonald (1998). As presented in figure (1.6), TCPS consists of multiple tap-changing shunt transformers, a boosting series transformer, and a set of thyristor arranged to select a combination of tap voltages to the boosting transformer. If the injected voltage angle is stipulated to $\pm 90°$, as can be seen from figure (1.7) which represents a phasor diagram of the system. The TCPS is called a quadrature booster, and the angle between the injected voltage and the line current can be determined from system parameters. The drawback of TCPS is that it is not capable to locally generate or absorb either real or reactive power. It is recommended that the TCPS is to be connected close to the generating node or be complemented by a shunt compensator to provide the required reactive power.

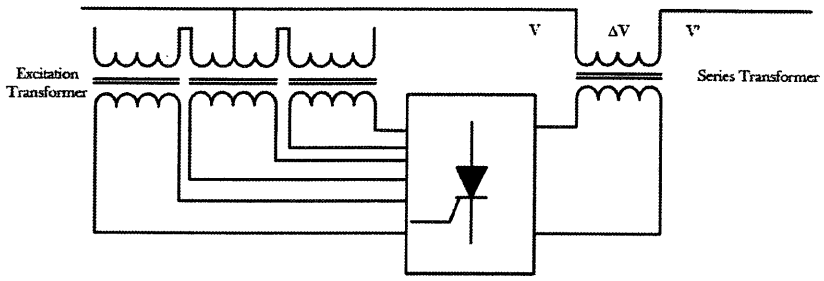


Figure (1.6)
Thyristor Controlled Phase Shifters (TCPS)

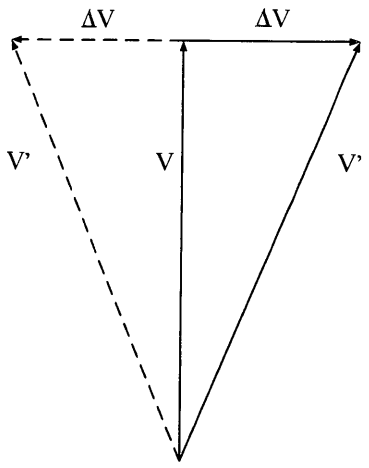


Figure (1.7)
TCPS Operation: Phasor Diagram

1.2.2 Voltage Source Converters Based FACTS Controllers

The first generation of FACTS controllers was based on thyristor technology, hence they have the turn-on capability only, while the turn-off of the device depends on the current coming to zero as per circuit and system conditions. Semiconductor devices such as Gate Turn-Off (GTO) Thryistor , Integrated Gate Biploar Transistor (IGBT), MOS Turn-Off Thyristor (MTO), and Integrated Gate Commutated Transistor (IGCT) have the turn off capability. The emergence of these devices has started the next generation of FACTS controllers based on the synchronous voltage source converters (VSC). The VSC based FACTS controllers are equipped with a dc storage device allowing a bi-directional flow of power between the device and the transmission system. Moreover, they have the capability of generating and absorbing of reactive power with the ac system.

1.2.2.1 Static Compensator (STATCOM)

Also known as Advanced Static Var Compensator (ASVC), is a shunt connected FACTS controller. It was developed to overcome the shortcomings of the conventional SVC as it uses switched reactors and switched ca-

pacitors. A STATCOM is comparable to a synchronous condenser which can supply variable reactive power and regulate the voltage of the bus where it is connected K. Padiyar (2007). A schematic representation of the STATCOM is shown in figure (1.8). The STATCOM is operated as when the injected voltage is greater than the bus voltage, the current flows through the tie reactance or coupling transformer from the VSC to the ac system, where it is 90° leading the voltage. Hence operating it either to generate reactive power, capacitive reactive power, or absorb reactive power, inductive reactive power and this can be seen from figure 1.9. This is done via the control of the magnitude of the injected voltage, through a PWM control signal.

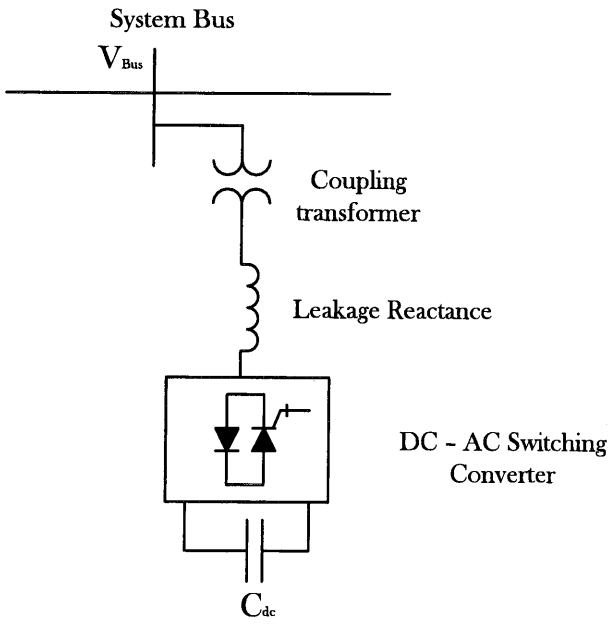
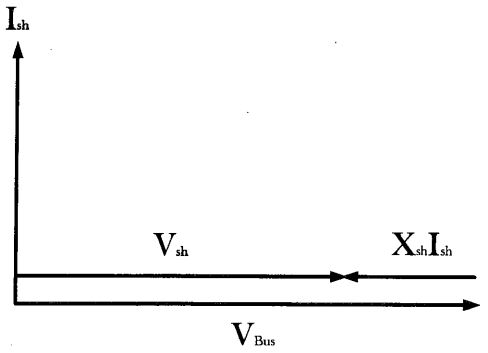
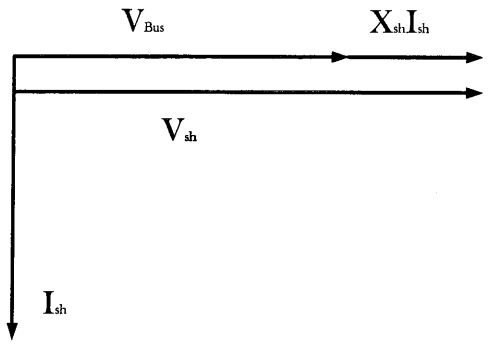


Figure (1.8)
STATCOM schematic representation



a. Generating Reactive Power



b. Absorbing Reactive Power

Figure (1.9)
STATCOM Operation

1.2.2.2 Static Synchronous Series Compensator (SSSC)

Static Synchronous Series Compensator (SSSC), is a series type FACTS device which employs the voltage source converter for compensation. The SSSC is similar to the STATCOM in construction the only difference is that it connected in series with the transmission line through a booster transformer, as shown in figure (1.10) .

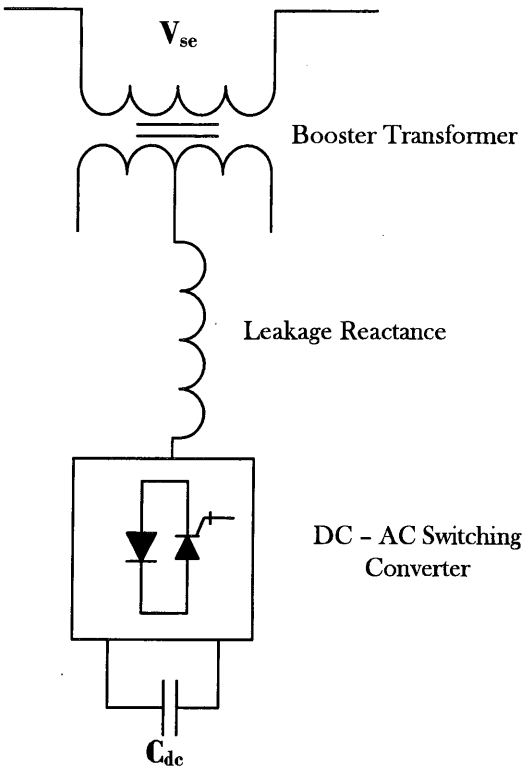


Figure (1.10)
Static Synchronous Series Compensator (SSSC)

The principle of operation of the SSSC is that through the injection of voltage in series with the transmission line the system parameters (angle and impedance) are varied. The injected voltage magnitude is fully controlled while the phase angle is kept in quadrature to the line current. However, the phase angle of the injected voltage can be either +90° or -90°, meaning that the voltage either be leading or lagging the current, thus operating either as series capacitance or series reactance to compensate the line impedance. Figure (1.11) , illustrates the SSSC operation in a phasor diagram, where $\mathbf{V}_s$ and $\mathbf{V}_r$ represents the sending and receiving buses between which the SSSC is connected $\mathbf{V}_L$ is the voltage drop across the transmission line. By injecting a controllable voltage $\mathbf{V_q}$ that is in-phase with $\mathbf{V}_L$ the voltage

drop across the line can be controlled and eventually controlling power flow through the line.

Same as the STATCOM, as being based on the voltage source converters, the SSSC is able to generate and absorb reactive power. The SSSC can exchange active and reactive power with the A.C system simply by varying the angle of the injected voltage. For this the capacitor serves as an energy source or sinks depending on the angle.

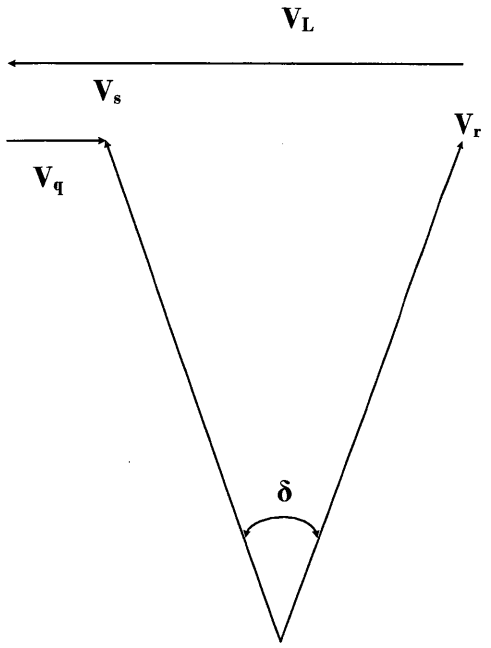


Figure (1.11)
SSSC Operation: Phasor Diagram

1.2.2.3 Interline Power Flow Controller (IPFC)

The conventional series capacitive compensation using fixed thyristor controlled or SSSC, are used to increase the transmittable real power over a given line and also balance loading of a normally encountered multiline transmission system. The problem with these controllers, that they are unable to control the reactive power flow in, and thus the proper load balancing through the line. This can be clearly seen when it is employed to control

power over a line with low X/R ratio. Since these devices are to reduce the line reactance to increase the transmitted power, the losses of the line will increase as the ratio decreases. Interline Power Flow Controller (IPFC), was introduced in 1998 by Gyugyi with Sen and Schader Hingorani et al. (2000). The introduction of IPFC was to address the problem experienced with conventional series compensation.

The IPFC consists of two voltage source converters connected back - to - back through a common DC link capacitor, as shown in figure (1.12). Each VSC operates as an independent SSSC, where it injects a controllable series voltage with respect to the selected bus voltage and line current. In its general form the IPFC employes a number of dc-to-ac converters each providing series compensation for a different line.

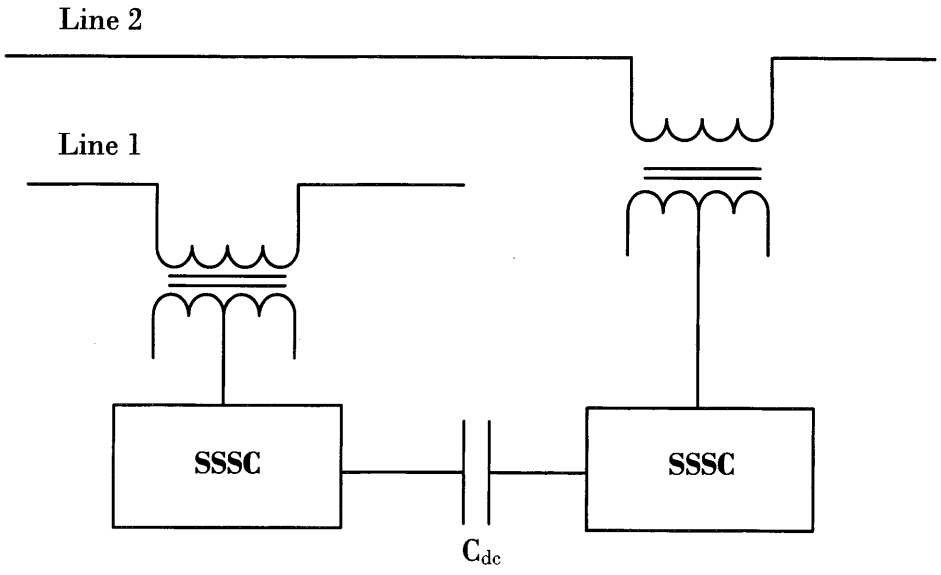


Figure (1.12)
Interline Power Flow Controller (IPFC)

1.3 Unified Power Flow Controller (UPFC)

The concept of UPFC was introduced by Gyugyi in 1991Gyugyi (1992). It is the most versatile VSC based FACTS controllers, capable of controlling any or all of the transmission system parameters (voltage,impedance, and angle), hence it is characterized by the adjective "unified" in its name Hingorani et al. (2000). UPFC can independently control both the real and reactive power flow in the line.

1.3.1 Construction of the UPFC

The UPFC is a hybrid FACTS controller, as it consists of two voltage source converters connected back to back through a common d.c link as illustrated in figure (1.13). Through the connection of two ac converters, a path is established in which the real power can freely flow between two a.c sides of the converters.

The series VSC, also termed as the booster converter, is connected to the line through a series coupling transformer similar to the SSSC. The shunt VSC or the excitation converter is connected to the system bus through a shunt coupling transformer same as the STATCOM. Hence the capabilities of the two devices are realized by a single FACTS controller.

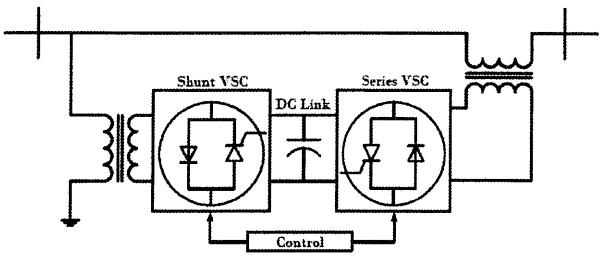


Figure (1.13)
Unified Power Flow Controller (UPFC)

1.3.2 Modes of Operation

The UPFC construction gives the advantage of controlling all the transmission system parameters (voltage,phase angle and impedance). This is

done by injecting voltage with appropriate magnitude and phase.

UPFC in concept is a synchronous voltage source (SVS) , that can be represented as a fundamental frequency voltage phasor $\mathbf{V_{pq}}$, with controllable magnitude V_{pq} and controllable phase angle ρ. The magnitude of the voltage phasor is controllable within a range of $0 \leq V_{pq} \leq V_{pqmax}$, which defines the compensation region of the UPFC. On the other hand, the phase angle is free to change as $0 \leq \rho \leq 2\pi$. The shunt converter of the UPFC acts primarily as a supply of active power to the series converter that is analogous to the SVS where it injects the controllable voltage in series with the transmission line. Each converter is capable of generating and absorbing reactive power independently, hence they give rise to reactive power compensation through the series converter and voltage support or Var compensation through the shunt converter.

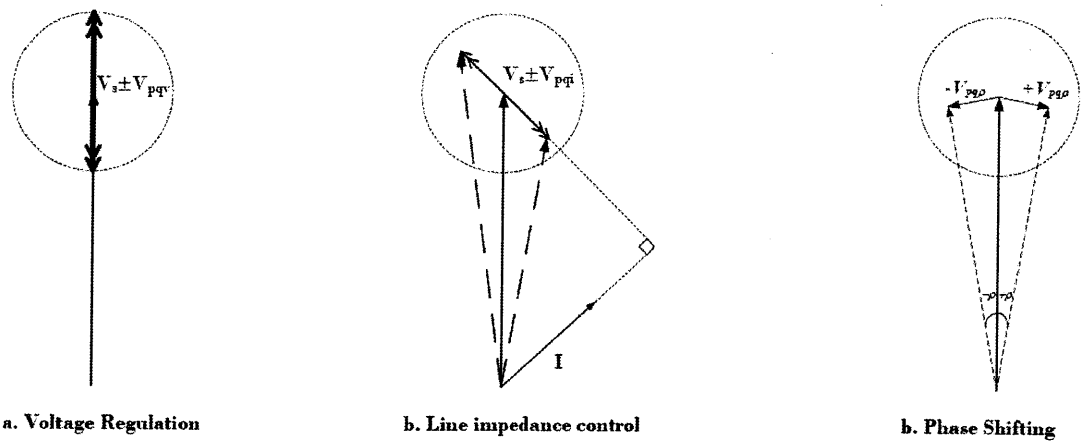
The voltage injected via the booster converter acts essentially as a synchronous ac voltage source, and as the current flows through this voltage source it results in an exchange of active and reactive powers with the AC system. The active power that is exchanged at the AC terminal is supplied from the shunt converter that draws power from the system to the DC link, while the reactive power is generated internally in the converter.

Figure (1.14), illustrates the phasor diagram of the control capabilities of the UPFC . For instance, the voltage regulation is done through the injection of an in-phase or anti-phase voltage, $\rho = 0$ and $0 \leq V_{pq} \leq V_{pqmax}$. Hence the effective sending end voltage is either increased or decreased in magnitude.

The series reactive compensation is done through injection of a quadrature voltage to the line current **I**, in which it emulates the action of a series inductive or series capacitive compensation. The type of compensation depends on the angle of the series injected voltage as it can be either +90° or -90°, and the level of the compensation depends on the magnitude of the injected voltage.

Phase angle regulation is done through an injection of a voltage component V_{pq} with a phase shift of ρ that if added to V_s will not change its magnitude.

Combining these modes, the UPFC multifunction power flow control is executed through simultaneous terminal voltage regulation.



a. Voltage Regulation b. Line impedance control b. Phase Shifting

Figure (1.14)
UPFC Control Capabilities

1.4 Motivation and Objective

The objectives of this research work are as follows:

1. Analyzing the system mathematically for load flow and dynamic studies and compare between different models of UPFC that have been used in literature.
2. Discussing biological inspired evolutionary optimization algorithms:

   (a) Biogeography Based Optimization (BBO) Algorithm

   (b) Particle Swarm Optimization (PSO) Algorithm

3. Investigating the capability of UPFC in damping power system oscillations through the use of a lead - lag compensator and use of the above mentioned algorithms to tune it.

4. Designing and simulating the performance of UPFC as MIMO system.

5. Comparing the performance of the system for the two case studies mentioned above in terms of speed, stability, accuracy and simplicity.

1.5 Publications

1. Comparison of Fundamental Frequency Model and PWM Based Model of UPFC, by S.A. Al-Qallaf, S.A. Al-Mawsawi, A. Haider, ICEE 2014 : International Conference on Electrical Engineering, Dubai, October 2014.

2. Investigation of Different Control Stratgies for UPFC Decoupled Model and the Impact of Location on Control Parameters, by S.A. Alqallaf, S.A. Al-Mawsawi, A. Haider, ICEE 2014 : International Conference on Electrical Engineering, Dubai, October 2014

3. Evolutionary Optimization Algorithms in Designing a UPFC Based POD Controller, WSEAS Transactions on Power Systems,5716-331 (15296) - under review.

4. Design of Robust UPFC Based Damping Controller Using Biogeography Based Optimization, Alexandria Engineering Journal, AEJ-D-14-00434 - under review.

1.6 Outline of The Thesis

The thesis is divided into six chapters . The first chapter is an introductory chapter, which discusses the concept behind FACTS controllers. It categorizes the FACTS controllers based on the technology employed into first generation and second generation devices. It then discusses the UPFC construction and modes of operations. The second chapter deals with the modeling of the UPFC for load flow studies and dynamic analysis. It presents comparison between two dynamic models for which one is selected for use in this study. The third chapter introduces the concept of biogeography based optimization (BBO) and particle swarm optimization (PSO) algorithms, it then proceeds to investigates the system capability to damp the power system oscillation. Using the optimization algorithms, a POD controller is designed using different objective functions. The fourth chapter, uses the optimization algorithms to tune simultaneous controllers to realize a MIMO UPFC control system. In the fifth chapter an assessment of the controller robustness and performance is done through several tests on the system. The conclusion and recommendation for future research work are presented in the sixth chapter.

Chapter 2

Unified Power Flow Controller Modeling

- 2.1 Overview
- 2.2 Unified Power Flow Controller Load Flow Modeling
- 2.3 Investigation of Installation location and Impact on control parameter
- 2.4 Unified Power Flow Controller Dynamic Modeling
- 2.5 Study System
- 2.6 Summary

Chapter 2
Unified Power Flow Controller Modeling

2.1 Overview

In order to evaluate the performance of a unified power flow controller (UPFC), mathematical models for steady state and dynamic analysis need to be developed. The steady state model is mainly concerned with the incorporation of the UPFC in load flow studies, while the dynamic model is developed to investigate the behavior of UPFC during transients ,the control capability, and controller design. This chapter is divided into two main sections, the first discusses the load flow models developed in literature and select one model for the aim of finding the initial operating conditions required for the dynamical analysis of the system. The dynamic modeling is discussed in the second section of this chapter, where two models are presented and discussed with a proposed control strategy. Based on a comparison between the two models and their control strategies, the chosen dynamical model is then implemented on a single machine infinite bus (SMIB) system with double transmission line circuit.

2.2 Unified Power Flow Controller Load Flow Modeling

Steady state analysis of a power system with the inclusion of the unified power flow controller (UPFC) would show the need of a model for this device to be incorporated in the load flow studies. In a load flow problem the real and reactive powers of a load bus, the real power and voltage magnitude of the generator bus, and the voltage magnitude and phase angle of a slack bus is to be specified. This section will discuss several models that were introduced in literature briefly, and it will take on a detailed discussion for the model introduced in Nabavi-Niaki & Iravani (1996). This model will

be used to find the initial operating conditions required for the dynamic analysis and control design.

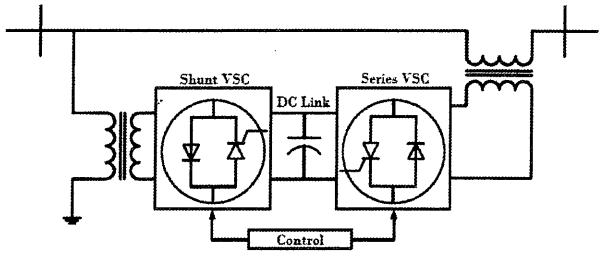


Figure (2.1)
Unified Power Flow Controller Schematic Diagram

Figure (2.1) shows a schematic diagram of a single line UPFC connected to a transmission line system. As discussed in chapter 1, the UPFC is composed of two voltage source converters (VSC) connected back to back through a common DC link capacitor. Converter 1 is connected to the power system in shunt through a shunt coupling transformer termed as the excitation transformer. Converter 2 is connected to the power system through a series coupling transformer known as boosting transformer.

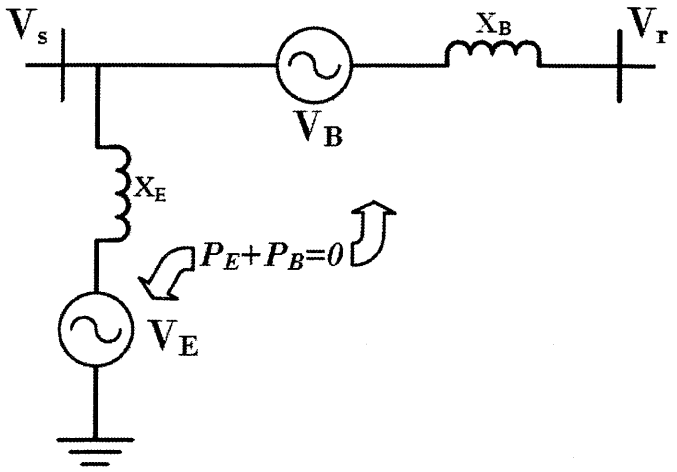


Figure (2.2)
Steady State UPFC Model

During steady state the UPFC is modeled by replacing the converters by fundamental frequency voltage sources in series with the coupling trans-

former leakage reactance, as shown in Figure (2.2).Vural & Tumay (2003). In this modeling approach the series voltage source $\mathbf{V_B}$ is converted into a current source in parallel to the transmission line. This current injection is transformed into an equivalent complex power injection at the sending and receiving buses of the UPFC. In this approach the shunt converter functions as a real power supply to the series converter, where its reactive power injection is not considered ,$Q_E = 0$Vural & Tumay (2003). Figure (2.3), illustrates how to obtain the power injection model of UPFC. The drawbacks of this model is that it did not consider the shunt converter capabilities by neglecting the reactive power injection. Moreover all major aspects of automatic UPFC parameters adjustment has not been addressed, also the adjustment of the power flow is done through trial and error procedure El-Sadek et al. (2006).

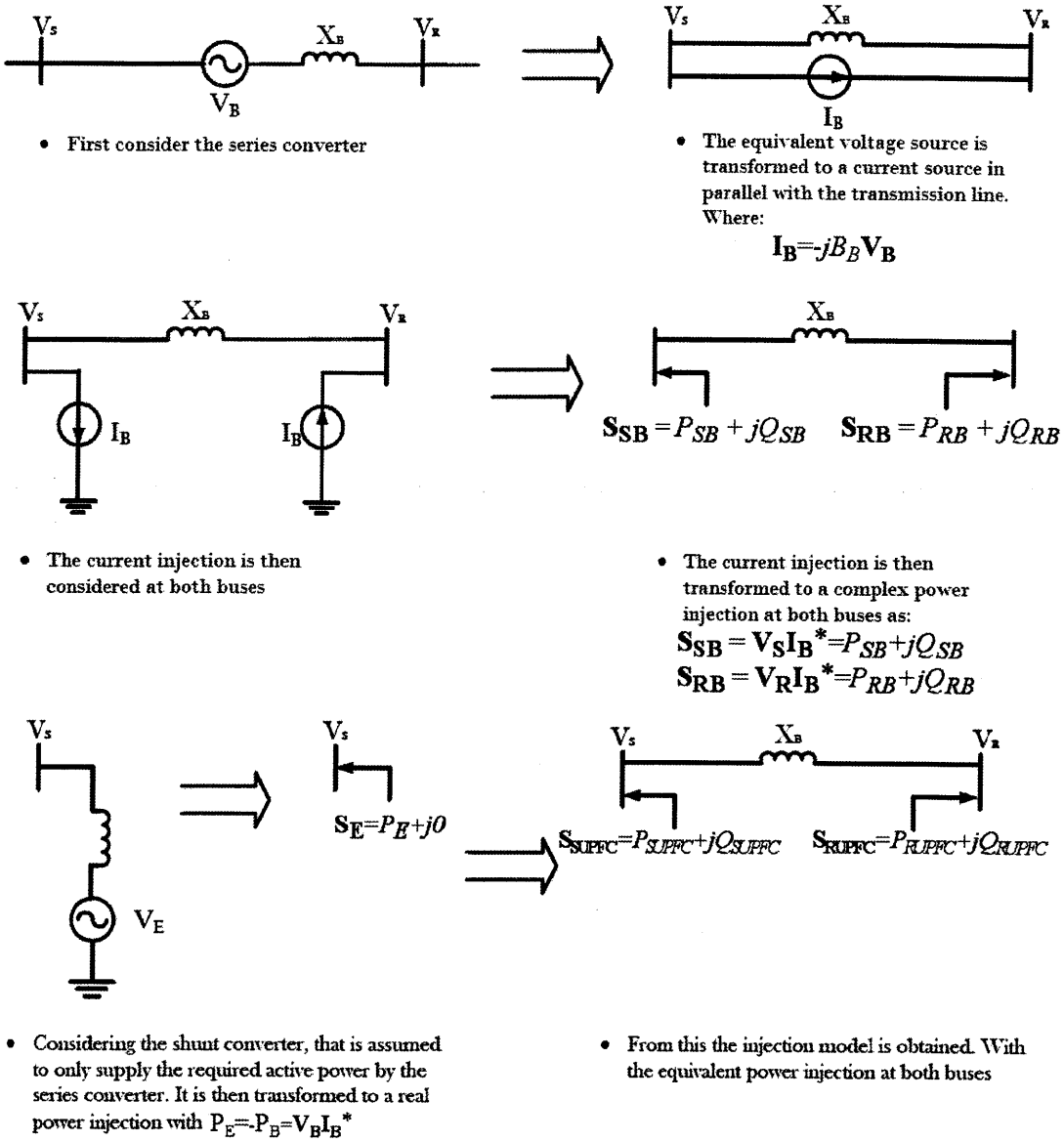


Figure (2.3)
UPFC Power Injection Model

Another load flow modeling approach was introduced in Fuerte-Esquivel et al. (2000). This comprehensive UPFC model uses the steady state equivalent circuit shown in figure (2.2) to derive an extension of the power flow equations. This model incorporates the UPFC directly in the existing New-

ton - Raphson load flow algorithm. This model suffers from a convergence and divergence problem, where a good initial condition could lead to convergence while a bad initialization may lead to divergence.

2.2.1 UPFC Decoupled Load Flow Model

Based on Nabavi-Niaki & Iravani (1996), it was deduced that the UPFC can be modeled as can be seen from figure (2.2). The operation of the voltage sources is not independent of each other, rather as mentioned above that the UPFC real power constraint should be satisfied:

$$P_E + P_B = 0 \tag{2.1}$$

By neglecting the coupling transformers losses and by assuming that the UPFC is a lossless system, the active power injection at the UPFC buses should be equal as net active power exchange with the AC system is zero. Hence:

$$P_{Et} + P_{Bt} = 0 \tag{2.2}$$

In order to incorporate the UPFC in the load flow studies, an innovative approach was presented by Nabavi-Niaki & Iravani (1996), where the UPFC is replaced by equivalent bus representation. Hence, the power system is transformed into a conventional power system which can be solved using any load flow procedure. The bus equivalent representation of the UPFC that was presented in Nabavi-Niaki & Iravani (1996) is shown in figure (2.4):

In this representation the UPFC is intended for simultaneous control where it will control the active power flow through the transmission line, regulate the receiving end voltage, and control reactive power injection to the sending end bus. Hence, the sending bus is set to a PQ - load bus and the receiving end bus is set to a PV generator bus. By the assumption that

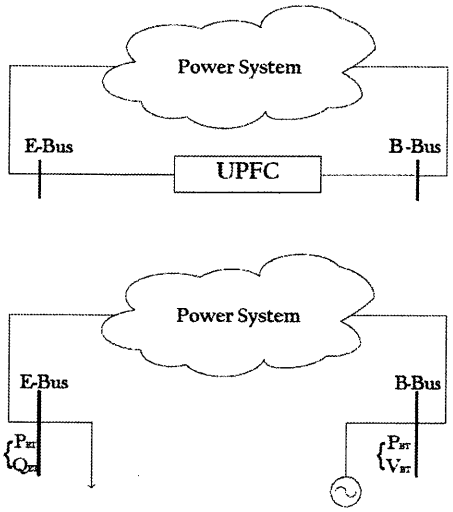


Figure (2.4)
UPFC Equivalent Bus Representation

the UPFC is a lossless system and from equation (2.2), it can be seen that the active power for the load bus and for the generator bus are equal and is set to the desired power flow in the transmission line that the UPFC should control. The reactive power at the load bus is the reactive power injection by the shunt converter, while the the generator bus voltage magnitude is set to the value at which the UPFC is desired to regulate.

Since in this scheme shown in figure (2.4), the UPFC is intended for simultaneous control of active power flow, reactive power compensation, and receiving bus voltage regulation. In a similar manner, different control schemes can be defined for simultaneous control (and with simple manipulation can be used for two or single parameter control), and this can be seen from figure (2.5), which is showing different control strategies using the decoupled model.

Figure (2.5a), shows a scheme where the UPFC is used for simultaneous control of the power flow through the transmission line and to regulate the voltage of the sending end bus. The double parameter control is achieved in scheme of (2.5b), where the both of the buses are set as a PQ buses, where the active power can be set from (2.2), and by setting the injected reactive

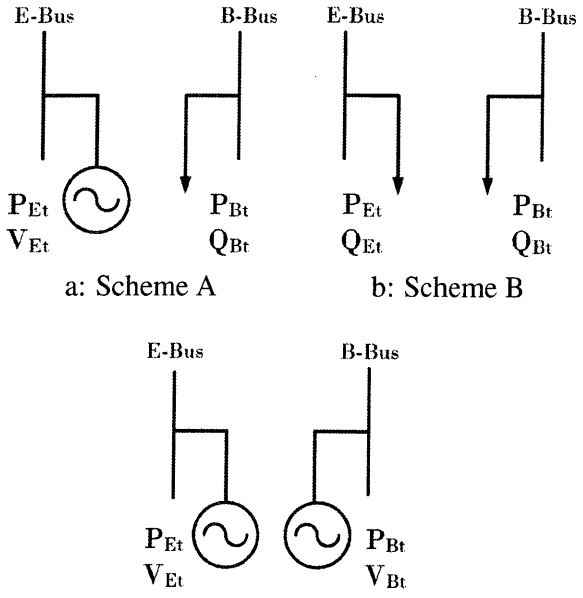


Figure (2.5)
UPFC Decoupled Model Different Control Schemes

power by the shunt convert $Q_{Et} = 0$ only the active power and reactive power flow in the line is controlled. Scheme 3 is used for active power flow and voltage regulation at both buses of the UPFC.

Once the UPFC control strategy is decided, the UPFC is replaced by its bus configuration equivalent and the load flow problem is solved using any load flow procedure. Once all the state variables of the power system with the decoupled representation of the UPFC are obtained, the UPFC control parameters are to be found and in order to do this the power injections for the UPFC model in figure (2.2) are given as:

$$P_{Etc} = \frac{V_{Et}V_E}{X_E}\sin(\delta_{Et} - \delta_E) + \frac{V_{Et}V_{Bt}}{X_B}\sin(\delta_{Et} - \delta_{Bt}) - \frac{V_{Et}V_B}{X_B}\sin(\delta_{Et} - \delta_B) \quad (2.3)$$

$$Q_{Etc} = \left(\frac{X_E + X_B}{X_E X_B}\right) V_{Et}^2 - \frac{V_{Et}V_E}{X_E}\cos(\delta_{Et} - \delta_E) - \frac{V_{Et}V_{Bt}}{X_B}\cos(\delta_{Et} - \delta_{Bt}) + \frac{V_{Et}V_B}{X_B}\cos(\delta_{Et} - \delta_B) \quad (2.4)$$

$$P_{Bt} = \frac{V_{Bt}V_{Et}}{X_B}\sin(\delta_{Bt} - \delta_{Et}) + \frac{V_{Bt}V_B}{X_B}\sin(\delta_{Bt} - \delta_B) \quad (2.5)$$

$$Q_{Bt} = \frac{V_{Bt}^2}{X_B} - \frac{V_{Bt}V_{Et}}{X_B}\cos(\delta_{Bt} - \delta_{Et}) - \frac{V_{Bt}V_B}{X_B}\cos(\delta_{Bt} - \delta_B) \quad (2.6)$$

And it can be seen that these equations are nonlinear, so in order to solve them Newton-Raphson method is used . The Jacobian matrix for this system of equations is found to be:

$$J = \begin{vmatrix} \frac{\partial P_{Et}}{\partial \delta_E} & \frac{\partial P_{Et}}{\partial V_E} & \frac{\partial P_{Et}}{\partial \delta_B} & \frac{\partial P_{Et}}{\partial V_B} \\ \frac{\partial Q_{Et}}{\partial \delta_E} & \frac{\partial Q_{Et}}{\partial V_E} & \frac{\partial Q_{Et}}{\partial \delta_B} & \frac{\partial Q_{Et}}{\partial V_B} \\ \frac{\partial P_{Bt}}{\partial \delta_E} & \frac{\partial P_{Bt}}{\partial V_E} & \frac{\partial P_{Bt}}{\partial \delta_B} & \frac{\partial P_{Bt}}{\partial V_B} \\ \frac{\partial Q_{Bt}}{\partial \delta_E} & \frac{\partial Q_{Bt}}{\partial V_E} & \frac{\partial Q_{Bt}}{\partial \delta_B} & \frac{\partial Q_{Bt}}{\partial V_B} \end{vmatrix} \quad (2.7)$$

Figure (2.6) illustrating a flow chart for the decoupled UPFC model used in a Newton-Raphson load flow solution.

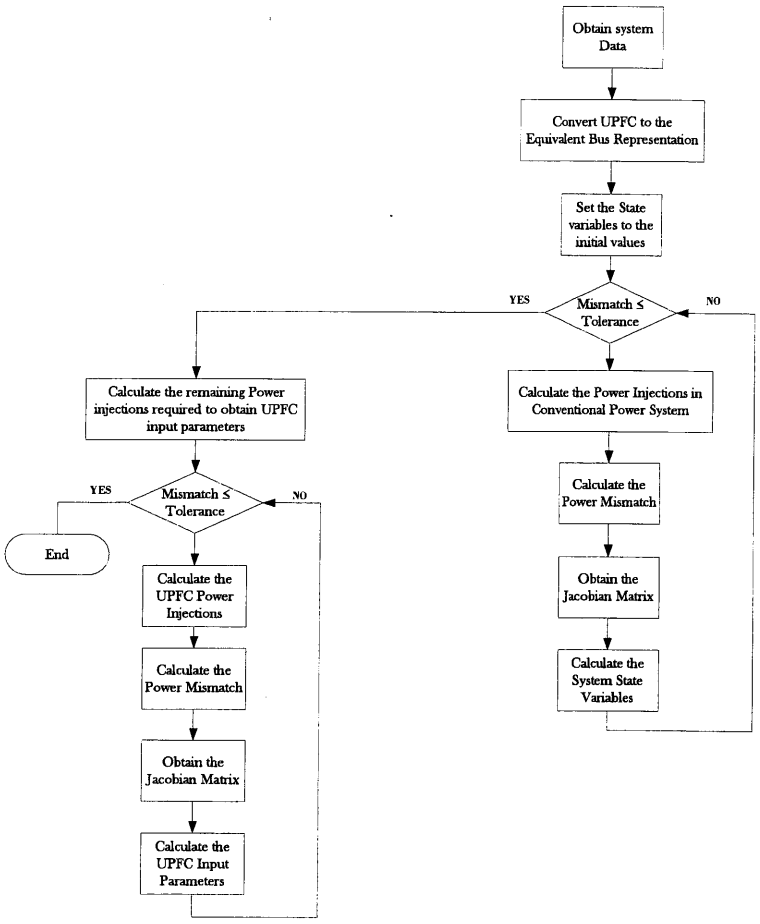


Figure (2.6)
Flow Chart of Newton-Raphson Algorithm for the UPFC Decoupled Load Flow Model

Compared to the two approaches in Vural & Tumay (2003); Fuerte-Esquivel et al. (2000), the decoupled method is easier to use, preserve the functionality, and it does not suffer from the problem of initial conditions.

2.3 Investigation of Installation location and Impact on control parameter

To investigate the impact of location of UPFC and the variation of setpoint on the control parameters, namely the modulation indexes, thus the UPFC decoupled model for different control strategy is to be implemented on a single machine infinite bus system. The system is shown in figure(2.7) :

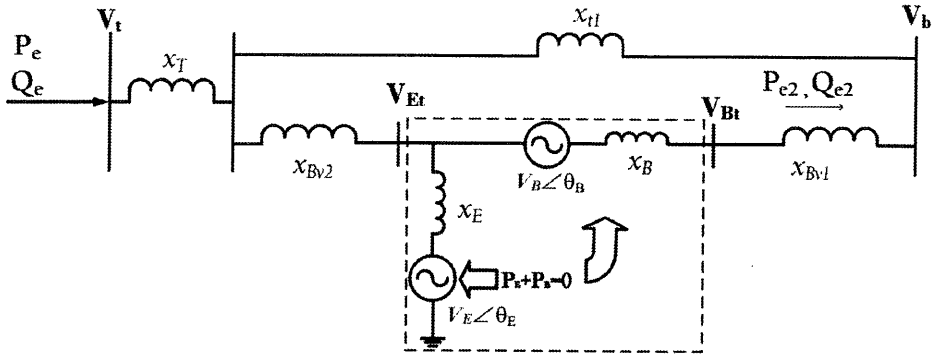


Figure (2.7)
Single machine infinite bus system with double transmission line circuit

For this study system the generator bus which is a PV bus where it injects an active power of 1.0 p.u and the bus voltage is being regulated at 1.05 p.u . The infinite bus has a constant voltage of $1\angle 0°$. In order to simulate the system, the UPFC is replaced by it equivalent bus model based on the control scheme to be used. So in order to study the effect of changing the setpoint on the modulation indexes different control schemes should be taken into account, in this research two schemes are considered to see the effect of variation of setpoint and location.

2.3.1 Case 1: PQ - PV bus configuration

In this scheme the UPFC is used to control the active power flow in the line, regulate the voltage of the receiving end, and shunt converter is used for

reactive power compensation. In this case each of the controlled variables is to be changed as the location of installation is changed while holding the other variables at a constant value.

2.3.1.1 Active Power

By varying the active power setpoint from 0.5 p.u to 0.65 p.u with the location, the following results were obtained:

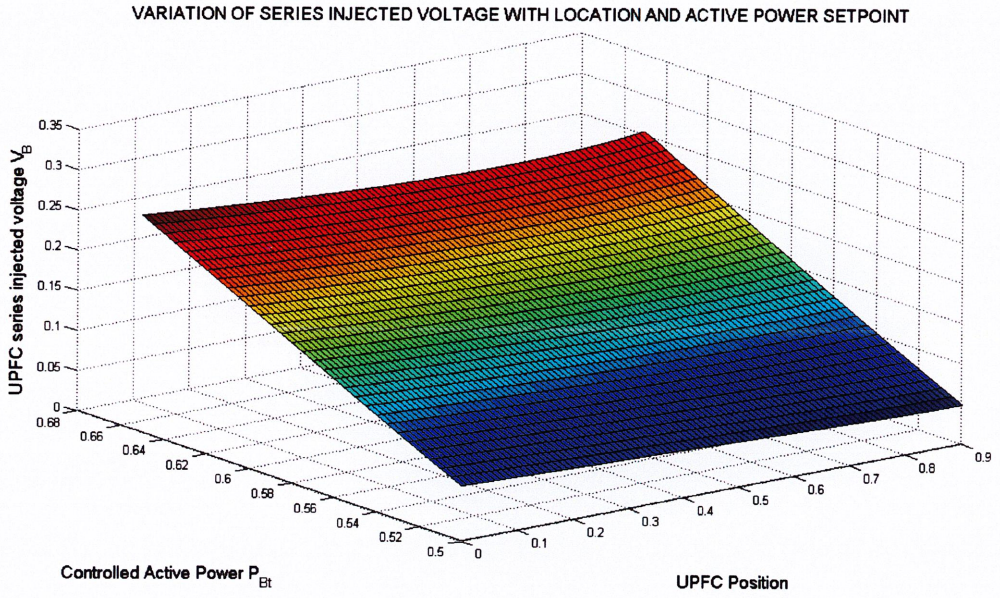


Figure (2.8)
Variation of series injected voltage V_B with active power setpoint and location variation

From figure (2.8), it can be seen that the series injected voltage increases linearly with the increase of setpoint regardless of the location. On the other hand, for a given setpoint on the surface shown in figure, the behavior of the injected voltage V_B is slightly nonlinear. At a 0.5 p.u active power setpoint, the variation of series voltage V_B seems to be linear as it drops from 0.068 p.u to 0.048 p.u as the location changes, while at a higher degree of active power compensation the behavior is nonlinear as the injected voltage V_B varies between 0.2691 p.u and 0.2525 p.u and the minimum is

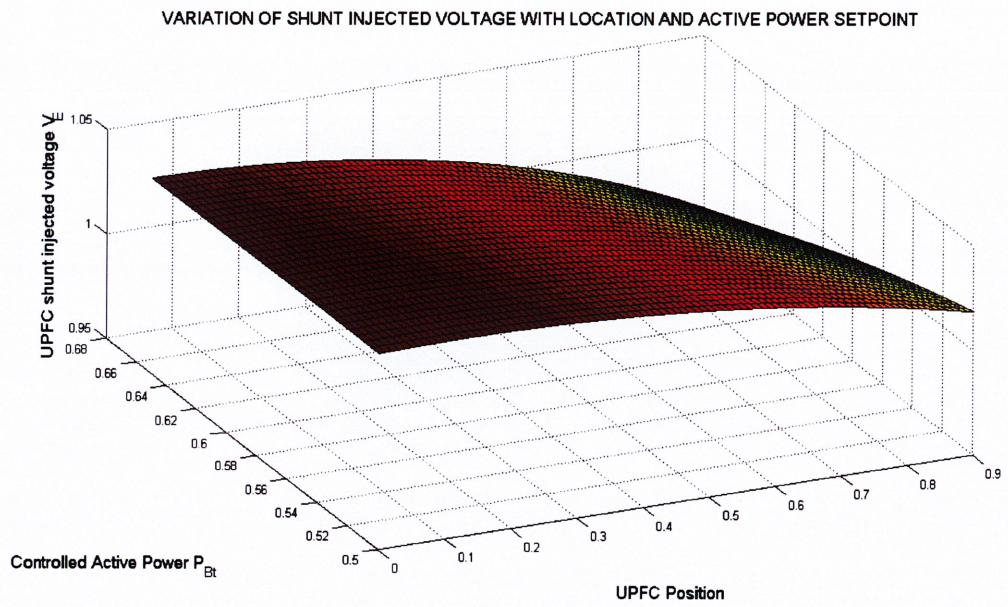


Figure (2.9)
Variation of shunt injected voltage V_E with active power setpoint and location variation

attained at 65% from the system intermediate bus. Thus the level of active power compensation is what decides the nature of the relation between the series injected voltage and the point of installation.

As for the shunt injected voltage V_E, it can be seen from figure (2.9) that for the UPFC connected at the intermediate bus the value is almost constant as the setpoint is varied, and that can be explained due to the change in the intermediate bus voltage V_{Et} hence the current in the shunt branch is changing. As the location is varied the injected voltage is varied, but it is almost constant for the variation in setpoint. Beyond the mid point position, the behavior of the controlled voltage V_E is varied as the setpoint is varied, and that is due to the increase in x_{Bv2} and with Q_{Et} being constant which means that the current is almost constant with the location variation. V_E behaves in a nonlinear manner as it reduces as the setpoint increases and that can be related to the increase in V_B as it should maintain the power balance between the UPFC branches in (2.1).

2.3.1.2 Reactive Power Q_{Et}

Varying the shunt injected reactive power Q_{Et} from -0.2 p.u to 0.2 p.u while all the other controlled parameters of the UPFC are kept constant, the following results were obtained:

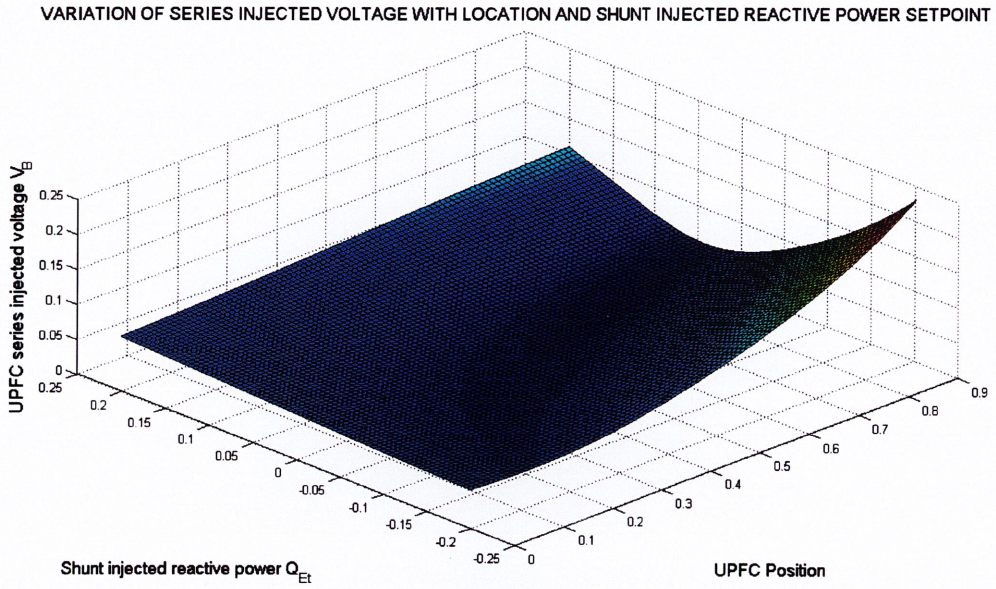


Figure (2.10)
Variation of series injected voltage V_B with reactive power Q_{Et} setpoint and location variation

From the figures (2.10) and (2.11), it can be seen that the variation in the series injected voltage V_B and the shunt injected voltage are V_E are inverted from each other as it is keep the power balance of the UPFC in (2.1). It can be seen that the variation of the series injected voltage V_B is linear as the the variation in setpoint until 20% from the intermediate bus, after which the the variation is nonlinear as it reaches its maximum at 90% of the line as it reaches upto 0.23 p.u at $Q_{Et} = -0.2$ p.u, from this the minimum value of V_E will be at the same point.

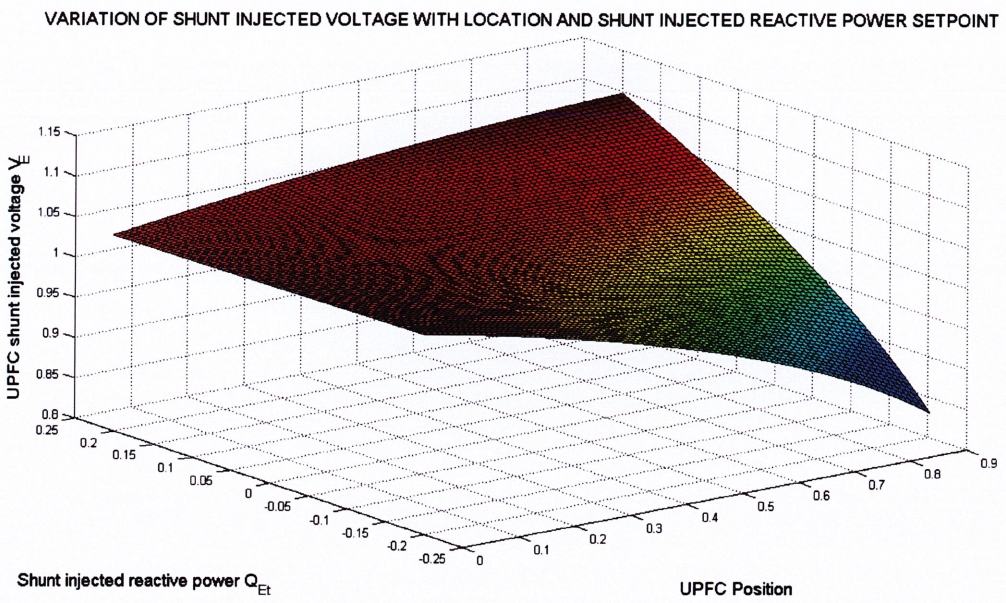


Figure (2.11)
Variation of shunt injected voltage V_E with reactive power Q_{Et} setpoint and location variation

2.3.1.3 Receiving End Voltage V_{Bt}

By varying the setpoint for the regulated receiving end bus voltage V_{Bt} , the variation in the injected voltages of the UPFC is shown in figures (2.12) and (2.13):

As can be seen from the figure (2.12), that the series injected voltage V_B decreases as the voltage setpoint is increased. The behavior of V_B is as described until the UPFC reaches 75% location, where the behavior change to be come nonlinear and it starts to increase until it reaches maximum at 90% at a setpoint of 0.9 p.u. As for the shunt injected voltage V_E , it seems that as the location is getting further from the intermediate bus the behavior changes until it reaches 90% location in the transmission line, the voltage increases as the setpoint is varied. From this it can be seen that the sensitivity of the the shunt injected voltage is affected by the location of installation while changing the UPFC receiving end bus voltage.

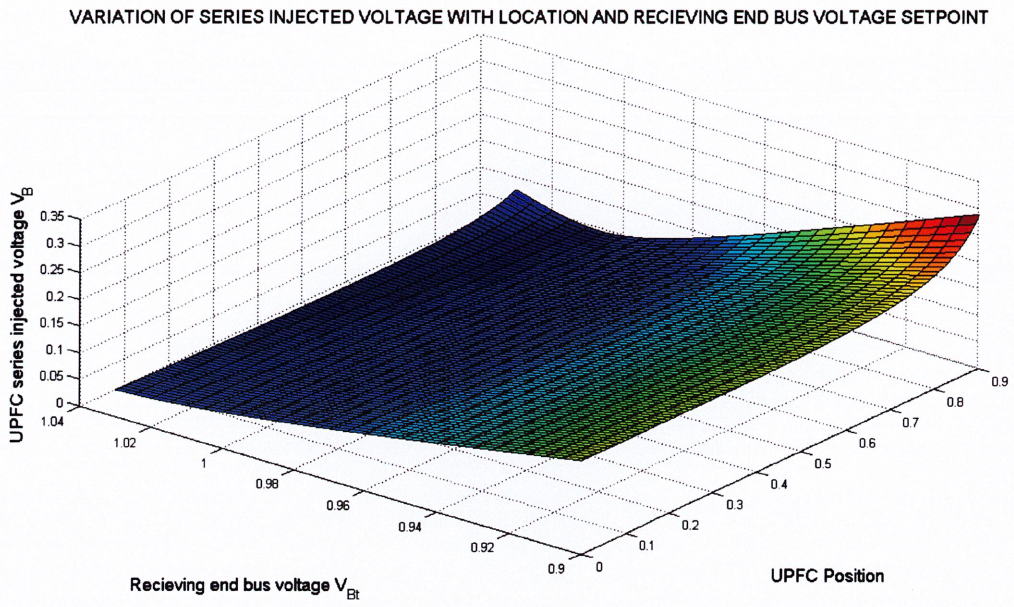


Figure (2.12)
Variation of series injected voltage V_B with receiving end voltage V_{Bt} setpoint and location variation

2.3.2 Case 2: PV - PQ Bus Configuration

In order to test the remaining scenarios and their effect on the UPFC control parameter, the following control scheme is to be considered where the active power and reactive power of the line are controlled as well as regulating the sending end voltage. Since the effect of active power variation with the location of installation was presented before, it will not be considered here and the rest of the cases are considered.

2.3.2.1 Reactive Power Q_{Bt}

In this case the controlled reactive power Q_{Bt} setpoint is varied in order to investigate the impact of the injected voltage, and by varying the location of installation of the UPFC it is going to be shown how does it affect the control parameters.By varying the reactive power from 0 p.u up to 0.2 p.u, the obtained results are shown in figures (2.14) and (2.15).

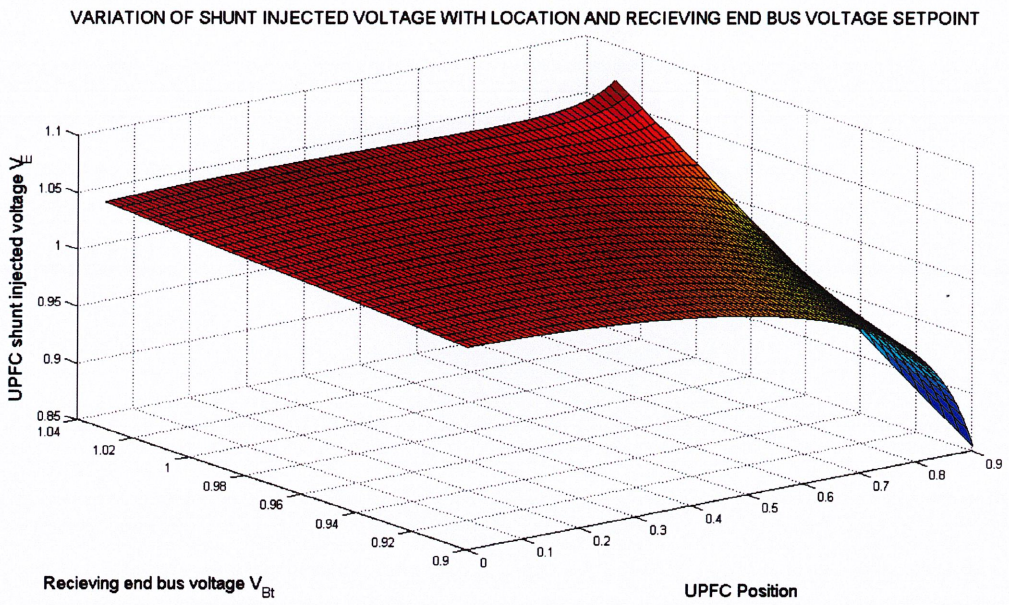


Figure (2.13)
Variation of shunt injected voltage V_E with receiving end voltage V_{Bt} setpoint and location variation

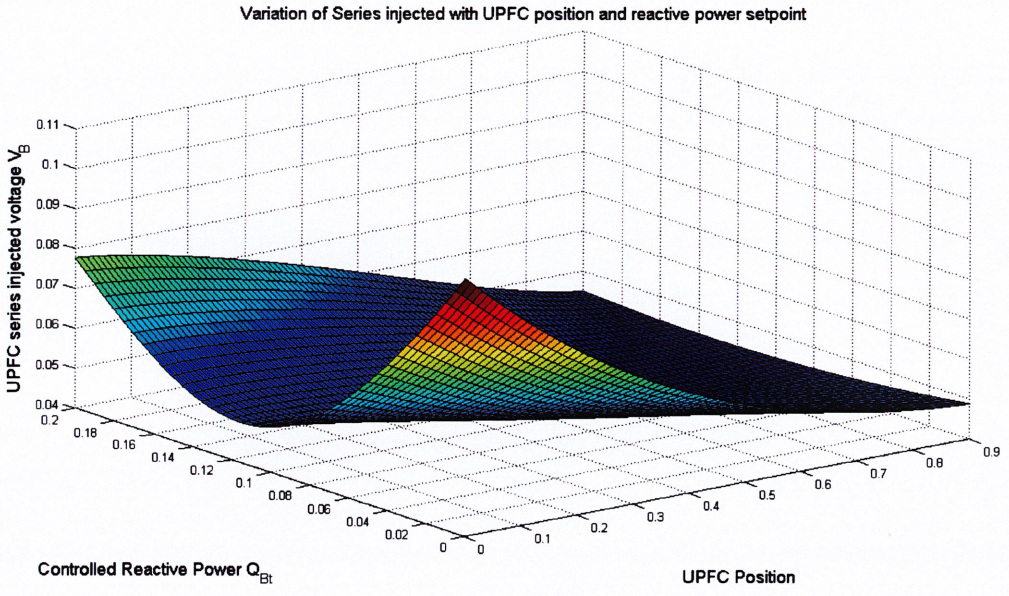


Figure (2.14)
Variation of series injected voltage V_B with reactive power Q_{Bt} setpoint and location variation

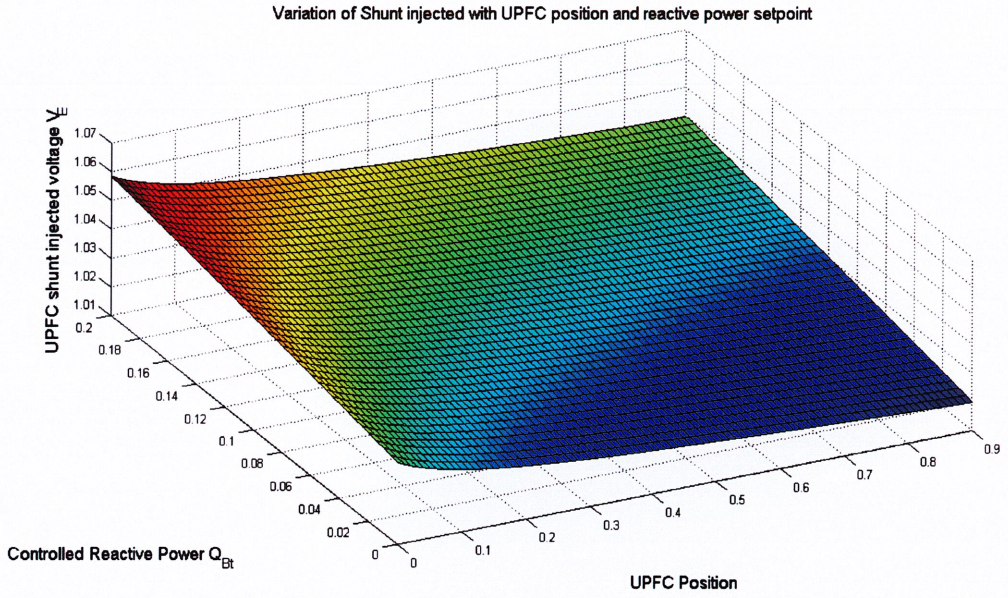


Figure (2.15)
Variation of shunt injected voltage V_E with reactive power Q_{Bt} setpoint and location variation

From figure (2.14), it can be seen that the series injected voltage V_B sensitivity to the variation in reactive power Q_{Bt} decreases as the location of the installation of the UPFC is getting further near to the infinite bus. As the distance increases the variation in V_B becomes less, at $x = 0$ the injected voltage value swings between 0.1 p.u and 0.05 p.u, and the variation can be seen as a nonlinear relation. But, at $x = 0.9$ it can be seen that the variation is small as it changes between 0.048 p.u and 0.045 p.u. As for the shunt injected voltage V_E , the variation is linear with the setpoint variation. The variation with the location of the UPFC did not affect the behavior of the V_E with the variation in Q_{Bt}.

2.3.2.2 Sending End Voltage V_{Et}

Through the variation of V_{Et} setpoint, which is the UPFC sending end bus voltage, with the location of installation, the behaviors of the concerned

control parameters are shown in figures (2.16) and (2.17).

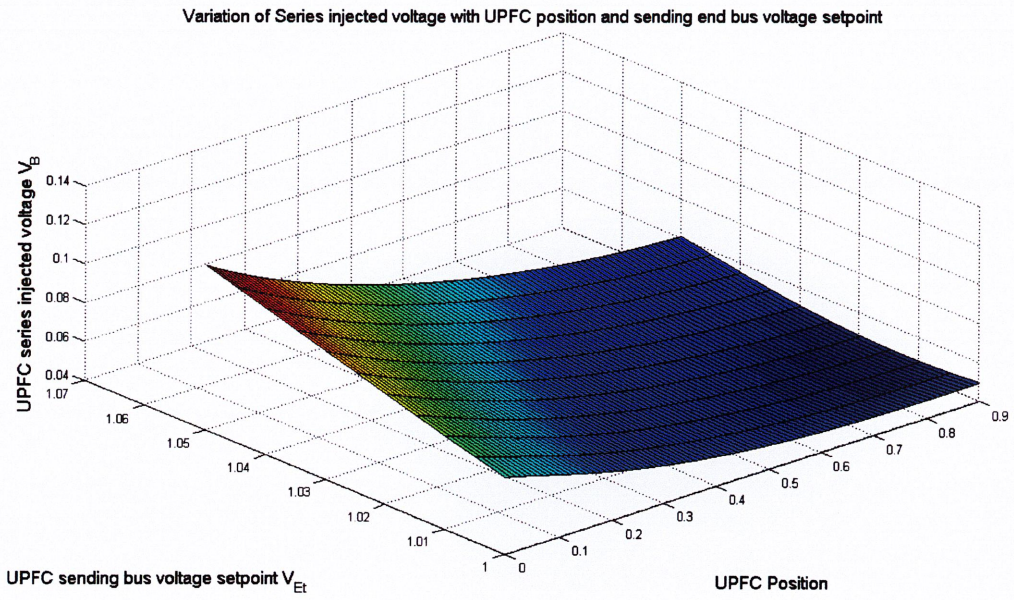


Figure (2.16)
Variation of series injected voltage V_B with sending end voltage V_{Et} setpoint and location variation

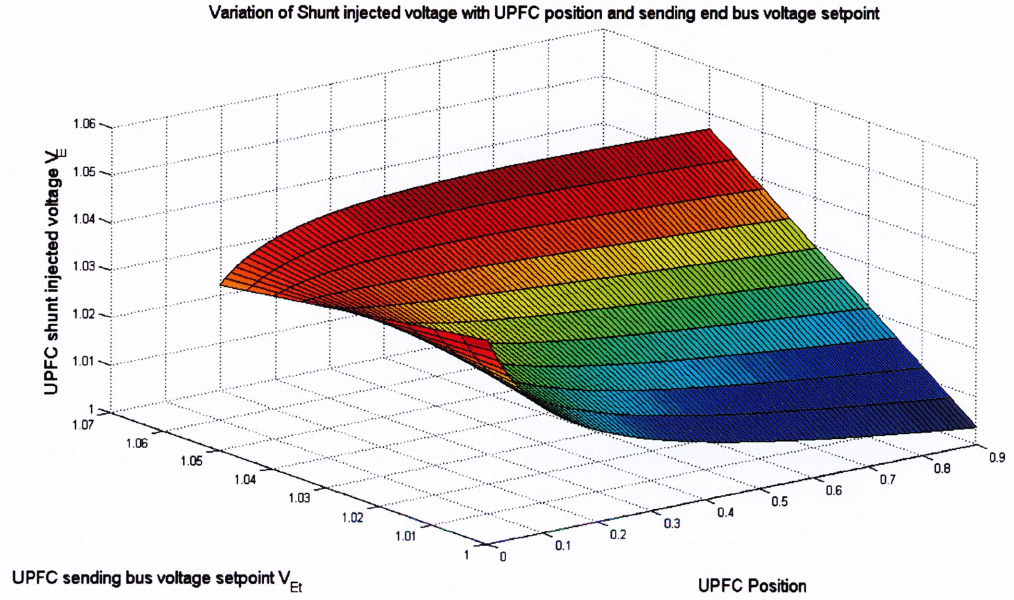


Figure (2.17)
Variation of shunt injected voltage V_E with sending end voltage V_{Et} setpoint and location variation

The series injected voltage V_B sensitivity decreases as the location of installation gets further from the intermediate bus, and that is the reverse in the shunt injected voltage V_E as it becomes more sensitive to the variation of location. The sensitivity of V_B is less compared to V_E , as the variation of V_B with the location can be seen from the slope $\frac{dV_B}{dV_{Et}}$ that did not much vary.

The decoupled model for the UPFC has been upgraded for different control schemes that can be modified for simultaneous control or single control with the manipulation of the setpoints for the injected powers in the bus equivalent model of the device. To measure the sensitivity of the UPFC control parameters, namely the injected voltages of the UPFC, varying the setpoint of the controlled parameters individually, one at a time, with the variation of the location where the UPFC is installed. It was shown that regardless of the controlled variable the variation of the injected voltages is the inverse of each other and that is to keep the active power exchange between the UPFC and the system at zero. Also, the control scheme has an impact on the sensitivity of the control parameters of the UPFC. The sensitivity of the injected voltage depends on the controlled variable and the location, and it was found that as the distance increases from the system intermediate bus the sensitivity increases except in case of line reactive power control. From this it can be seen that the effect of position on the controlled parameters of the UPFC is significantly affected by the location of installation. However, this will only be significant if the limits of UPFC injected voltages is considered and that by considering the ratings of the UPFC series and shunt converters, and thus it can be seen that installation location could be a factor in limiting the range of controllability of the UPFC for active and reactive power compensation.

2.4 Unified Power Flow Controller Dynamic Modeling

Several references in literature have addressed the topic of the UPFC dynamic modeling. In Smith et al. (1997), a dynamic model for the UPFC was introduced for transient and small signal stability analysis. The problem with the proposed modeling approach was that it did not consider the DC link dynamics which could lead to implications during transients. In Son & Lasseter (2004), a Newton type current injection model is used for transient stability studies. The model consists of a controllable voltage source added in series with the transmission line, plus two current sources added in shunt to balance power flow through the device. As the model has considered the power balance constraint for the UPFC, it has neglected the dynamics of the DC link also. Thus, this model may not be suitable for dynamic analysis.

This section presents two dynamic models that have been proposed in K. R. Padiyar & Kulkarni (1998) and Nabavi-Niaki & Iravani (1996). It discusses the control strategies that were proposed for these two models in literature. It highlights the major advantages and disadvantages of the two models and their respective control strategies.

2.4.1 Fundamental Frequency Based Dynamic Modeling

In K. R. Padiyar & Kulkarni (1998), a detailed dynamic model for the UPFC was introduced. Figure (2.18) shows a schematic diagram of the UPFC placed in a two bus system with the current flow orientation in the AC and DC sides. In this modeling approach the dynamics associated with the series converter, shunt converter, and the UPFC dc link capacitor are considered.

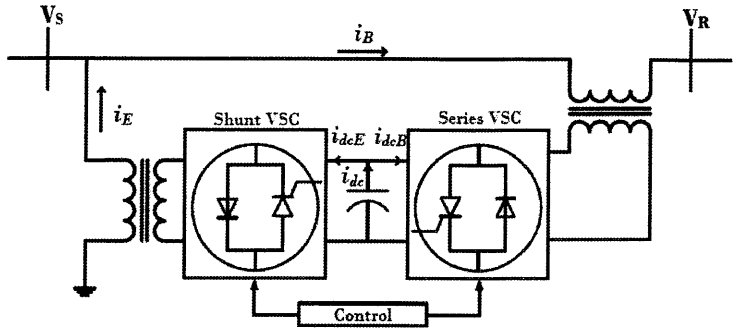


Figure (2.18)
UPFC with associated DC and AC currents

let $\mathbf{V_S}$ be the sending end bus voltage and $\mathbf{V_r}$ be the receiving end bus voltage. $\mathbf{I_B}$ is the transmission line current passing through the boosting transformer while $\mathbf{I_E}$ is the shunt converter current passing through the excitation transformer. $\mathbf{V_B}$ is the series injected voltage and $\mathbf{V_E}$ is the shunt injected voltage. The currents at the DC side of the UPFC are given as: i_{dc}, the supplied current from the DC link capacitor, i_{dcE}, the DC shunt converter current, and i_{dcB} is the DC series converter current.

By replacing the VSCs of the UPFC with a controllable fundamental frequency voltage sources, a model similar to the steady state model introduced in figure (2.2) is obtained. The difference arise when the model of the coupling transformer is considered to be represented by its resistance and leakage reactance. This can be seen from figure (2.19).

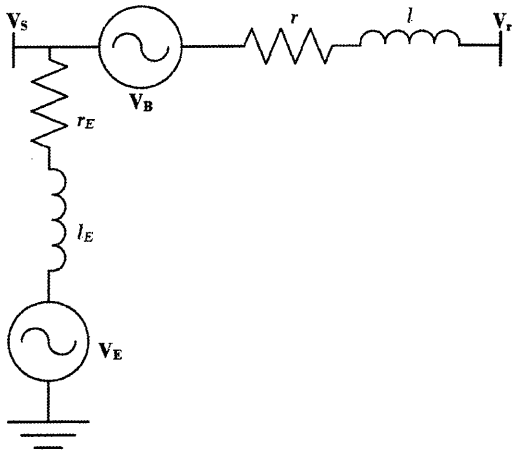


Figure (2.19)
Detailed Fundamental Frequency UPFC Model

From the circuit shown in figure (2.19), the dynamics of the shunt and series converter can be deduced as:

$$\begin{vmatrix} \frac{di_{Ea}}{dt} \\ \frac{di_{Eb}}{dt} \\ \frac{di_{Ec}}{dt} \end{vmatrix} = \begin{vmatrix} -\frac{r_E}{l_E} & 0 & 0 \\ 0 & -\frac{r_E}{l_E} & 0 \\ 0 & 0 & -\frac{r_E}{l_E} \end{vmatrix} \begin{vmatrix} i_{Ea} \\ i_{Eb} \\ i_{Ec} \end{vmatrix} + \begin{vmatrix} \frac{1}{l_E} & 0 & 0 \\ 0 & \frac{1}{l_E} & 0 \\ 0 & 0 & \frac{1}{l_E} \end{vmatrix} \begin{vmatrix} v_{Ea} - v_{sa} \\ v_{Eb} - v_{sb} \\ v_{Ec} - v_{sc} \end{vmatrix} \tag{2.8}$$

$$\begin{vmatrix} \frac{di_{Ba}}{dt} \\ \frac{di_{Bb}}{dt} \\ \frac{di_{Bc}}{dt} \end{vmatrix} = \begin{vmatrix} -\frac{r}{l} & 0 & 0 \\ 0 & -\frac{r}{l} & 0 \\ 0 & 0 & -\frac{r}{l} \end{vmatrix} \begin{vmatrix} i_{Ba} \\ i_{Bb} \\ i_{Bc} \end{vmatrix} + \begin{vmatrix} \frac{1}{l} & 0 & 0 \\ 0 & \frac{1}{l} & 0 \\ 0 & 0 & \frac{1}{l} \end{vmatrix} \begin{vmatrix} v_{sa} + v_{Ba} - v_{ra} \\ v_{sb} + v_{Bb} - v_{rb} \\ v_{sc} + v_{Bc} - v_{rc} \end{vmatrix} \tag{2.9}$$

where , r and l are the resistance and leakage inductance of the boosting transformer and the transmission line, r_E and l_E are the shunt converters resistance and leakage inductance.

By transforming equations (2.8) and (2.9) to the dq- reference frame, the following two equations are obtained:

$$\begin{vmatrix} \frac{di_{Ed}}{dt} \\ \frac{di_{Eq}}{dt} \\ \frac{di_{E0}}{dt} \end{vmatrix} = \begin{vmatrix} 0 & -\omega_o & 0 \\ \omega_o & 0 & 0 \\ 0 & 0 & 0 \end{vmatrix} \begin{vmatrix} i_{Ed} \\ i_{Eq} \\ i_{E0} \end{vmatrix} + \begin{vmatrix} -\frac{r_E}{l_E} & 0 & 0 \\ 0 & -\frac{r_E}{l_E} & 0 \\ 0 & 0 & -\frac{r_E}{l_E} \end{vmatrix} \begin{vmatrix} i_{Ed} \\ i_{Eq} \\ i_{E0} \end{vmatrix} + \begin{vmatrix} \frac{1}{l_E} & 0 & 0 \\ 0 & \frac{1}{l_E} & 0 \\ 0 & 0 & \frac{1}{l_E} \end{vmatrix} \begin{vmatrix} v_{Ed} - v_{sd} \\ v_{Eq} - v_{sq} \\ v_{E0} - v_{s0} \end{vmatrix} \tag{2.10}$$

$$\begin{vmatrix} \frac{di_{Bd}}{dt} \\ \frac{di_{Bq}}{dt} \\ \frac{di_{B0}}{dt} \end{vmatrix} = \begin{vmatrix} 0 & -\omega_o & 0 \\ \omega_o & 0 & 0 \\ 0 & 0 & 0 \end{vmatrix} \begin{vmatrix} i_{Bd} \\ i_{Bq} \\ i_{B0} \end{vmatrix} + \begin{vmatrix} -\frac{r}{l} & 0 & 0 \\ 0 & -\frac{r}{l} & 0 \\ 0 & 0 & -\frac{r}{l} \end{vmatrix} \begin{vmatrix} i_{Bd} \\ i_{Bq} \\ i_{B0} \end{vmatrix} + \begin{vmatrix} \frac{1}{l} & 0 & 0 \\ 0 & \frac{1}{l} & 0 \\ 0 & 0 & \frac{1}{l} \end{vmatrix} \begin{vmatrix} v_{sd} + v_{Bd} - v_{rd} \\ v_{sq} + v_{Bq} - v_{rq} \\ v_{s0} + v_{B0} - v_{r0} \end{vmatrix} \tag{2.11}$$

In this research the zero axis currents are neglected since only balanced power systems are considered. Thus, results that the dynamic equations of the shunt and series converters can be re-written as:

$$\frac{di_{Ed}}{dt} = -\frac{\omega_B r_E}{x_E} i_{Ed} - \omega_o i_{Eq} + \frac{\omega_B}{x_E} (v_{Ed} - v_{sd}) \tag{2.12}$$

$$\frac{di_{Eq}}{dt} = -\frac{\omega_B r_E}{x_E} i_{Eq} + \omega_o i_{Ed} + \frac{\omega_B}{x_E} (v_{Eq} - v_{sq}) \tag{2.13}$$

$$\frac{di_{Bd}}{dt} = -\frac{\omega_B r}{x} i_{Bd} - \omega_o i_{Bq} + \frac{\omega_B}{x} (v_{sd} + v_{Bd} - v_{rd}) \tag{2.14}$$

$$\frac{di_{Bq}}{dt} = -\frac{\omega_B r}{x} i_{Bq} + \omega_o i_{Bd} + \frac{\omega_B}{x} (v_{sq} + v_{Bq} - v_{rq}) \tag{2.15}$$

where
ω_o: system operating frequency in rad/sec
ω_B : system base frequency in rad/sec

Figures (2.20) and (2.21) show block diagrams representation of the equations above, from which it can be seen the coupling of the system.

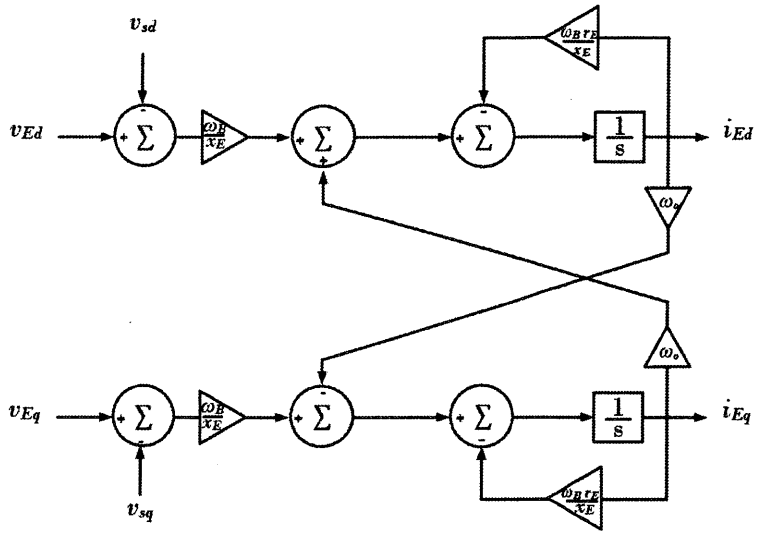


Figure (2.20)
Shunt Converter Block Diagram Representation

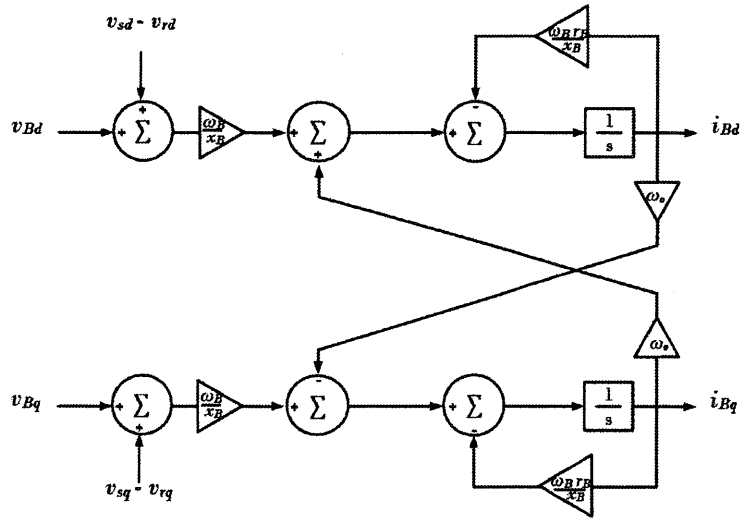


Figure (2.21)
Series Converter Block Diagram Representation

From figure (2.18), by applying Kirchoff Current Law at the dc capacitor node:

$$i_{dc} = i_{dcE} + i_{dcB} \tag{2.16}$$

By considering the three phase active power flow at the AC side of the shunt converter. Transforming the AC quantities to the dq reference frame:

$$P_E = 3Re\left\{(v_{Eq} + j\, v_{Ed})\ (i_{Eq} + j\, i_{Ed})^*\right\} \tag{2.17}$$

$$P_E = \frac{3}{2}\left(v_{Eq}\, i_{Eq} + v_{Ed}\, i_{Ed}\right) \tag{2.18}$$

On the dc side the real power flowing out of the shunt converter is given by:

$$P_{DCE} = v_{dc}\, i_{dcE} \tag{2.19}$$

Since the losses are neglected, the power at both sides of the converter are equal:

$$P_{DCE} = P_E \tag{2.20}$$

$$v_{dc}\, i_{dcE} = \frac{2}{3}\left(v_{Eq}\, i_{Eq} + v_{Ed}\, i_{Ed}\right) \tag{2.21}$$

$$i_{dcE} = \frac{2}{3\, v_{dc}}\left(v_{Eq}\, i_{Eq} + v_{Ed}\, i_{Ed}\right) \tag{2.22}$$

Similarly, the series converter three phase power can be represented as:

$$P_B = 3Re\left\{(v_{Bq} + j\, v_{Bd})\,(i_{Bq} + j\, i_{Bd})^*\right\} \tag{2.23}$$

$$P_B = \frac{3}{2}\left(v_{Bq}\, i_{Bq} + v_{Bd}\, i_{Bd}\right) \tag{2.24}$$

The real power at the dc side of the series converter is:

$$P_{dcB} = v_{dc}\, i_{dcB} \tag{2.25}$$

Since system is lossless:

$$P_{dcB} = P_B \tag{2.26}$$

Thus we get:

$$i_{dcB} = \frac{2}{3v_{dc}} \left(v_{Bq}\, i_{Bq} + v_{Bd}\, i_{Bd} \right) \tag{2.27}$$

The dc link dynamics is given by:

$$\frac{dv_{dc}}{dt} = -\frac{i_{dc}}{C_{dc}} \tag{2.28}$$

$$\frac{dv_{dc}}{dt} = -\omega_B\, x_{dc}\, i_{dc} \tag{2.29}$$

by substituting equations (2.16) ,(2.22)and (2.27) in (2.29) :

$$\frac{dv_{dc}}{dt} = -\frac{2}{3}\frac{\omega_B\, x_{dc}}{v_{dc}} \left(v_{Eq}\, i_{Eq} + v_{Ed}\, i_{Ed} + v_{Bq}\, i_{Bq} + v_{Bd}\, i_{Bd} \right) \tag{2.30}$$

Therefore, equations (2.12) to (2.15) and equation (2.30) are the dynamics representation of the UPFC is a two bus system that is shown in figure (2.19).

2.4.1.1 Control Strategy

Based on the model presented earlier a control strategy for power flow control, bus voltage regulation, and DC voltage regulation is discussed here. The control strategy is intended to control both active power, reactive power, bus voltage and dc link voltage. The control strategies used were proposed in K. R. Padiyar & Kulkarni (1998), Yam & Haque (2004) and shown in figure(2.22).

For power flow control, consider the complex power injection into the

receiving bus:

$$\mathbf{S_r} = P_r + \jmath Q_r \tag{2.31}$$

The active and reactive received powers in dq - reference frame are found as:

$$P_r = v_{rq} i_{Bq} + v_{rd} i_{Bd} \tag{2.32}$$

$$Q_r = v_{rd} i_{Bq} - v_{rq} i_{Bd} \tag{2.33}$$

The power injection setpoint can be translated into current setpoints of the series converter as follows:

$$i^*_{Bq} = \frac{P^*_r\, v_{rq} + Q^*_r\, v_{rd}}{\triangle} \tag{2.34}$$

$$i^*_{Bd} = \frac{P^*_r\, v_{rd} - Q^*_r\, v_{rq}}{\triangle} \tag{2.35}$$

where:

P^*_r: desired active power setpoint

Q^*_r: desired reactive power setpoint

$\triangle = v^2_{rq} + v^2_{rd}$

Similarly, for the bus voltage and dc link voltage regulation consider the complex power injection by the shunt converter:

$$\mathbf{S_E} = \mathbf{V_s}\, \mathbf{I^*_E} \tag{2.36}$$

Decomposing the voltage and current into the DQ components, this gives:

$$\begin{aligned}\mathbf{S_E} &= (v_{sq} + j\, v_{sd})\,(i_{Eq} - j\, i_{Ed}) \\ &= (V_s\, \cos\theta_s\, i_{Eq} + V_s\, \sin\theta_s\, i_{Ed}) + j\,(V_s\, \sin\theta_s\, i_{Eq} - V_s\, \cos\theta_s\, i_{Ed}) \\ &= V_s\,[(i_{Eq}\, \cos\theta_s + i_{Ed}\, \sin\theta_s) - j\,(i_{Ed}\, \cos\theta_s - i_{Eq}\, \sin\theta_s)] \end{aligned} \quad (2.37)$$

$$\mathbf{S_E} = V_s\,[i_{psh} - j\, i_{rsh}] \quad (2.38)$$

where i_{psh} is the real or active current and i_{rsh} is the reactive or imaginary current, and they are given as:

$$i_{psh} = i_{Ed}\, \cos\theta_s + i_{Eq}\, \sin\theta_s \quad (2.39)$$

$$i_{rsh} = i_{Ed}\, \cos\theta_s - i_{Eq}\, \sin\theta_s \quad (2.40)$$

Through cascade control loop as in K. R. Padiyar & Kulkarni (1998), the real current i_{psh} is regulated by a PI controller by the dc voltage whereas the reactive $i_{rsh}$is regulated by a PI controller by the ac bus voltage. Thus the current setpoints for the shunt converter is obtained as:

$$i^*_{Ed} = i_{psh}\, \sin\theta_s + i_{rsh}\, \cos\theta_s \quad (2.41)$$

$$i^*_{Eq} = i_{psh}\, \cos\theta_s - i_{rsh}\, \sin\theta_s \quad (2.42)$$

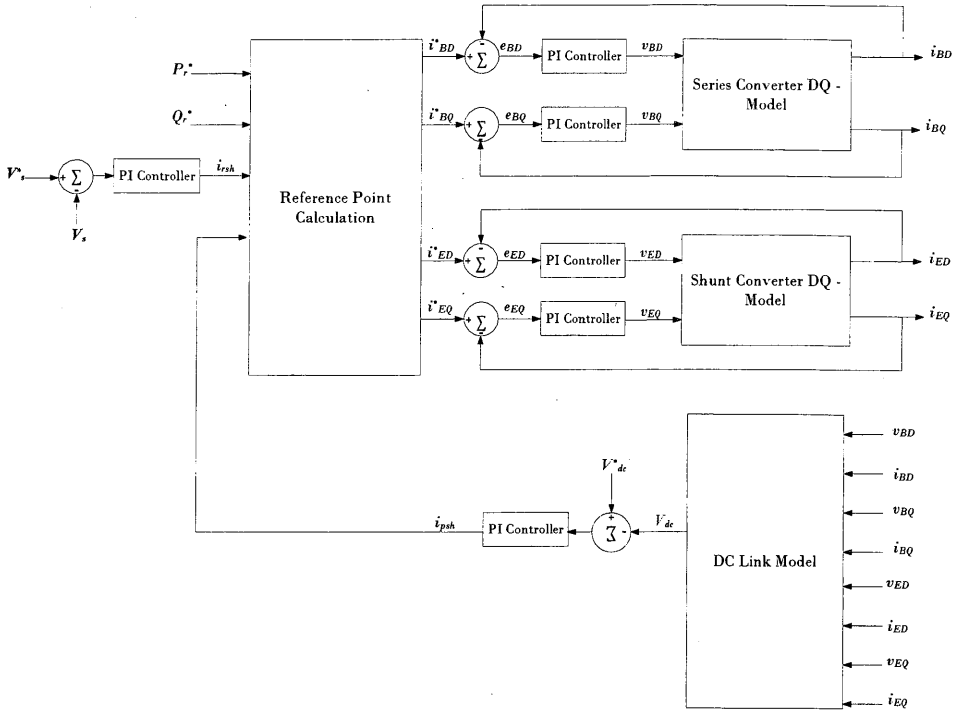


Figure (2.22)
Fundamental frequency based control strategy

2.4.2 Pulse Width Modulation Based Dynamic Modeling

Another modeling approach was introduced by Nabavi - Niaki and Iravani in Nabavi-Niaki & Iravani (1996). This model is based on the three phase circuit illustrated in figure (2.23). Based on the pulse width modulation (PWM) technique used to control the converters, this modeling approach considered the injected voltages to be a pure sine wave signals by neglecting the high order frequency components introduced due to switching. Thus:

$$v_{Eabc} = \frac{m_E\, v_{dc}}{2} \cos\left(\omega t + \delta_E \pm \frac{2\pi}{3}\right) \qquad (2.43)$$

$$v_{Babc} = \frac{m_B\, v_{dc}}{2} \cos\left(\omega t + \delta_B \pm \frac{2\pi}{3}\right) \tag{2.44}$$

m_E and m_B are amplitude modulation ratios, δ_E and $\delta_B$are phase angles of the voltage source converters control signal.

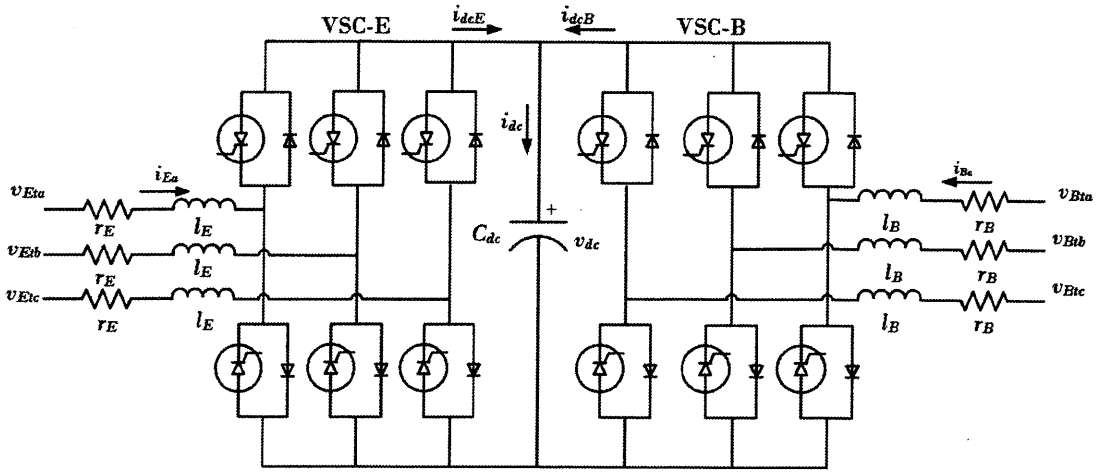


Figure (2.23)
UPFC Three Phase Schematic Diagram

Let (v_{Etabc}) be the three phase AC side terminal voltage of the shunt converter, and (v_{Btabc}) is the three phase AC side terminal voltage of the series converter.

The dynamics of the shunt and series converters can be obtained as:

$$\begin{vmatrix} \frac{di_{Ea}}{dt} \\ \frac{di_{Eb}}{dt} \\ \frac{di_{Ec}}{dt} \end{vmatrix} = \begin{vmatrix} -\frac{r_E}{l_E} & 0 & 0 \\ 0 & -\frac{r_E}{l_E} & 0 \\ 0 & 0 & -\frac{r_E}{l_E} \end{vmatrix} \begin{vmatrix} i_{Ea} \\ i_{Eb} \\ i_{Ec} \end{vmatrix} - \frac{m_E\, v_{dc}}{2l_E} \begin{vmatrix} \cos(\omega t + \delta_E) \\ \cos\left(\omega t + \delta_E + \frac{2\pi}{3}\right) \\ \cos\left(\omega t + \delta_E + \frac{4\pi}{3}\right) \end{vmatrix}$$
$$+ \begin{vmatrix} \frac{1}{l_E} & 0 & 0 \\ 0 & \frac{1}{l_E} & 0 \\ 0 & 0 & \frac{1}{l_E} \end{vmatrix} \begin{vmatrix} v_{Eta} \\ v_{Etb} \\ v_{Etb} \end{vmatrix} \tag{2.45}$$

$$\begin{vmatrix} \frac{di_{Ba}}{dt} \\ \frac{di_{Bb}}{dt} \\ \frac{di_{Bc}}{dt} \end{vmatrix} = \begin{vmatrix} -\frac{r_B}{l_B} & 0 & 0 \\ 0 & -\frac{r_B}{l_B} & 0 \\ 0 & 0 & -\frac{r_B}{l_B} \end{vmatrix} \begin{vmatrix} i_{Ba} \\ i_{Bb} \\ i_{Bc} \end{vmatrix} - \frac{m_B\, v_{dc}}{2l_B} \begin{vmatrix} \cos(\omega t + \delta_B) \\ \cos\left(\omega t + \delta_B + \frac{2\pi}{3}\right) \\ \cos\left(\omega t + \delta_B + \frac{4\pi}{3}\right) \end{vmatrix} + \begin{vmatrix} \frac{1}{l_B} & 0 & 0 \\ 0 & \frac{1}{l_B} & 0 \\ 0 & 0 & \frac{1}{l_B} \end{vmatrix} \begin{vmatrix} v_{Bta} \\ v_{Btb} \\ v_{Btb} \end{vmatrix} \quad (2.46)$$

The DC link dynamics can be obtained in a manner similar to what have been illustrated in the previous model as:

$$\frac{dv_{dc}}{dt} = \frac{m_E}{2C_{dc}} \begin{vmatrix} \cos(\omega t + \delta_E) & \cos\left(\omega t + \delta_E + \frac{2\pi}{3}\right) & \cos\left(\omega t + \delta_E + \frac{4\pi}{3}\right) \end{vmatrix} \begin{vmatrix} i_{Ea} \\ i_{Eb} \\ i_{Ec} \end{vmatrix} + \frac{m_B}{2C_{dc}} \begin{vmatrix} \cos(\omega t + \delta_B) & \cos\left(\omega t + \delta_B + \frac{2\pi}{3}\right) & \cos\left(\omega t + \delta_B + \frac{4\pi}{3}\right) \end{vmatrix} \begin{vmatrix} i_{Ba} \\ i_{Bb} \\ i_{Bc} \end{vmatrix} \quad (2.47)$$

Applying Park's transformation for the above equations:

$$\begin{vmatrix} \frac{di_{Ed}}{dt} \\ \frac{di_{Eq}}{dt} \\ \frac{di_{E0}}{dt} \end{vmatrix} = \begin{vmatrix} 0 & -\omega_o & 0 \\ \omega_o & 0 & 0 \\ 0 & 0 & 0 \end{vmatrix} \begin{vmatrix} i_{Ed} \\ i_{Eq} \\ i_{E0} \end{vmatrix} + \begin{vmatrix} -\frac{r_E}{l_E} & 0 & 0 \\ 0 & -\frac{r_E}{l_E} & 0 \\ 0 & 0 & -\frac{r_E}{l_E} \end{vmatrix} \begin{vmatrix} i_{Ed} \\ i_{Eq} \\ i_{E0} \end{vmatrix} - \frac{m_E v_{dc}}{2l_E} \begin{vmatrix} \cos\delta_E \\ \sin\delta_E \\ 0 \end{vmatrix} + \begin{vmatrix} \frac{1}{l_E} & 0 & 0 \\ 0 & \frac{1}{l_E} & 0 \\ 0 & 0 & \frac{1}{l_E} \end{vmatrix} \begin{vmatrix} v_{Etd} \\ v_{Etq} \\ v_{Et0} \end{vmatrix} \quad (2.48)$$

$$\begin{vmatrix} \frac{di_{Bd}}{dt} \\ \frac{di_{Bq}}{dt} \\ \frac{di_{B0}}{dt} \end{vmatrix} = \begin{vmatrix} 0 & -\omega_o & 0 \\ \omega_o & 0 & 0 \\ 0 & 0 & 0 \end{vmatrix} \begin{vmatrix} i_{Bd} \\ i_{Bq} \\ i_{B0} \end{vmatrix} + \begin{vmatrix} -\frac{r_B}{l_B} & 0 & 0 \\ 0 & -\frac{r_B}{l_B} & 0 \\ 0 & 0 & -\frac{r_B}{l_B} \end{vmatrix} \begin{vmatrix} i_{Bd} \\ i_{Bq} \\ i_{B0} \end{vmatrix} - \frac{m_B v_{dc}}{2l_B} \begin{vmatrix} \cos\delta_B \\ \sin\delta_B \\ 0 \end{vmatrix} + \begin{vmatrix} \frac{1}{l_B} & 0 & 0 \\ 0 & \frac{1}{l_B} & 0 \\ 0 & 0 & \frac{1}{l_B} \end{vmatrix} \begin{vmatrix} v_{Btd} \\ v_{Btq} \\ v_{Bt0} \end{vmatrix} \tag{2.49}$$

$$\frac{dv_{dc}}{dt} = \frac{3m_E}{4C_{dc}} \begin{vmatrix} \cos\delta_E & \sin\delta_E & 0 \end{vmatrix} \begin{vmatrix} i_{Ed} \\ i_{Eq} \\ i_{E0} \end{vmatrix} + \frac{3m_B}{4C_{dc}} \begin{vmatrix} \cos\delta_B & \sin\delta_B & 0 \end{vmatrix} \begin{vmatrix} i_{Bd} \\ i_{Bq} \\ i_{B0} \end{vmatrix} \tag{2.50}$$

By neglecting the transformer transients and resistances in the above equations. Moreover, as only balanced operation is considered the zero axis currents are omitted from the equations. This leads to:

$$\begin{vmatrix} v_{Etd} \\ v_{Etq} \end{vmatrix} = \begin{vmatrix} 0 & x_E \\ -x_E & 0 \end{vmatrix} \begin{vmatrix} i_{Ed} \\ i_{Eq} \end{vmatrix} + \frac{m_E v_{dc}}{2} \begin{vmatrix} \cos\delta_E \\ \sin\delta_E \end{vmatrix} \tag{2.51}$$

$$\begin{vmatrix} v_{Btd} \\ v_{Btq} \end{vmatrix} = \begin{vmatrix} 0 & x_B \\ -x_B & 0 \end{vmatrix} \begin{vmatrix} i_{Bd} \\ i_{Bq} \end{vmatrix} + \frac{m_B v_{dc}}{2} \begin{vmatrix} \cos\delta_B \\ \sin\delta_B \end{vmatrix} \tag{2.52}$$

$$\frac{dv_{dc}}{dt} = \frac{3m_E}{4C_{dc}} \begin{vmatrix} \cos\delta_E & \sin\delta_E \end{vmatrix} \begin{vmatrix} i_{Ed} \\ i_{Eq} \end{vmatrix} + \frac{3m_B}{4C_{dc}} \begin{vmatrix} \cos\delta_B & \sin\delta_B \end{vmatrix} \begin{vmatrix} i_{Bd} \\ i_{Bq} \end{vmatrix} \tag{2.53}$$

Hence the UPFC dynamic model is represented only with dynamics of the DC link as given in equation (2.53).

2.4.2.1 Control Strategy

Based on this modeling approach, the control signals for the UPFC are explicitly shown as the modulation indexes and the phase angles of the injected voltages. Therefore a direct control of these variables by the outputs of the system can be done. A multiple PI controllers are used in this control strategy for active power, reactive power, bus voltage, and dc link voltage control. The selection of the output control signals for the UPFC system shown in figure (2.24) are: $U_P = \delta_B$, $U_Q = m_B$, $U_{AC} = m_E$, and $U_{DC} = \delta_E$.

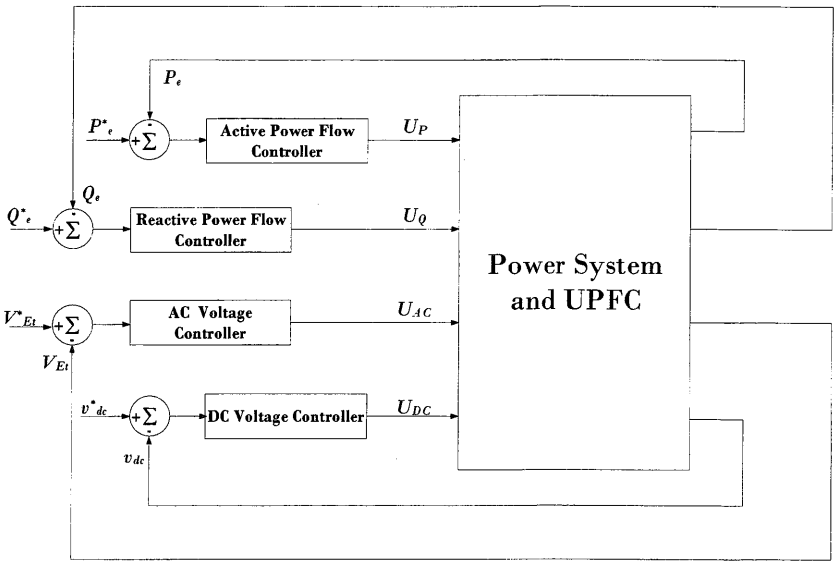


Figure (2.24)
PWM based control strategy

Comparing the two UPFC models and their respective proposed control strategies, it can be seen that the first modeling approach has three major shortcomings when compared with the second approach. First, that this

model is a detailed model that considers the transmission line dynamics. Hence, if it is to be used for a multi-bus multi-UPFC system, it is not an appropriate choice due to the number of differential equations that are to be considered in the simulation (Generators, transmission lines, and UPFCs). Secondly, is that the real control signals are implicit unlike the second model. Therefore there is a need to convert these signals to the UPFC inputs signals (modulation index and firing angles). Finally, the number of the controllers required to be tuned not to mention that it has a cascade control loop making it more difficult to tune. Due to these reasons, the second model with its control strategy is adopted in this research. The next section presents the power system dynamics study system with PWM based UPFC dynamic model incorporated that will be used throughout this research. And by using the decoupled load flow model of the UPFC the system initial conditions for the dynamic study can be obtained.

2.5 Study System

Considering the SMIB test system shown in figure (2.25) with the proposed UPFC model this leads to the system to become as shown in figure (2.25):

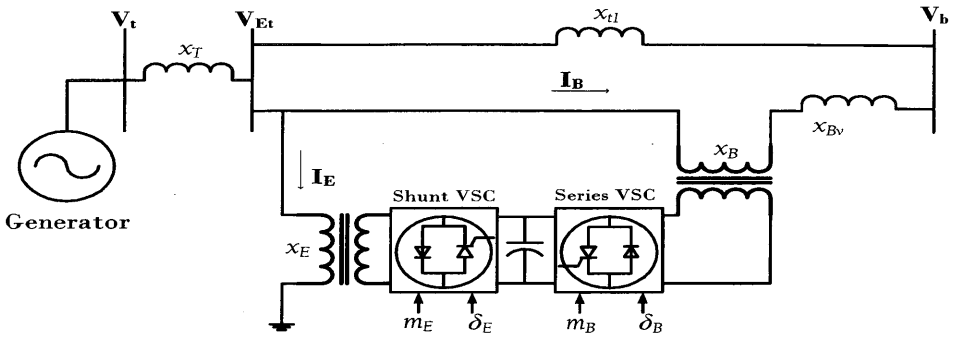


Figure (2.25)
SMIB system equipped with UPFC

The nonlinear model of the SMIB system shown in figure (2.25) is given as:

$$\frac{d\delta}{dt} = \omega_B \, \omega_r \tag{2.54}$$

$$\frac{d\omega_r}{dt} = \frac{1}{M} \left(-D \, \omega_r + P_m - P_e \right) \tag{2.55}$$

$$\frac{dE'_q}{dt} = \frac{1}{T'_{do}} \left(-E'_q + E_{fd} - \left(x_d - x'_d \right) i_d \right) \tag{2.56}$$

$$\frac{dE_{fd}}{dt} = \frac{1}{T_A} \left(-E_{fd} + K_A \left(V_{ref} - V_t \right) \right) \tag{2.57}$$

where:

$$P_e = v_d \, i_d + v_q \, i_q \tag{2.58}$$

$$V_t = \sqrt{v_q^2 + v_d^2} \tag{2.59}$$

$$v_q = E'_q - x'_d \, i_d \tag{2.60}$$

$$v_d = x_q \, i_q \tag{2.61}$$

Equations (2.54) to (2.57) illustrates a 1.0 model of a synchronous generator with IEEE ST1A excitation system. Such a model have been widely adopted for dynamic studies of power system and has been used in M. Abido (2005); M. A. Abido et al. (2006); M. Abido (2009); Al-Awami et al. (n.d.), where equations (2.58) to (2.61) are the algebraic equations of the model. P_m and P_e are the input mechanical power output electric power of the generator respectively; M is the generator moment of inertia; D is the inertia constant of the generator, $\omega_B$is the base synchronous speed, δ and ω_r are the generator rotor angel and generator relative angular speed respectively; E'_q,E_{fd} and V_t are the internal generator voltage, generator field voltage,

and generator terminal voltage respectively. T'_{do} is the open circuit field time constant of the generator, T_A and K_A are the time constant and gain of the excitation system respectively, and V_{ref} is the generator reference voltage. The system data of this study system along with the UPFC is given in appendix A.

In order to simulate the following system, the network currents are to be expressed in terms of the system state and input variables (refer to appendix B.1). The currents are found as:

$$i_{Ed} = \frac{x_{Bt}}{x_{d\Sigma}} E'_q - \frac{x_{d1}}{x_{d\Sigma}} \frac{m_E v_{dc}}{2} \sin\delta_E + \frac{x_{d2}}{x_{d\Sigma}} \frac{m_B v_{dc}}{2} \sin\delta_B + \frac{x_{d3}}{x_{d\Sigma}} V_b \cos\delta \quad (2.62)$$

$$i_{Eq} = \frac{x_{q1}}{x_{q\Sigma}} \frac{m_E v_{dc}}{2} \cos\delta_E - \frac{x_{q2}}{x_{q\Sigma}} \frac{m_B v_{dc}}{2} \cos\delta_B - \frac{x_{q3}}{x_{q\Sigma}} V_b \sin\delta \quad (2.63)$$

$$i_{Bd} = \frac{x_{Et}}{x_{d\Sigma}} E'_q + \frac{x_{d2}}{x_{d\Sigma}} \frac{m_E v_{dc}}{2} \sin\delta_E - \frac{x_{d4}}{x_{d\Sigma}} \frac{m_B v_{dc}}{2} \sin\delta_B - \frac{x_{d5}}{x_{d\Sigma}} V_b \cos\delta \quad (2.64)$$

$$i_{Bq} = \frac{x_{q2}}{x_{q\Sigma}} \frac{m_E v_{dc}}{2} \cos\delta_E - \frac{x_{q4}}{x_{q\Sigma}} \frac{m_B v_{dc}}{2} \cos\delta_B - \frac{x_{q5}}{x_{q\Sigma}} V_b \sin\delta \quad (2.65)$$

$$i_d = \frac{x_{c1}}{x_{d\Sigma}} E'_q - \frac{x_{Bt}}{x_{d\Sigma}} \frac{m_E v_{dc}}{2} \sin\delta_E + \frac{x_{Et}}{x_{d\Sigma}} \frac{m_B v_{dc}}{2} \sin\delta_B - \frac{x_{c2}}{x_{d\Sigma}} V_b \cos\delta \quad (2.66)$$

$$i_q = \frac{x_{Bt}}{x_{q\Sigma}} \frac{m_E v_{dc}}{2} \cos\delta_E - \frac{x_{Et}}{x_{q\Sigma}} \frac{m_B v_{dc}}{2} \cos\delta_B + \frac{x_{c2}}{x_{q\Sigma}} V_b \sin\delta \quad (2.67)$$

By this a full descriptive model is obtained for the SMIB system in

shown figure (2.25).

2.6 Summary

1. Different load flow models for UPFC have been proposed in literature, such as the power injection model, the comprehensive load flow model, and the decoupled load flow model. Between these models the decoupled model has been widely adopted due to the simplicity of use and implementation.

2. The decoupled load flow model for UPFC can be modified from the original bus convention to different bus conventions in order to achieve different control schemes.

3. Investigating the impact of installation location on the UPFC control parameters (V_E and V_B) resulted in the following:

   (a) By varying the setpoint of the active power flow through the transmission line with varying the installation location, it was observed that the controlled and injected voltages (V_E and V_B) were more sensitive to the variation of the setpoint of active power flow than the installation location, and that is due to that the system considered for the study was a lossless system.

   (b) Through the variation of the setpoint of the reactive power flow, it was seen that for the series injected voltage V_B the sensitivity is highest for the variation in setpoint rather than for the location, but as the location increases it becomes less sensitive to the setpoint variation as the location increases. As for the shunt controlled voltage V_E, the sensitivity of location is almost negligible.

   (c) Varying the setpoint of the UPFC receiving end bus voltage V_{Bt} while also varying the installation location, have shown that the series injected voltage V_B has almost consistent behavior until it reaches 90% of the line, where the behavior is becoming nonlinear. As for the shunt controlled voltage V_E, it is almost constant through the line until it reaches around 75% from the infinite bus

the sensitivity of the parameter increases and it becomes more sensitive to setpoint variation.

(d) As for the variation of reactive power injection Q_{Et} versus the location variation, it can be seen that the sensitivity of the series injected voltage V_B is linear, but as the UPFC progresses to travel through the line the voltage becomes more nonlinear nonlinear dependent to setpoint. As for the shunt controlled voltage V_E it becomes more sensitive to the setpoint variation as the locations of the UPFC comes nearest to the infinite bus.

(e) While for the variation of the UPFC sending end bus voltage V_{Et} setpoint with the location, it was seen that the series injected voltage V_B becomes less sensitive to setpoint variation as it progresses through its travel througout the line. Where for the shunt controlled voltage V_E the sensitivity increases for the setpoint as the location varies.

4. From this the UPFC control parameters are more sensitive to the setpoint variation more than the location variation if compared.

5. Several UPFC dynamic models have been introduced in literature, two have been considered in this research.

6. Comparing the two dynamic models it was found that the PWM based UPFC model is more suitable for the use of multimachine system, as the model based control strategy is less complicated compared with the fundamental frequency UPFC model.

7. Introduced the study system to be used in this research where the PWM UPFC model is incorporated within that system, where the UPFC decoupled load flow model is used to initialized the parameters for the dynamic studies to be considered in later chapters.

Chapter 3

Evolutionary Optimization Based Controller

- 3.1 Overview
- 3.2 Biogeography Based Optimization
- 3.3 Particle Swarm Optimization
- 3.4 Introduction to FACTS based Power System Stabilizers
- 3.5 UPFC Based Damping Controller
- 3.6 Controller Design
- 3.7 Simulation Result

Chapter 3
Evolutionary Optimization Based Controller

3.1 Overview

In the past few decades the subject of evolutionary algorithm (EA) attracted an increasing attention due to its ease of implementation and wide adaptation. As per published work, evolutionary algorithms have been applied in various fields not to mention power systems only. Making it an interesting field of research. This chapter will present two evolutionary algorithms: Biogeography Based Optimization (BBO) algorithm and Particle Swarm Optimization(PSO) algorithm. These two algorithms are then used to design a Power Oscillation Damping (POD) controller for the system discussed in chapter 2. The chapter is divided into four main sections: the first and second sections introduce the evolutionary algorithms stated earlier. The third section introduces FACTS based POD controllers and their structure. For the design of the POD controllers, the fourth section discusses different objective functions used to find the optimal set of parameters for the POD controller.

3.2 Biogeography Based Optimization

3.2.1 Biogeography

Biogeography is the science concerned with the study of geographical distribution of species over time and space, their extinction, diversity, and the causes leading to these distribution patterns. The early studies of biogeography are dated back to the 19th century by Alfred Wallace Wallace (2011) and Charles DarwinDarwin & Bynum (2009). Most of the work in biogeography was descriptive and historical, except for the work of Eugene Munroe's in 1948 where he presented a quantitative study for biogeographyMonroe

(1948). This continued until the 1960s, where Robert MacArthur and Edward Wilson presented a mathematical model for biogeography in their book The *Theory of Island Biogeography.* The mathematical model of biogeography describes speciation (evolution of new species), the migration of species between neighboring islands, and the extinction of species.

Simon in Simon (2013), stated that the term island in biogeography is descriptive rather than literal. In biogeography, an island is a habitat that is geographically isolated from other habitats. Where in a classical sense, an island is isolated from other habitats by water. From this an island can be an isolated areas by deserts, rivers, mountain ranges, predators, man made artifacts, or any other type of obstacles.

Habitat suitability index (HSI), is a measure of suitability of a habitat to support species. For this a geographical areas that are friendly to life are said to have high HSI. Features that correlate with HSI include rainfall, vegetative diversity, topographic diversity, land area and temperature. These variables that characterize the habitability of an island are termed as suitability index variables(SIV). Hence the SIV is an independent variable while HSI is a dependent variable.

Islands with high HSI tend to support large number of species, while low HSI islands can only support few number of species. In high HSI islands will have high emigrations of species, not that because they want to but due to the accumulation of random effects on large number of species with large population. Emigration occurs when species ride flotsam, swim, fly or ride wind to neighboring islands. With the emigration, the species will not vanish from the island only a few representatives will leave the island. Based on Simon assumption in Simon (2013), that when an emigration occurs this results in the extinction of the specie from the island which is necessary in the development of the BBO. High HSI islands not only have high emigration rates, but also have low immigration rates due to that the number of species on such islands is large. Hence, the new species that arrive to the

islands will have low probability of survival due to the competitive nature on the resources in the island.

Islands having low HSI have high immigration rates due to the low populations, this occurs by the virtue that these islands have a lot of geographical area for additional species. It has been found that species diversity correlates with HSI, so the more species arrive to the low HSI islands the chance will increase for them to become a high HSI habitats.

MacArthur and Wilson MacArthur (1967), has illustrated the model of species abundance on a single island as shown in figure (3.1). Immigration rate λ and emigration rates are functions of the number of species in the island.

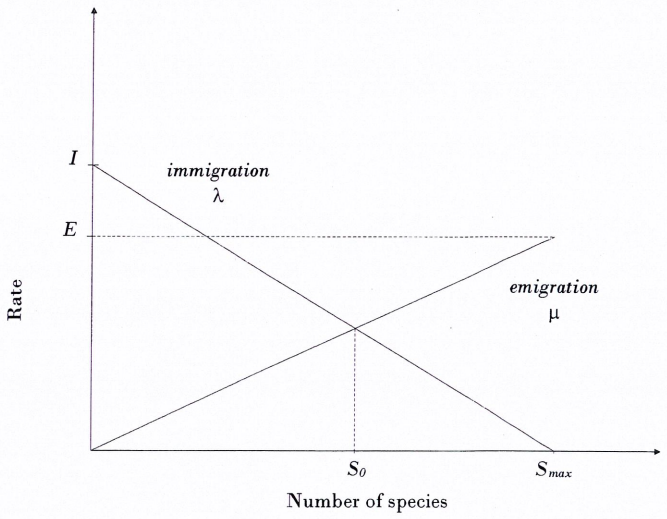


Figure (3.1)
Species migration model of an island, based on [MacArthur and Wilson,1967MacArthur (1967)]

Based on the model in figure (3.1), as initially the island is uninhabited (zero species) the immigration rate will be at its maximum I. Hence, as more species immigrate to the island, it becomes more crowded and by this the immigration rate decreases. This continues until the maximum number of species S_{max} that the island can support is reached. As the immigration rate decreases as new species inhabit the island, the emigration rate will

increase. The emigration rate will be zero initially as there are no species in the island. As the number of species increase the emigration rate will increase reaching its maximum E when maximum supported species S_{max} are in the island. At the point where the immigration rate and emigration rate are equal, the island is said to be at equilibrium and the number of species at this point is S_0 . Hence, for equilibrium to be satisfied:

$$\lambda_{s_0} = \mu_{s_0} \tag{3.1}$$

When the island is at equilibrium S_0 there will be a number of occasional excursions that alter the species count in the island. λ_s and μ_s are the immigration and emigration rates respectively for an island with S number of species. From figure (3.1), for an island having S number of species the emigration rate and immigration rate can be found as:

$$\lambda_s = I\left(1 - \frac{S}{S_{max}}\right) \tag{3.2}$$

$$\mu_s = E\frac{S}{S_{max}} \tag{3.3}$$

The excursions that could lead to a change in the species count of an island can be either positive (increase in number of species) or negative (decrease in number of species). Positive excursions such as large piece of flotsam arriving from a neighboring island, or statistically unlikely high number of births. Negative excursions can be diseases, temporary introduction of a new predator, or a natural catastrophe.

Let P_s be the probability of an island containing S species at time t, as the time flows from t to $t + \Delta t$ the probability P_s will change as follows:

$$P_s\left(t + \Delta t\right) = P_s\left(t\right)\left(1 - \lambda_s\Delta t - \mu_s\Delta t\right) + P_{s-1}\left(t\right)\lambda_{s-1}\Delta t + P_{s+1}\left(t\right)\mu_{s+1}\Delta t \tag{3.4}$$

Δt is assumed to be small enough so that the probability of more than

one migration between t and $t + \Delta t$ can be ignored Simon (2008),Simon (2013). To have S species at time $t + \Delta t$, one of the following conditions must hold:

1. There were S species at time t, and no immigration nor emigration occurred between t and $t + \Delta t$.
2. There were $S - 1$ species at time t, and one species immigrated.
3. There were $S + 1$ species at time t, and one species emigrated.

Taking the limit of equation (3.4) as $\Delta t \to 0$:

$$\dot{P}_s = \begin{cases} -(\lambda_s + \mu_s) P_s + \mu_{s+1} P_{s+1} & S = 0 \\ -(\lambda_s + \mu_s) P_s + \lambda_{s-1} P_{s-1} + \mu_{s+1} P_{s+1} & 1 \leq S \leq S_{max} - 1 \\ -(\lambda_s + \mu_s) P_s + \lambda_{s-1} P_{s-1} & S = S_{max} \end{cases} \tag{3.5}$$

By defining $n = S_{max}$ and $P = [P_0 \cdots P_n]^T$, and by arranging the $(n + 1)$ equations from equation (3.5) into a single matrix equation we get:

$$\dot{P} = AP \tag{3.6}$$

where

$$A = \begin{vmatrix} -(\lambda_0 + \mu_0) & \mu_1 & 0 & \cdots & 0 \\ \lambda_0 & -(\lambda_1 + \mu_1) & \mu_0 & \ddots & \vdots \\ \vdots & \ddots & \ddots & \ddots & \vdots \\ \vdots & \ddots & \lambda_{n-2} & -(\lambda_{n-1} + \mu_{n-1}) & \mu_n \\ 0 & \cdots & 0 & \lambda_{n-1} & -(\lambda_n + \mu_n) \end{vmatrix} \tag{3.7}$$

For a special case of $E = I$ and from equations (3.2) and (3.3):

$$A = E \begin{vmatrix} -1 & 1/n & 0 & \cdots & 0 \\ 1 & -1 & 2/n & \ddots & \vdots \\ \vdots & \ddots & \ddots & \ddots & \vdots \\ \vdots & \ddots & 2/n & -1 & 1 \\ 0 & \cdots & 0 & 1/n & -1 \end{vmatrix}$$
$$= EA' \tag{3.8}$$

From Simon (2013), in steady-state $t \to \infty$, hence $\dot{P}(\infty) = AP(\infty) = EA'P(\infty) = 0$; from that $P(\infty)$is the eigenvector corresponding to the zero eigenvalues. Thus we get:

$$P(\infty) = \frac{v(0)}{\sum_{k=0}^{n} v_k(0)} \tag{3.9}$$

where

$$v(0) = [v_0(0) \cdots v_k(0)] \tag{3.10}$$

and

$$v_k(0) = \binom{n}{k} = \frac{n!}{k!(n-k)!} \tag{3.11}$$

3.2.2 Biogeography-Based Optimization

Biogeography-Based Optimization (BBO), introduced by SimonSimon (2008) is a population based stochastic based evolutionary algorithm. As can be seen from the island biogeography theory, biogeography is nature's way to achieve optimal condition of life through the distribution of species

among islands. This can be translated to a mathematical optimization problem, in which a number of candidate solutions referred to as population and each solution from the population is termed as individual. An individual that performs well on the objective function is analogous to high HSI islands, and the individuals that perform poor on the objective function are analogous to low HSI islands. As in biogeography theory that high HSI islands having lower immigration rate thus it will be more reluctant to change than the low HSI islanfs having immigration rates. Therefore, a good individual will have low tendency to change than poor individuals. On the other hand, the high HSI islands have high emigration rate and hence tendency to share its features with the low HSI islands having low emigration rates. Thus, the good individuals will share its features with the poor individuals. The addition of new features to poor individuals may raise the quality of those individuals.

In BBO each individual is represented by an identical species count curve with $E = I$ for simplicity, as illustrated in figure (3.2). In figure (3.2) S_1 represents a poor individual which is analogous to a low HSI island, while S_2 represents a good individual that is analogous to high HSI island. It can be seen that S_1 will have a high immigration rate and low emigration rate, where for S_2 it is the other way around. The migration model shown below is called a linear migration model where λ and μ are both linear functions of the cost.

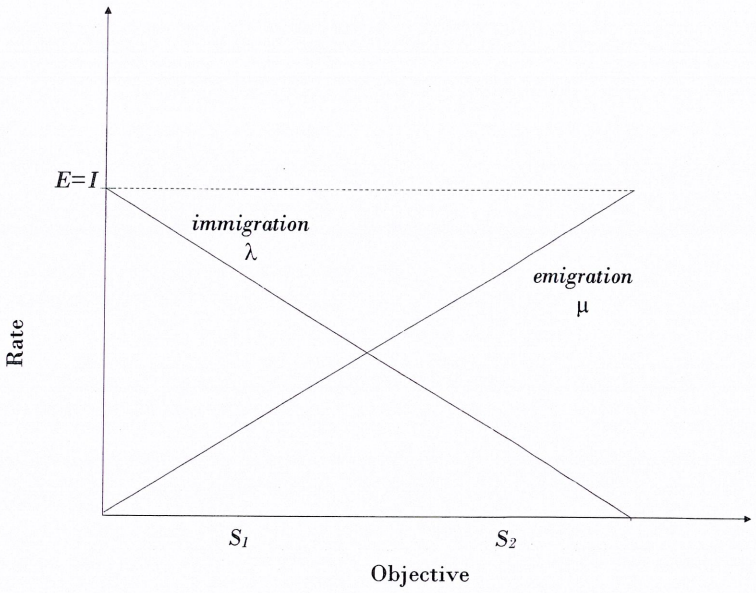


Figure (3.2)
BBO individual species count curve with $E = I$

3.2.2.1 BBO Migration

Consider the following constrained optimization problem:

$$\min_{x \epsilon \mathbb{R}^n} f(\mathbf{x}) \tag{3.12}$$

where $x = [x_1, x_2, \cdots, x_n]^T$.

x would be an individual which is analogous to an island, and x_i would be analogous to SIV of an island. Hence when a migration occurs the SIV's of an island will either immigrate to the individual or they will emigrate from the individual. In BBO a use of migration rates of each individual to probabilistically share information between individuals. There are different ways to implement migration in BBO, but in this study the original BBO developed in Simon (2008) will be used which is referred to as partial immigration based.

Suppose that there are a population of size N and that x_k is the k-th individual in the population where $k \in [1, N]$, and the size of the optimiza-

tion problem is n. $x_k(s)$ is the s-th independent variable in the individual, where $s \in [1, n]$. Based on the cost function evaluation the immigration probability λ_k, is given for the k-th individual and for all of its solution features $s \in [1, n]$, so in each generation there would be a probability of $\lambda_k$that this individual will be replaced.

Once a solution feature is selected to be replaced, then selection of the emigrating solution feature is done based on the emigrating probability of that individual $\{\mu_i\}$.

Algorithm (3.1) shows the pseudo code for the migration operator of BBO.

Algorithm 3.1 Habitat migration

```
for i = 1 to N
    z_i = x_i
    for s = 1 to n
        Select x_i with probability ∝ λ_i
        if rand(0,1) < λ_i then
            for j = 1 to N
                Select x_j with probability ∝ μ_j
                if rand(0,1) < μ_j then
                    z_i(s) ← x_j(s)
                end if
            end for
        end if
    end for
end for
```

3.2.2.2 BBO Mutation

In BBO there are two main operators , i.e, migration and mutation. Simon Simon (2008), has referred to mutation of SIV to be analogous to the introduction of an excursion to a habitat that will drive it away from its equilibrium point and that can happen randomly. An example is the arrival

of large piece of flotsam to the island. Mutation rates are determined through the species count probabilities using equation (3.5).

From figure (3.2), it can be seen that for low species count and high species count both have relatively low probabilities. While for medium species count they have high probabilities for change as they are near the equilibrium point.

To calculate the species count probabilities there are two methods:

First Method: Setting an equal initial species count probabilities to all individuals $P(0)$, and through an iterative procedure the steady state probability $P(\infty)$ can obtained.

Second Method: Using the equations (3.9),(3.10), and (3.11) to calculate $P(\infty)$.

After obtaining the probabilities, the mutation rates can be found as:

$$m_i = m_{max}\left(1 - \frac{P_i}{P_{max}}\right) \tag{3.13}$$

where

m_i : the i-th individual mutation rate

m_{max} : the maximum mutation rate, typical between and.

P_i : i-th individual species count probability

P_{max} : Maximum species count probability from all individuals

In algorithm (3.2) the pseudo code for the mutation operator of BBO is illustrated.

Algorithm 3.2 Habitat Mutation

for i = 1 to N

Compute probability P_i
for s = 1 to n
Select SIV $x_i(s)$ with probability $\propto P_i$
if rand < m_i
replace $x_i(s)$ with a randomly generated SIV
end if
end for

end for

3.2.2.3 BBO Elitism

Elitism is a way of making sure that the best individual in evolutionary algorithms are retained in the population from one generation to the next. Since there is a danger that good solution might be lost, elitism prevent this from happening. This can be done in BBO like any other EA.

The BBO algorithm flow chart is illustrated in figure (3.3).

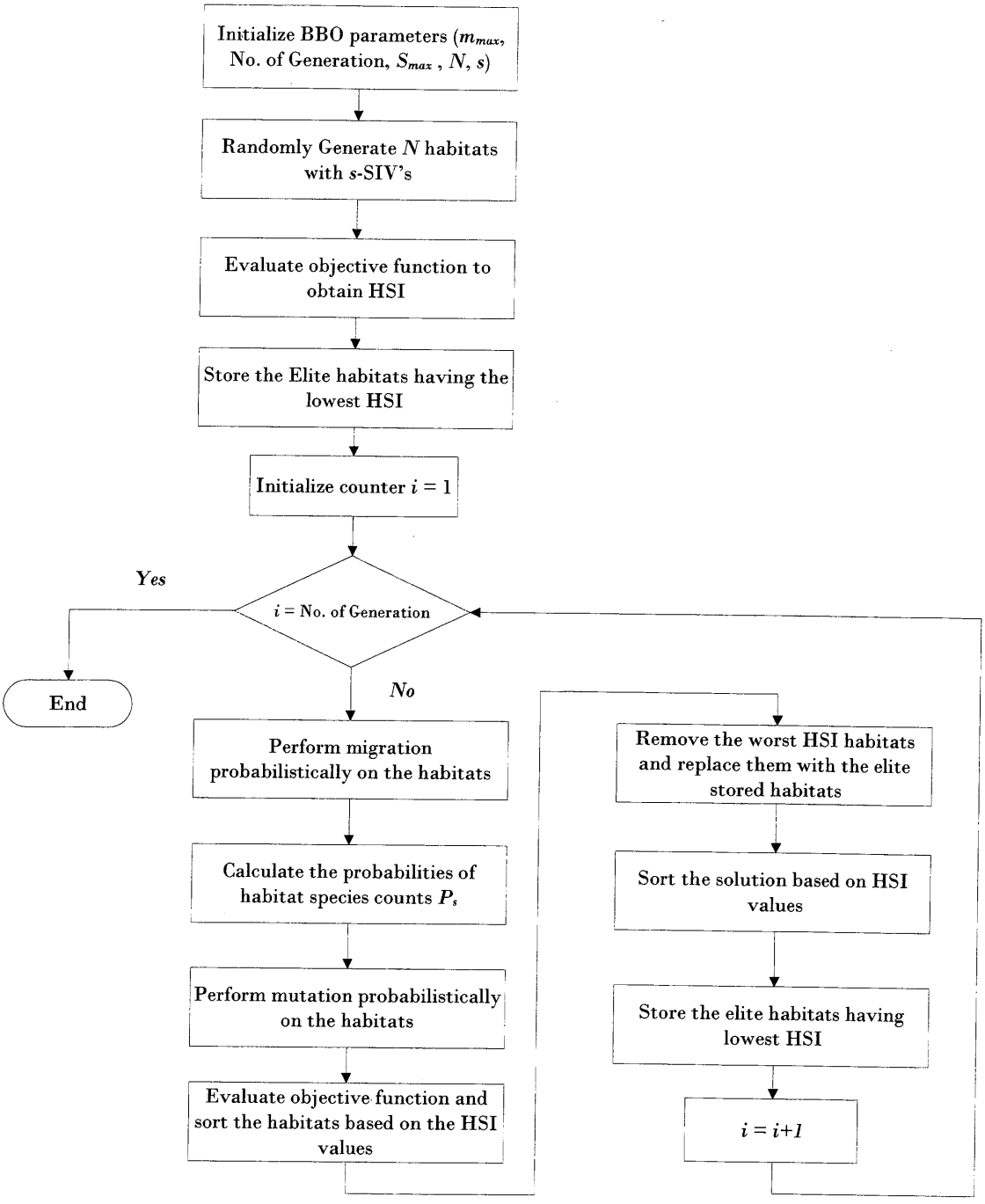


Figure (3.3)
Biogeography-Based Optimization Flowchart

3.3 Particle Swarm Optimization

Particle swarm optimization (PSO) was introduced by Kennedy and Eberhart in 1995, J. Kennedy et al. (1995). PSO is a population based iterative search algorithm that manipulates a number of candidate solutions, referred to as particles, in order to find the optimum. The PSO was discovered through simulation of simple social models. It imitates the swarm behavior such as birds flocking and fish schooling, and this behavior is referred to as swarm intelligenceYang (2010). The PSO, unlike BBO, does not use the mutation operator.

Observation of bird flocks, school of fishes, bee swarms, and animal herds have shown that the collective effort of a group is usually more rewarding than the individual effortHomans (1958).From this, in order for a group to achieve a certain goal each member of the group has certain capabilities in order to achieve the goal. While working in a group, the individual behavior is governed by two forces: the first is his perception to achieve the goal, and the second is the social dynamics. All the members of the group, swarm, share the experience of pursuing a common goal , and each individual learns not only from its own experience, but also from the experience of its neighbors. This speeds up the search process significantlyRakitianskaia (2011).

This algorithm searches the space of an objective function by adjusting the trajectories of individual particles, as these trajectories form piecewise path in a quasi-stochastic manner. The movement of a swarming particles consists of two major components: stochastic component and a deterministic component. Each particle is attracted toward the position of the current global best g_{best} and it own personal best location p_{best} in history, while in the same time it has tendency to move randomly Yang (2010).

When a particle i attains a location better than the one attained before in its history, it updates the personal best location with the new attained one. As mentioned before that all particles has a personal best location that can be

altered at any time during the iterations. The aim is to find the global best among all the current personal best until the objective no longer improve or after a certain number of iterations. Figure (3.4), shows a schematic representation of the motion of the particles, where xp_{best} is the particle best location, and $xg_{best} = \min\{f(x_i)\}$ for $i = 1, 2, \cdots, n$ is the current global best.

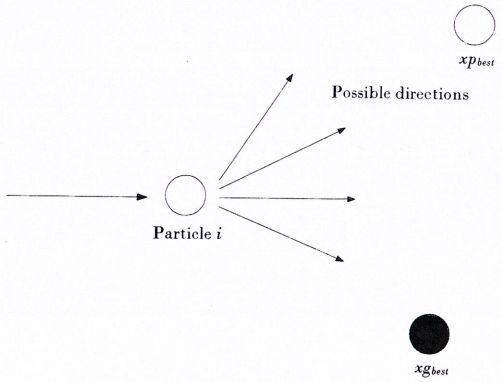


Figure (3.4)
Schematic Representation of the motion of particles in PSO, moving towards the global best xg_{best} and the current best xp_{best} for each particle

3.3.1 Particle Swarm Optimization Algorithm

PSO operates on a set (swarm) of candidate individuals (particles) . For a $n-$ dimensional optimization problem, a particle is represented by an $n-$ dimensional vector $\overrightarrow{x}$ also referred to as particle position. Every particle has a fitness value, that indicates the quality of the candidate solution. The swarm will move in a $n-$dimensional search space which represents its environment. In addition to the position of the particle within the search space, it has a velocity vector $\overrightarrow{v}$. The velocity of the particle determines the step size the particle takes in a generation, and the direction it takes. The so-

cial interaction is emulated by the formation of neighborhood in the swarm. As each particle remembers its own best location, it also query neighboring particles for their best position discovered so far. In this study, the neighborhood size is taken as the full swarm.

PSO searches for an optimum by moving the particles through the search space. At each time step, t, the position $x_i(t)$ of the particle i is modified by adding the particle velocity to the previous position vector:

$$\overrightarrow{x_i}(t) = \overrightarrow{x_i}(t-1) + \overrightarrow{v_i}(t) \tag{3.14}$$

The velocity vector determines the step size inside the search space and direction of the particle. The velocity vector is determined as:

$$\overrightarrow{v_i}(t) = \omega \overrightarrow{v_i}(t-1) + c_1 \overrightarrow{r_1}(\vec{x}_{pbest,i} - \overrightarrow{x_i}(t)) + c_2 \overrightarrow{r_2}(\vec{x}_{gbest} - \overrightarrow{x_i}(t)) \tag{3.15}$$

where ω is the inertia weight , controlling the influence of the previous velocity values on the new velocity. c_1 and c_2 are the acceleration coefficients used to scale cognitive and social components respectively. r_1 and r_2 are vectors with each component sampled from a uniform distribution $U(0,1)$; $x_{pbest,i}$ is the i-th particle best location attained through generations and x_{gbest} is the global best location found in the swarm.

Algorithm 3.3 Particle swarm Optimization Algorithm

Initialize population
Evaluate objective function
store g_{best} and p_{best}
for $t = 1$ to G
for $i = 1$ to n

for $j = 1$ to p
Update the j-th component of the i-th velocity vector:
$v_{i,j}^{t} =$
$\omega v_{i,j}^{t-1} + c_1 r_1 \left(x_{ipbest} - x_i^{t-1}\right) + c_2 r_2 \left(x_{gbest} - x_i^{t-1}\right)$
Update the j-th component of the i-th displacement vector:
$x_{i,j}^{t} = x_{i,j}^{t-1} + v_{i,j}^{t}$
end for
Evaluate the objective function for the new velocity vector obtained $f\left(\overrightarrow{x_i}\right)$:
if $f\left(\overrightarrow{x_i}\right) < f\left(\vec{x}_{ipbest}\right)$
$\vec{x}_{ipbest} = \overrightarrow{x_i}$
end if
if $f\left(\overrightarrow{x_i}\right) < f\left(\vec{x}_{gbest}\right)$
$\vec{x}_{gbest} = \overrightarrow{x_i}$
end if

end for
end for

3.3.1.1 Velocity Clamping

It has be noted that the basic PSO algorithm suffered from undesirable dynamical properties, notably the particle velocities need to be limited in order to control their trajectoriesClerc & Kennedy (2002). It was suggested by Kennedy and Eberhart J. F. Kennedy et al. (2001) to keep the velocity within sensible bounds by putting limits on the maximum that the particle

is allowed to attain in every dimension. To implement velocity clamping:

$$v_{ij} = \begin{cases} v_{max,j} & if \quad v_{ij} > v_{max,j} \\ -v_{max,j} & if \quad v_{ij} < -v_{max,j} \\ v_{ij} & otherwise \end{cases} \tag{3.16}$$

Velocity clamping can be viewed as a control over the exploration - exploitation balance of PSO. A large v_{max} allows more change in each particle from one generation to the next, which emphasizes exploration. A small v_{max} restricts changes in particles, which emphasizes exploitation Simon (2013).

3.3.1.2 Inertia Weighting

From equation (3.15), the inertia weight was defined to control the velocity of the particle from one generation to the next, as if it was not defined the velocity tends to become constant. However, it was found empirically that decreasing inertia weight during the optimization process may provide better performance. Based on Eberhart & Shi (2000), it is often advisable to decrease the ω from 0.9 at the first generation up to 0.4 at the last generation. This helps slow down the velocity of each particle as the generation count increases, hence improves convergence.

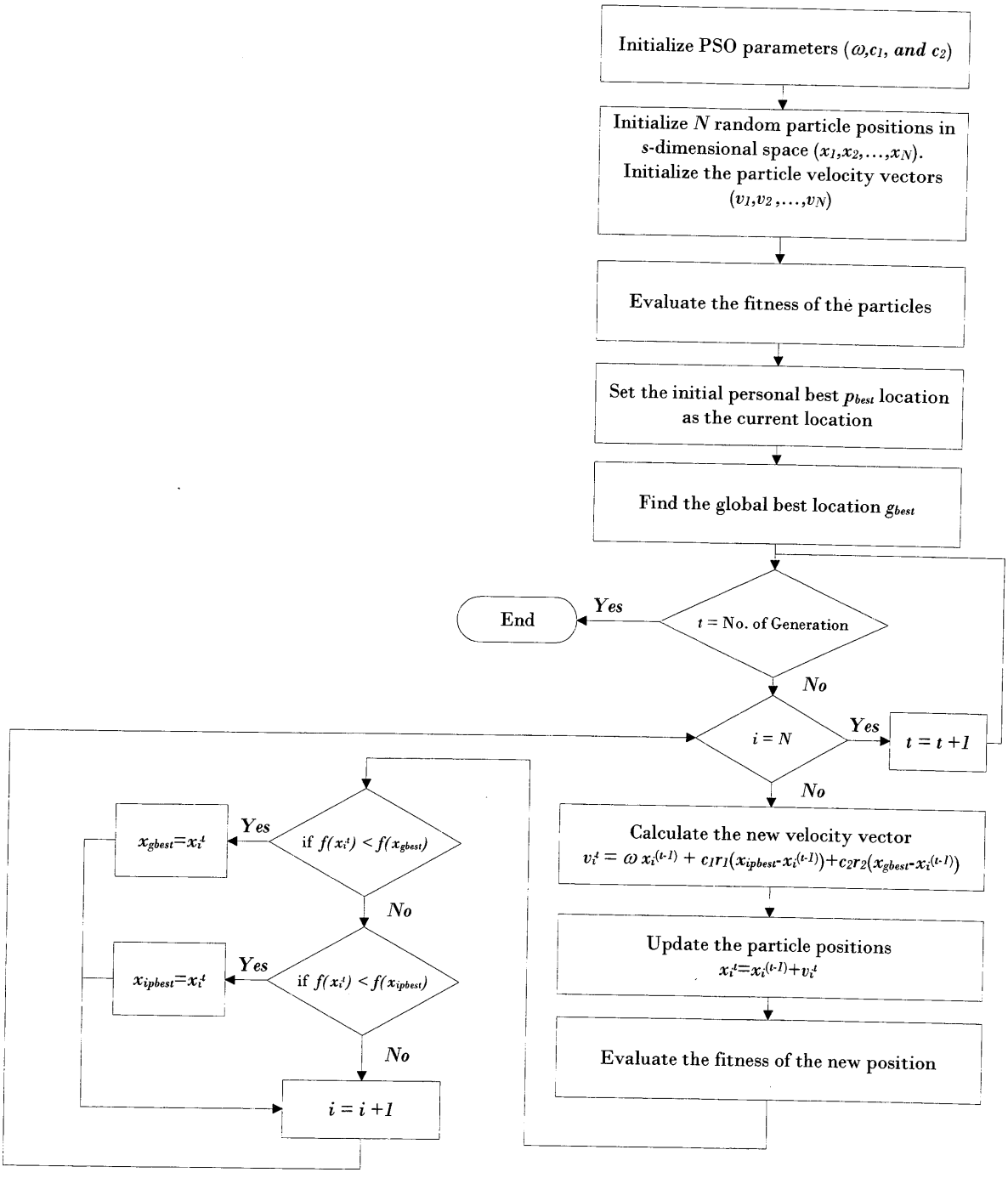


Figure (3.5)
Particle Swarm Optimization Flowchart

3.4 Introduction to FACTS based Power System Stabilizers

In the past few decades the power system networks has explosively increased in size due to the constant demand for power. This gave rise to interconnection of power network, thus increasing the complexity of the system. This was caused due to the restricted and limited resources and the strict environmental constraints. The demand for power will never get less, as it grows day by day. The interconnection between remotely located power systems gave rise to low frequency oscillations in the range of 0.1 ~ 3.0 Hz. This type of instability can endanger the system security and limit power transfer, since if these oscillations are not well damped they will keep growing in magnitude until loss of synchronism occurs K. Padiyar (2008); Al-Awami et al. (n.d.).

This problem gave rise to a solution through the use of power system stabilizers (PSS) , which are intended to provide damping to generator oscillations. The PSS is a supplementary controller in the excitation systems. The PSS will provide satisfactory operation under unusual or abnormal conditions which maybe encountered at times K. Padiyar (2008). While PSS are effective in damping power oscillations, they suffer a drawback of being liable to cause great variations in voltage profile and they may even result in leading power factor operation under sever disturbance conditions Rahim & Nassimi (1996).

On the other hand, FACTS controllers have come up as another solution for this problem. From their introduction, the FACTS controllers were intended to solve various power system steady state control problems such as voltage regulation, power flow control, and transfer capability enhancement. The damping of the power system oscillations was introduced as a supplementary function, which has been extensively investigated and studied M. Abido (2009). Due to these capabilities, FACTS control installation provide a better solution over PSS.

WangWang (2000), has investigated the capabilities of Static Var Compensator (SVC), Controllable Series Compensator (CSC), and Phase Shifters (PS) to damp power system oscillations in an SMIB system. In Rahim & Nassimi (1996), a coordinated control of PSS and SVC was introduced. Several references in literature has investigated the capability of the Thyristor Controlled Series Capacitor (TCSC) to damp the power system oscillations through different approaches. In Panda & Padhy (2007), a Genetic Algorithm (GA) based power system stabilizer using TCSC was investigated.

STATCOM capability to damp power system oscillations exceeded the capability of the SVC M. Abido (2009). In M. Abido (2005), a singular value decomposition (SVD) to investigate the controllability of poorly damped electromechanical modes via STATCOM input channels.

As the most versatile FACTS controller, UPFC had become an interesting field of research for damping power system oscillations. In Nabavi-Niaki & Iravani (1996), a UPFC based stabilizer to mitigate torsional oscillations using shunt converter phase angle as a control signal was designed and investigated. Abido *et al* M. A. Abido et al. (2006), has introduced a particle swarm based stabilizer using UPFC in which he has investigated the controllability of the UPFC different input channels in damping power system oscillations. It was observed that the shunt converter phase angle provide a better controllability for damping electromechanical oscillations compared to the other input channels. In Al-Awami et al. (n.d.), a coordinated control design for UPFC and PSS based on particle swarm was developed.

3.5 UPFC Based Damping Controller

The structure of the damping controller is shown in figure (3.6). It consists of a washout circuit which is provided to eliminate the steady state bias from the output of the damping controller. The washout circuit acts as a high pass filter that passes all the frequencies of interests. In this research

the value of T_w is chosen to be 5 M. Abido (2005); M. A. Abido et al. (2006); M. Abido (2009); Ajami & Gholizadeh (2012); Al-Awami et al. (n.d.).

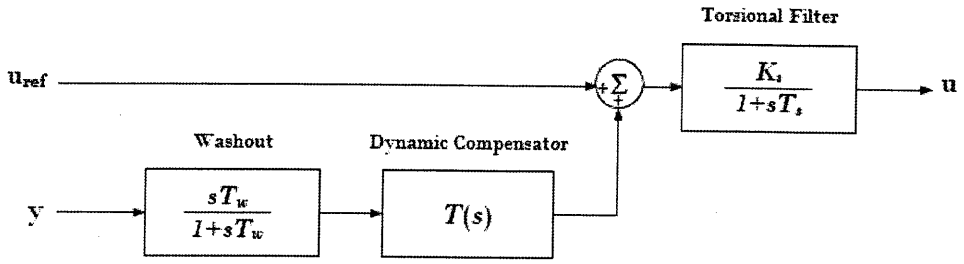


Figure (3.6)
UPFC Based Damping Controller

A common practice for the design of the dynamic compensator is the use of a two stage lead-lag stage compensator. This practice has been widely used and accepted even for FACTS based damping controllers. On the other hand, a use of PID controllers as dynamic compensator in power system stabilizers has been reported, but it has been rarely used. In Oonsivilai & Marungsri (2008), a PID controller design based on particle swarm optimization for a multimachine system was proposed. In this research a two stage lead-lag compensator will be used, as its parameters (T_1 to T_4) can be directly translated from the range of frequencies of interest.

$$T(s) = K_p \frac{(1+sT_1)}{(1+sT_2)} \frac{(1+sT_3)}{(1+sT_4)} \tag{3.17}$$

Seen here is the transfer function of the compensator given by (3.17).

As for the damping control signal y , one of the variables selected is the deviation in rotor angular velocity $\Delta\omega$. Another variable that have been reported in literature was the generator electrical power P_e which in fact approximates the accelerating power since the variations in the mechanical power are slowK. Padiyar (2008). In this research, there will be no deviation from the common practice in the use of rotor relative velocity.

Based on the conclusion reached by Abido in M. A. Abido et al. (2006), δ_E provides a better controllability for the electromechanical mode oscilla-

tions than other UPFC input channels. The proposed damping controller is based on the shunt converter phase angle, as shown in figure (3.7):

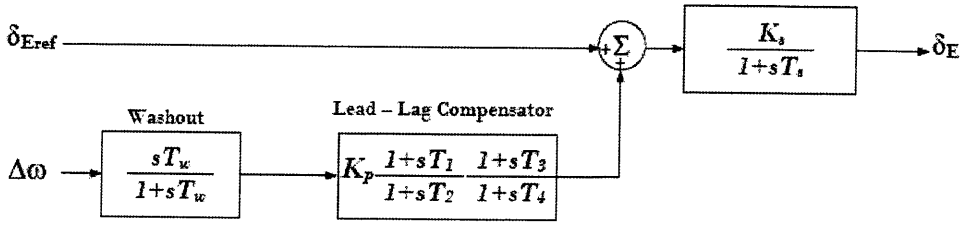


Figure (3.7)
UPFC Based Damping Controller Using δ_E Input channel

The eigenvalues of the system without POD controller are shown in table (3.1), and from this it can be seen that the system is unstable

Table (3.1)
System eigenvalues under nominal loading condition without POD controller

Eigenvalues
-15.73
-4.80
$0.64 \pm j3.70$
-1.28

3.5.1 System Linearized Model

In order to assess the stability of the system, and to construct an objective function based on the system eigenvalues, a linearized model of the system is to be determined (refer to Appendix B.2). For this purpose, the system has to be linearized around different operating points. The linear model is given by:

$$\dot{x} = A\,x + B\,u \tag{3.18}$$

where x is the state vector and u is the input vector :

$$x = \begin{bmatrix} \Delta\delta & \Delta\omega & \Delta E'_q & \Delta E_{fd} & \Delta v_{dc} \end{bmatrix}^T \tag{3.19}$$

$$u = \begin{bmatrix} \Delta m_E & \Delta\delta_E & \Delta m_B & \Delta\delta_B \end{bmatrix} \tag{3.20}$$

where A and B are:

$$A = \begin{bmatrix} 0 & \omega_B & 0 & 0 & 0 \\ -\frac{K_1}{M} & -\frac{D}{M} & -\frac{K_2}{M} & 0 & -\frac{K_{pd}}{M} \\ -\frac{K_4}{T'_{do}} & 0 & -\frac{K_3}{T'_{do}} & \frac{1}{T'_{d0}} & -\frac{K_{qd}}{T'_{do}} \\ -\frac{K_A K_5}{T_A} & 0 & -\frac{K_A K_6}{T_A} & -\frac{1}{T_A} & -\frac{K_A K_{vd}}{T_A} \\ K_7 & 0 & K_8 & 0 & -K_9 \end{bmatrix} \tag{3.21}$$

$$B = \begin{bmatrix} 0 & 0 & 0 & 0 \\ -\frac{K_{pe}}{M} & -\frac{K_{p\delta e}}{M} & -\frac{K_{pb}}{M} & -\frac{K_{p\delta b}}{M} \\ -\frac{K_{qe}}{T'_{do}} & -\frac{K_{q\delta e}}{T'_{do}} & -\frac{K_{qb}}{T'_{do}} & -\frac{K_{q\delta b}}{T'_{do}} \\ -\frac{K_A K_{ve}}{T_A} & -\frac{K_A K_{v\delta e}}{T_A} & -\frac{K_A K_{vb}}{T_A} & -\frac{K_A K_{v\delta b}}{T_A} \\ K_{ce} & K_{c\delta e} & K_{cb} & K_{c\delta b} \end{bmatrix} \tag{3.22}$$

where $K_1 - K_9$, K_{pu},K_{qu}, and K_{cu} are the linearization constants.

3.5.2 Objective Function

In order to find the optimal set of parameters of the damping controller using BBO and PSO, an objective function needs to be formulated then optimized. Several time domain based performance indices have been proposed in literature, such as integral of time multiplied by the absolute value of error (ITAE) criterion. In other performance indices such as eigenvalue based functions, the parameters are tuned in stabilizing power systems. This section presents two objective functions that are used to design a robust damping controller.

3.5.2.1 Eigenvalue Based Objective Function

In this approach, the damping coefficients of the eigenvalues are to be maximized. Then the damping coefficient ζ_i of the i-th eigenvalue is defined through the following equation:

$$\zeta_i = -\frac{\alpha_i}{\sqrt{\alpha_i^2 + \beta_i^2}} \tag{3.23}$$

Where α_i and β_i are the real and imaginary parts of the dominant eigenvalue respectively. A well damped power system is said to have a damping for all eigenvalues greater than 5% Rogers (2000). Thus, the objective of the optimization problem is to achieve a damping for all eigenvalues greater than 5% over the range of the operating points.

Let Ξ_p be a vector of the damping factors of all eigenvalues of the p-th operating point in the set, where $p = 1, 2, .., n$ for n operating points. Then the objective function to be maximized is:

$$\max \ J_e \tag{3.24}$$

where $J_e = \min(\min(\Xi_p))$

3.5.2.2 Time Based Objective Function

For a robust tuning using the ITAE criterion, the objective function for set of operating points is designed as:

$$J_t = \sum_{i=1}^{p} \left(\int t|\Delta\omega_i|dt \right) \tag{3.25}$$

In both cases, the eigenvalue based objective function is to be maximized, while the time based objective function is to be minimized. The objective functions are subject to the following constraints for the parameters of the controller in (3.17):

$$\begin{aligned} K_{pmin} \leq K_p \leq K_{pmax} \\ T_{1mn} \leq T_1 \leq T_{1max} \\ T_{2min} \leq T_2 \leq T_{2max} \\ T_{3min} \leq T_3 \leq T_{3max} \\ T_{4min} \leq T_4 \leq T_{4max} \end{aligned} \tag{3.26}$$

where the values of the optimization problem constraints are defined in table(3.2) and can be found in M. Abido (2005); M. A. Abido et al. (2006); Ajami & Gholizadeh (2012); Al-Awami et al. (n.d., 2007):

Table (3.2)
Optimization constraints for the POD controller design

	Min.	Max.
K_p	-100	100
T_1 to T_4	0.01	1.5

In both cases only a DC voltage regulator is incorporated in the system in order to stabilize the DC link voltage. The parameters for the DC regulator are obtained before hand and kept constant during the optimization process.

3.6 Controller Design

In order to find the optimal set of controller parameters, the controllers are tuned using BBO and PSO for 30 different operating conditions, where the generator active power P_e is varied between 0.2 p.u to 1.2 p.u and the reactive power Q_e is varied between -0.4 p.u to 0.4 p.u, hence covering almost all the possible operating conditions of the system. During the simulation the DC voltage regulator is incorporated in the system in order to stabilize the DC link voltage. The parameters for the DC regulator are obtained through fine tuning ($K_{dp} = -6.05$ and $K_{di} = -1.15$) and kept constant during the optimization process.

3.6.1 Robust Eigenvalue Based Damping Controller Design

For BBO using a maximum mutation rate of 0.005, and for PSO the acceleration coefficients are chosen based on M. A. Abido et al. (2006) as $c_1 = c_2 = 2.05$. The inertia weight ω is defined as linear function of the generation decreasing from 0.9 to 0.4. The program is run for 100 generations and a population of 100 individuals for both algorithms. Table (3.3) , shows the gains of the controllers:

Table (3.3)
Damping Controller Parameters Using BBO and PSO for eigenvalue based objective function

	BBO	PSO
K_p	-98.5099	-89.8943
T_1	1.0814	0.0578
T_2	0.5190	0.6519
T_3	0.0520	1.4808
T_4	0.6451	0.6807
ζ	0.3005	0.3003

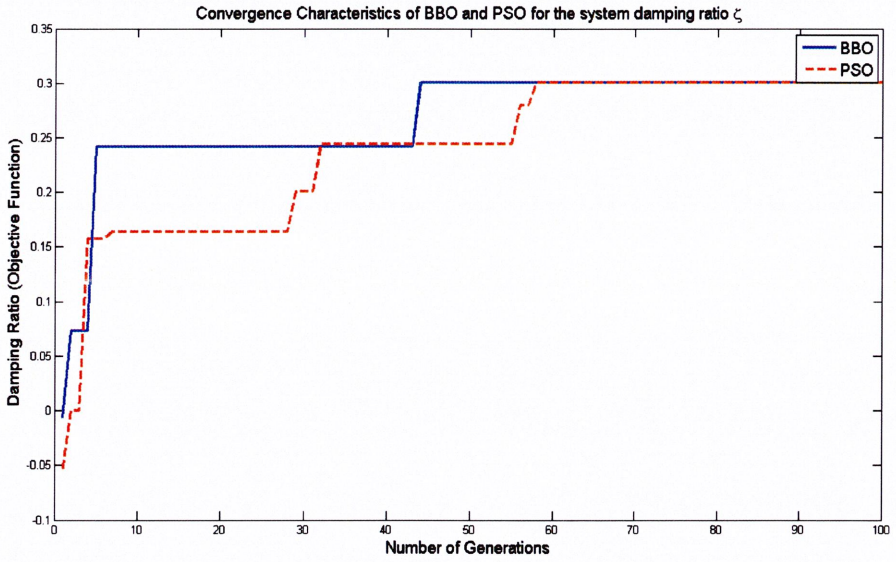


Figure (3.8)
Convergence characteristic for Eigenvalue based objective function for BBO algorithm and PSO algorithm

From figure (3.8), it can be seen that BBO and PSO has reached almost the same value of the minimum damping ratio of all eigenvalues for the 30 different operating conditions, as it has reached $\zeta = 0.3005$ and $\zeta = 0.3003$ for BBO and PSO respectively. The difference is in the convergence rate as can be seen, where BBO has reached its optimal value of the objective function in 44 generations and PSO has reached it in 58 generations.

3.6.2 Robust Time-value Based Damping Controller

Using the same parameter initialization for both BBO and PSO as has been done in the previous objective function, the following results were obtained, as the gain and time constants are given in Table (3.4):

Table (3.4)
Damping Controller Parameters Using BBO and PSO for time-value based objective function

	BBO	PSO
K_p	-94.8712	-98.9509
T_1	0.0143	1.4550
T_2	0.3284	0.6472
T_3	0.7778	0.0544
T_4	0.7126	0.7519
J_{ITAE}	0.1231	0.0920

The convergence characteristics for both of the algorithms can seen in figure 3.9:

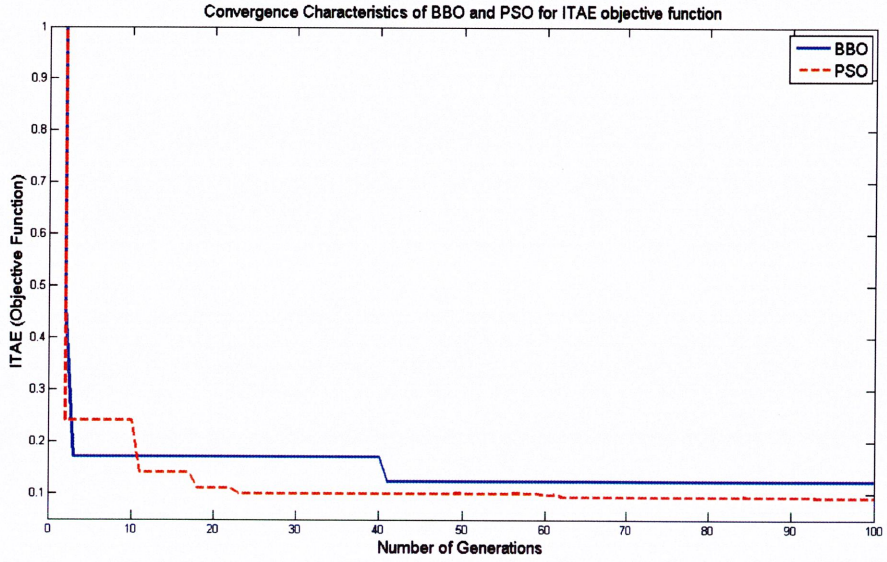


Figure (3.9)
Convergence characteristic for time-value based objective function for BBO algorithm and PSO algorithm

From figure 3.9 and from table 3.4, it can be seen that PSO has reached a minimum value compared to BBO.

3.7 Simulation Result

In order to test the performance of the designed damping controllers, each one of them is tested at nominal generator loading with no system uncertainty. At this loading condition the system is simulated for a 10% step change in mechanical power input (P_m).

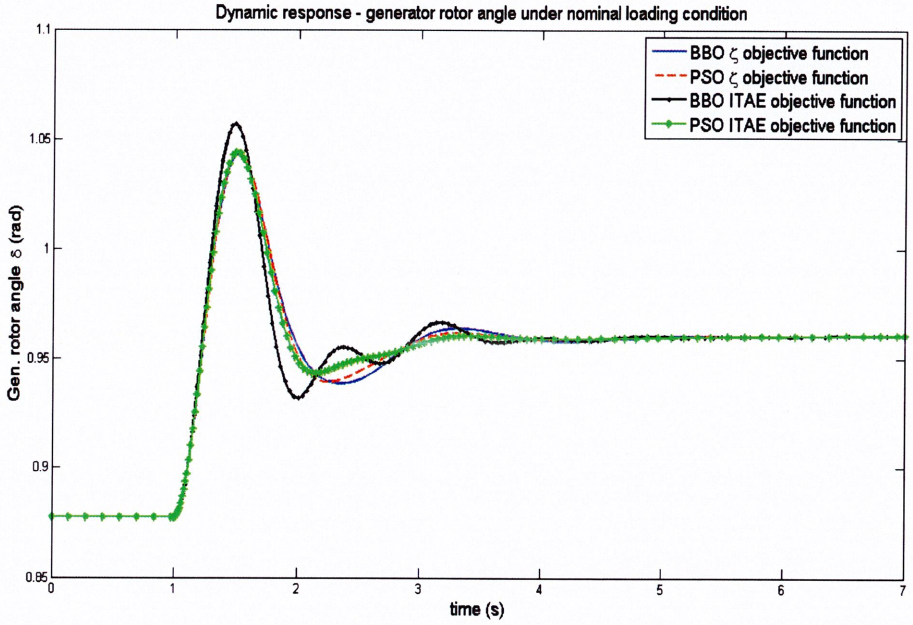


Figure (3.10)
Rotor Angle δ variation

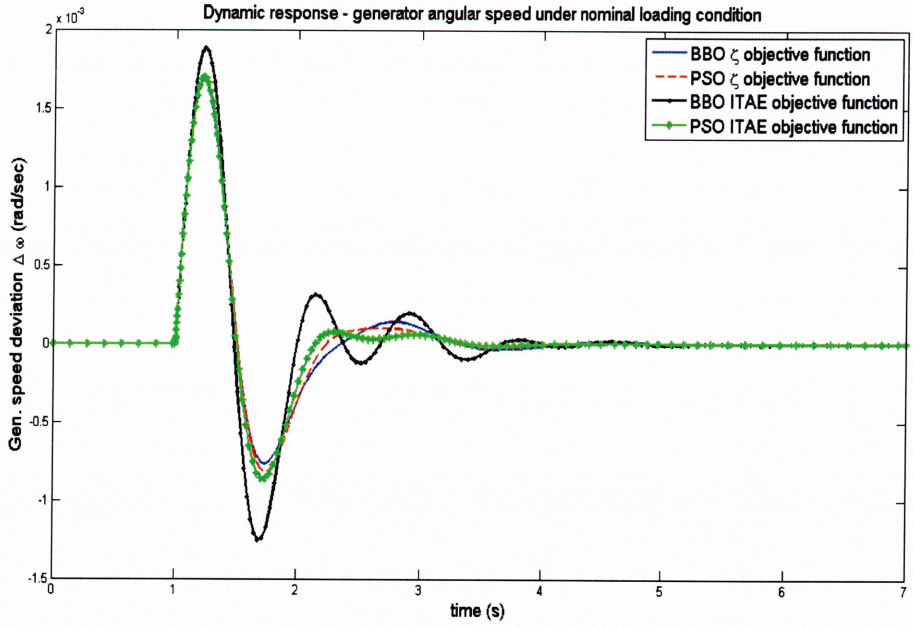


Figure (3.11)
Deviation in rotor angular velocity $\Delta\omega$

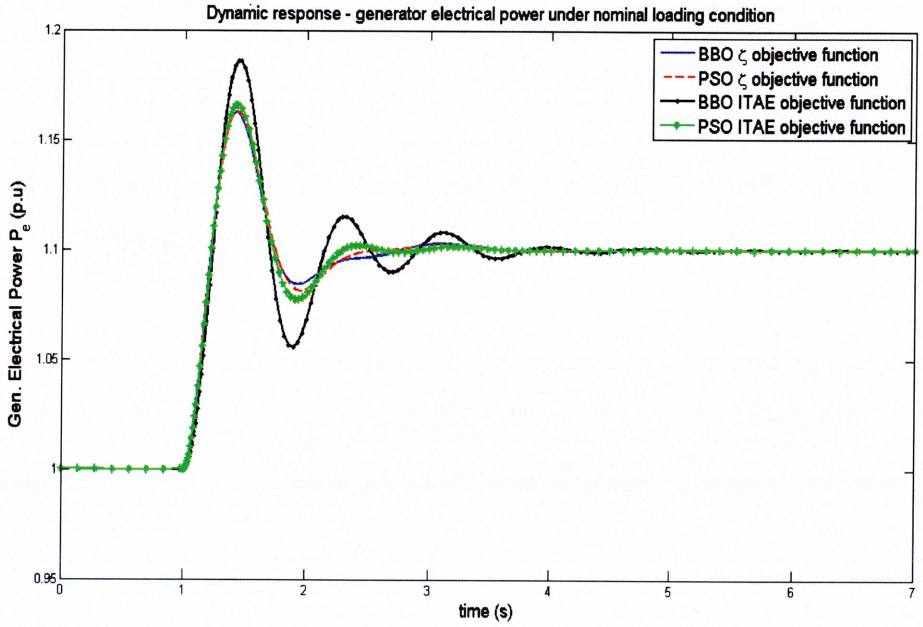


Figure (3.12)
Generator Electrical Power P_e

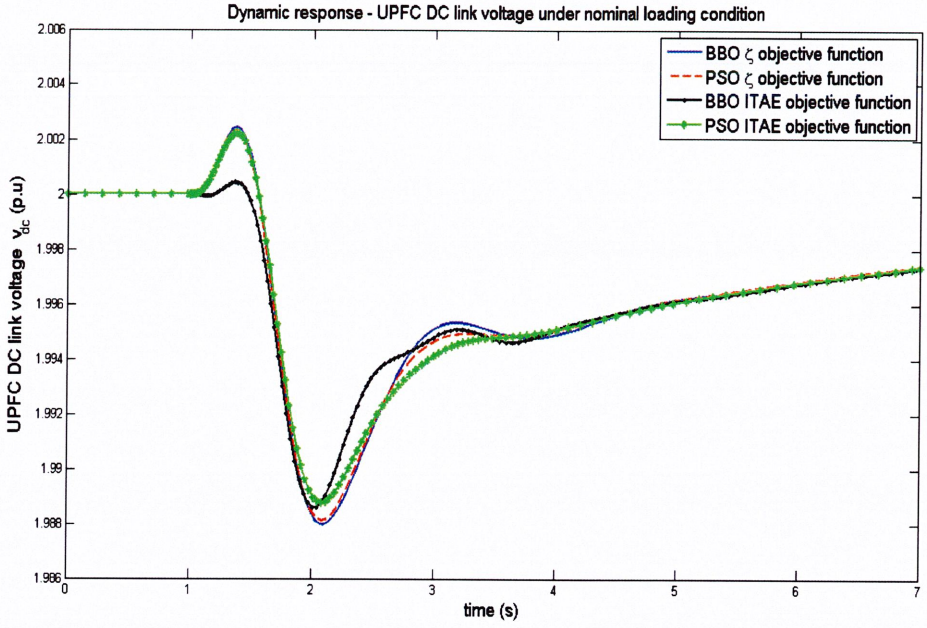


Figure (3.13)
UPFC DC link voltage v_{dc}

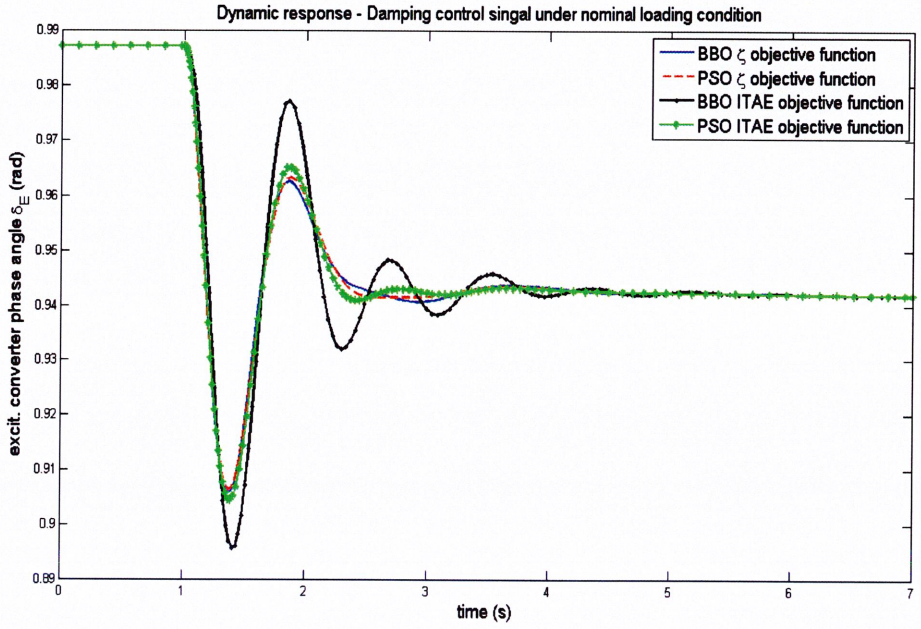


Figure (3.14)
Damping control signal δ_E

Table (3.5)
System eigenvalues with stabilizer installed

	BBO tuned stabilizer using ζ objective function	PSO tuned stabilizer using ζ objective function	BBO tuned stabilizer using ITAE objective function	PSO tuned stabilizer using ITAE objective function
System eigenvalues	-15.6785 -13.3227 EM:$-2.8118 \pm$ $j7.3595$ -5.1159 $-1.4128 \pm j3.3711$ -1.2571 $-0.1877 \pm j0.0108$	-15.6761 -12.4907 EM:$-2.8216 \pm$ $j6.9025$ -5.1108 $-1.6758 \pm j3.3447$ -1.0766 $-0.1880 \pm j0.0092$	-16.6768 -15.6434 EM:$-1.4423 \pm$ $j7.4855$ -5.1220 $-1.5499 \pm j3.5504$ -1.3688 $-0.1877 \pm j0.0109$	-15.6771 -12.8068 EM:$-2.4156 \pm$ $j6.8958$ -5.1097 $-1.8793 \pm j3.1526$ -1.0380 $-0.1878 \pm j0.0104$

Table (3.5), shows the system eigenvalues after the installation of the POD controllers. It can be seen that the system is stable, as all the eigenvalues fall in the left side of the complex plane. By comparing the system responses for the designed damping controller, there are two points that can be concluded from the figures (3.10) to (3.14). The first point, is that the performance of a designed damping based on the damping ratio ζ has a better performance compared to an ITAE based damping controller, and that can be shown from the settling time in table (3.6):

Table (3.6)
Damping controllers settling time and response attained peaks

Damping controller	Settling time	Peak
BBO ζ damping controller	2.9633	0.0017
PSO ζ damping controller	2.7031	0.0017
BBO ITAE damping controller	2.6445	0.0019
PSO ITAE damping controller	1.1556	0.0017

The second point is that even with BBO having an almost similar damping ratio as PSO tuned damping çontroller, the settling time varies and that is due to the effect of the DC voltage regulator. From this it can be seen that BBO and PSO had similar results for the ζ based damping controllers, while in minimization of the ITAE based objective function it was seen that PSO had a superior results compared to BBO. It can be seen that the ITAE BBO tuned POD controller is having the largest settling time, and ITAE PSO tuned POD is having the least.

Chapter 4

Unified Power Flow Controller Mult-Input Multi-Output Controller Design

- 4.1 Overview
- 4.2 UPFC MIMO control system
- 4.3 Control System Design
- 4.4 Simulation Results

Chapter 4

Unified Power Flow Controller Multi-Input Multi-Output Controller Design

4.1 Overview

The unified power flow controller (UPFC) was designed in order to control all the parameters of the transmission network, namely the magnitude of bus voltage, phase angle, and the transmission line impedance and that is to control the active and reactive power flow in the transmission line. With the configuration of the UPFC, more control functions can be realized, for instance the bus voltage regulation at the point of connection through the injection of reactive power by the shunt converter can be done. Moreover, the UPFC has been reported to be able to damp power oscillations, and that was investigated in the previous chapter. With this multiple control functions the UPFC is regarded as a multi-input multi-output (MIMO). In Wang (2002), an investigation of the interaction between different control loops, and based on that it has attempted to design a MIMO PI controller with decoupling controllers between the control loops. In Taher et al. (2010), a robust μ- synthesis decentralized controller for UPFC was designed, in that approach a DC voltage regulator, power flow controller, and a damping controller were designed. In this approach the MIMO system is transformed to equivalent mutli-input single output (MISO) control systems. Al-Awami *et al Al-Awami et al. (2007),* has used another approach in designing UPFC MIMO control system through using PSO to tune multiple controllers of the UPFC, DC voltage regulator, Power flow controller, and damping controller simultaneously, with the emphasis of the design was on the damping controller. The UPFC multiple controllers were tuned at a single operating point for multiple disturbances. The results were then simulated at a nonlinear system for a single system disturbance at different operating conditions.

In this research, the same approach that was used in Al-Awami et al.

(2007) is going to be utilized as that the decoupling of the controllers can deteriorate the performance of the control system Seborg et al. (2006). The MIMO control system, power flow control, DC voltage regulation, AC bus voltage regulation, and damping controller will be tuned using the two optimization algorithms discussed in the previous chapter.

4.2 UPFC MIMO control system

The structure of the control system is shown in figure (4.1), in this configuration the damping controller is associated with the DC voltage regulator where the control variable being it the excitation converter phase angle δ_E. The active power flow control is going to be controlled through the manipulation of the boosting converter modulation index m_B, which has been done in Al-Awami et al. (n.d.); M. A. Abido et al. (2006); Taher et al. (2010, 2012), while the AC bus voltage regulation is achieved through the control of excitation converter modulation index m_E.

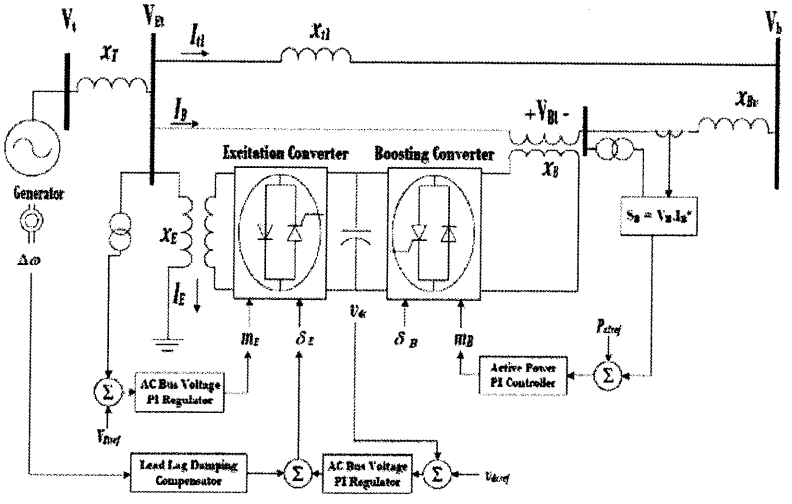


Figure (4.1)
UPFC MIMO control system structure

The multivariable controller structure is illustrated in figure(4.2):

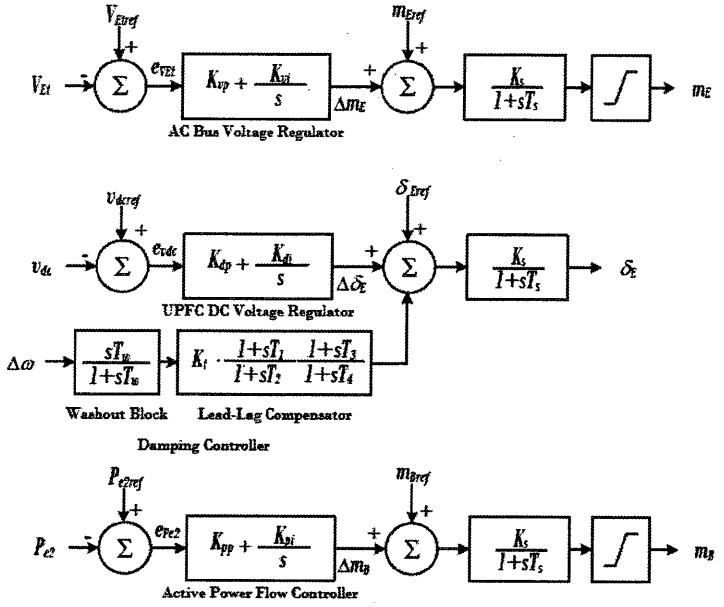


Figure (4.2)
Multiloop controllers for UPFC

4.3 Control System Design

To design a multivariable control system for the UPFC using the evolutionary optimization algorithms that were discussed in the previous chapter, an objective function is to be formulated and then optimized. From this perspective, there are several methods to design the MIMO controller. In Al-Awami et al. (2007), an ITAE based objective function was to be minimized, the objective function contained all the error signals of the controlled variables and this is done in purpose to tune the controllers simultaneously. The system was given two disturbances: an impulse disturbance in the input mechanical power, and a step change in the setpoint of the power flow in the compensated line. The optimization was carried at a single operating point. In this research a single operating point optimization will be carried out first with the same structure as in Al-Awami et al. (2007) in order to find the optimal set of gains for PI controllers and the gain and the time constants for a two stage lead-lag compensator to damp power system oscillations as has

been done in the previous chapter. The difference here, is that an AC bus voltage regulator will be incorporated in the system and the disturbances introduced will be:

1. A 10% step change in mechanical power P_m
2. A 2.5% step change in setpoint of P_{e2}

In order to find the optimal set of gains and time constants the following objective function is considered:

$$J_{ITAE} = \int_0^{t_{sim}} t\,|\Delta\omega|dt + \int_0^{t_{sim}} t\,|\Delta P_{e2}|dt + \int_0^{t_{sim}} t\,|\Delta v_{dc}|dt + \int_0^{t_{sim}} t\,|\Delta V_{Et}|dt \tag{4.1}$$

The above objective function is to be minimized:

$$\begin{aligned}
&min \quad J_{ITAE} \\
&Subject\ to \\
&K_{pp}^{min} \leq K_{pp} \leq K_{pp}^{max} \\
&K_{ip}^{min} \leq K_{ip} \leq K_{ip}^{max} \\
&K_{dp}^{min} \leq K_{dp} \leq K_{dp}^{max} \\
&K_{di}^{min} \leq K_{di} \leq K_{di}^{max} \\
&K_{vp}^{min} \leq K_{vp} \leq K_{vp}^{max} \\
&K_{vi}^{min} \leq K_{vi} \leq K_{vi}^{max} \\
&K_{p}^{min} \leq K_{p} \leq K_{p}^{max} \\
&T^{min} \leq T \leq T^{max}
\end{aligned} \tag{4.2}$$

The optimization problem constraints are as given in table4.1:

Table (4.1)
Optimization problem constraints

	Minimum	Maximum
K_{pp}	-0.5	0.5
K_{ip}	0	5
K_{dp}	-10	0
K_{di}	-5	0
K_{vp}	0	5
K_{vi}	0	15
K_p	-100	100
T_{min}	0.01	1.5

At nominal generator loading condition and by considering BBO maximum mutation rate as 0.05, and for PSO the acceleration coefficients are chosen as $c_1 = c_2 = 2.05$, and the inertia weight ω is defined as linear function of the generation decreasing from 0.9 to 0.4. The program is ran for 100 generations for all algorithms. The following results were obtained as:

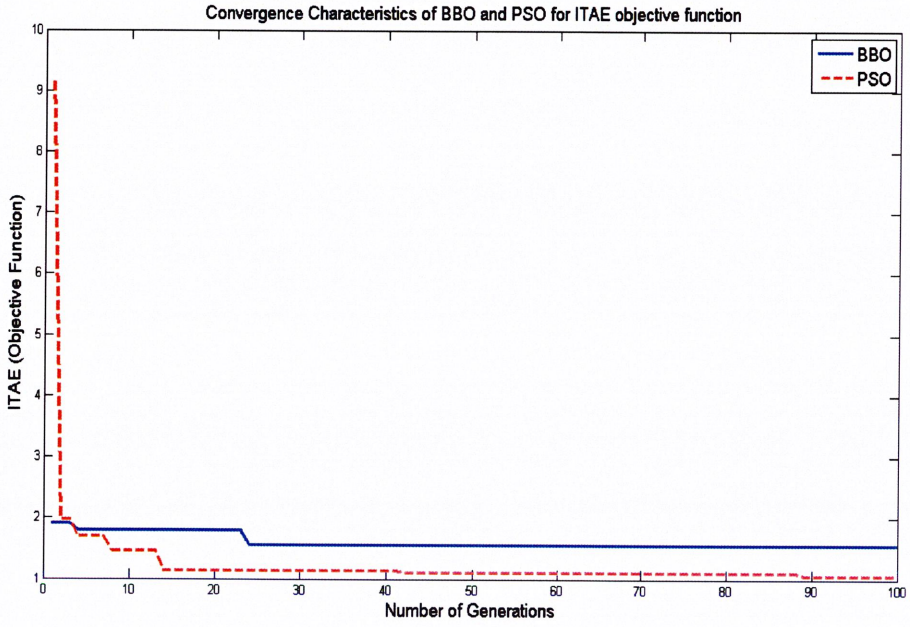


Figure (4.3)
Convergence characteristics for BBO and PSO for tuning MIMO controller using ITAE objective function

From figure (4.3), it can be seen that PSO has the minimum value of the objective function. The BBO has saturated after 24 generations.

Table (4.2)
UPFC MIMO controllers parameters using BBO and PSO

		BBO	PSO
Power flow controller	K_{pp}	-0.3042	0.1664
	K_{ip}	2.6602	4.6536
DC voltage regulator	K_{dp}	-6.2967	-7.0429
	K_{di}	-4.5062	-4.6774
AC bus voltage regulator	K_{vp}	4.4366	1.1029
	K_{vi}	9.6876	4.3276
POD controller	K_p	-75.5118	-71.9378
	T_1	0.8917	1.1755
	T_2	0.4514	0.8576
	T_3	0.0349	0.0287
	T_4	0.4890	0.3203

4.4 Simulation Results

In order to assess the system performance of both of the controllers, the system is simulated for a 10% step change in input power at nominal loading condition.

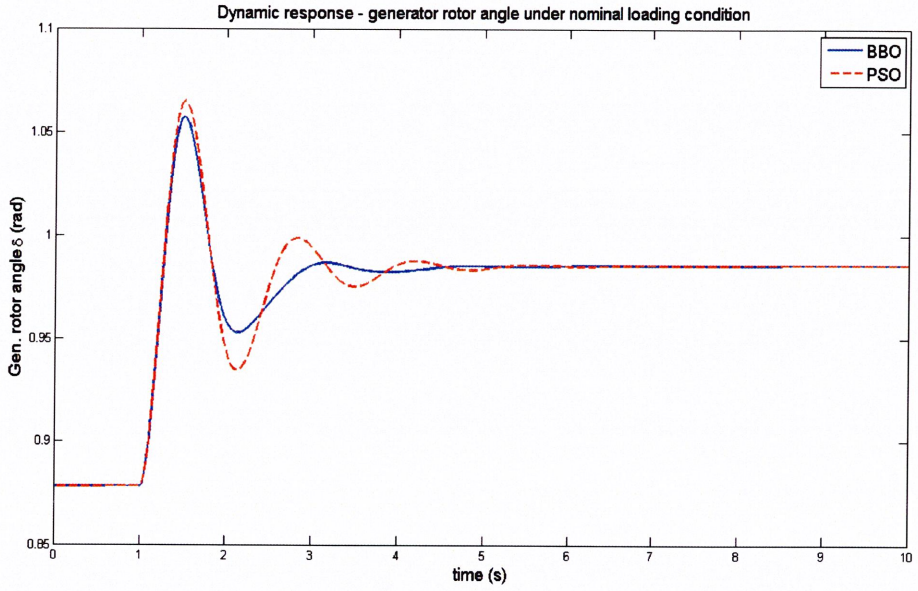


Figure (4.4)
Dynamic response of UPFC MIMO control system - Generator rotor angle δ

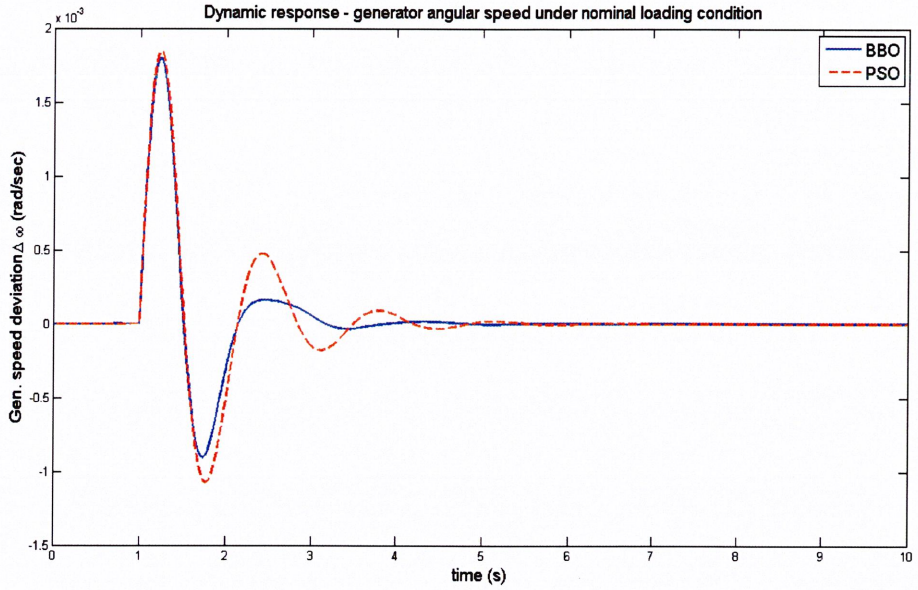


Figure (4.5)
Dynamic response of UPFC MIMO control system - Generator angular speed $\Delta\omega$

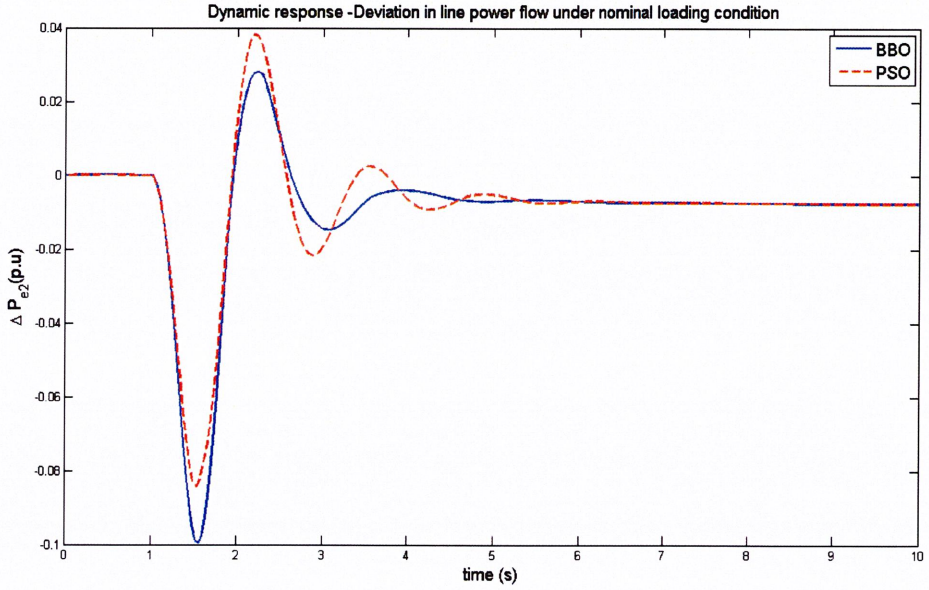


Figure (4.6)
Dynamic response of UPFC MIMO control system - Deviation in regulated power flowΔP_{e2}

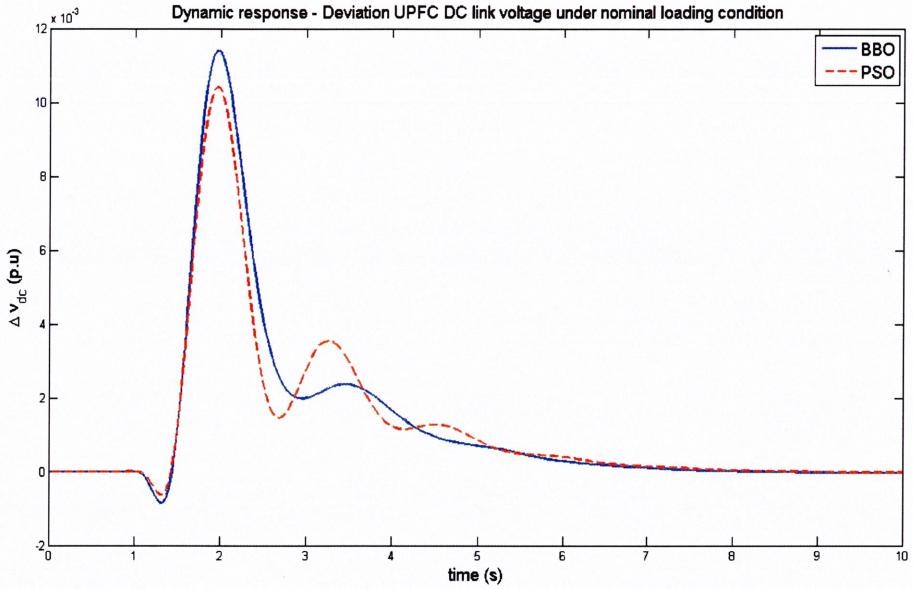


Figure (4.7)
Dynamic response of UPFC MIMO control system - Deviation in UPFC DC link voltage v_{dc}

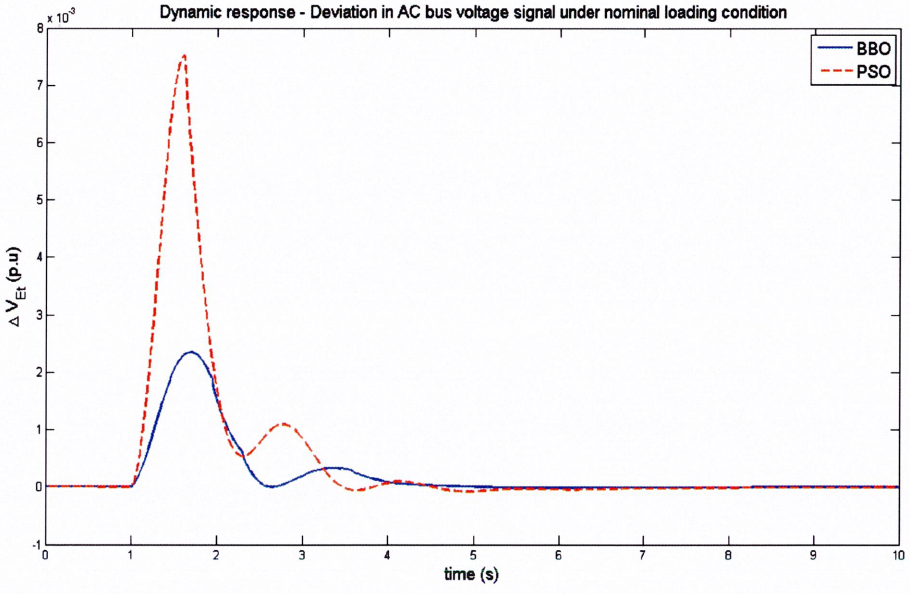


Figure (4.8)
Dynamic response of UPFC MIMO control system - Deviation in AC bus regulated voltage ΔV_{Et}

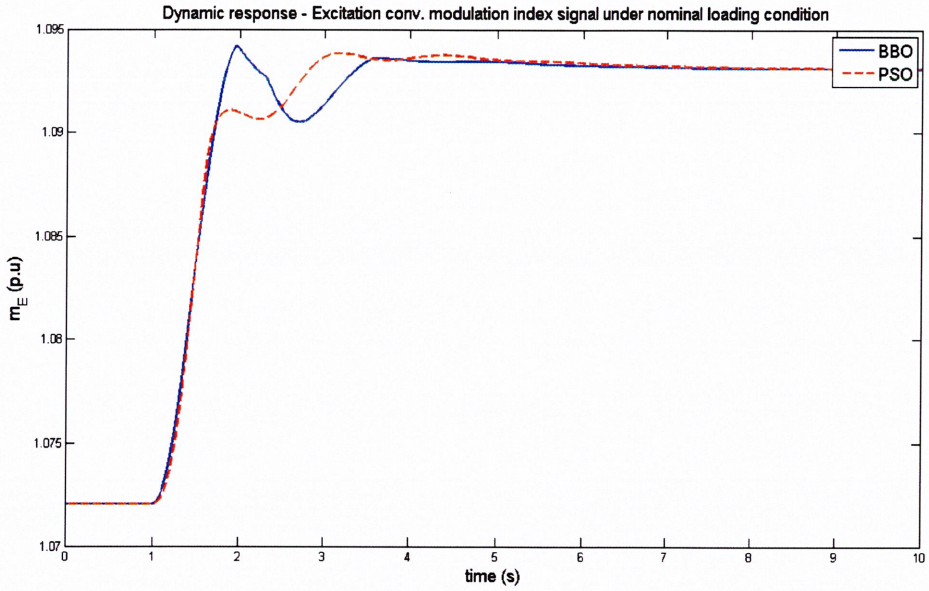


Figure (4.9)
Dynamic response of UPFC MIMO control system - Excitation converter modulation index m_E

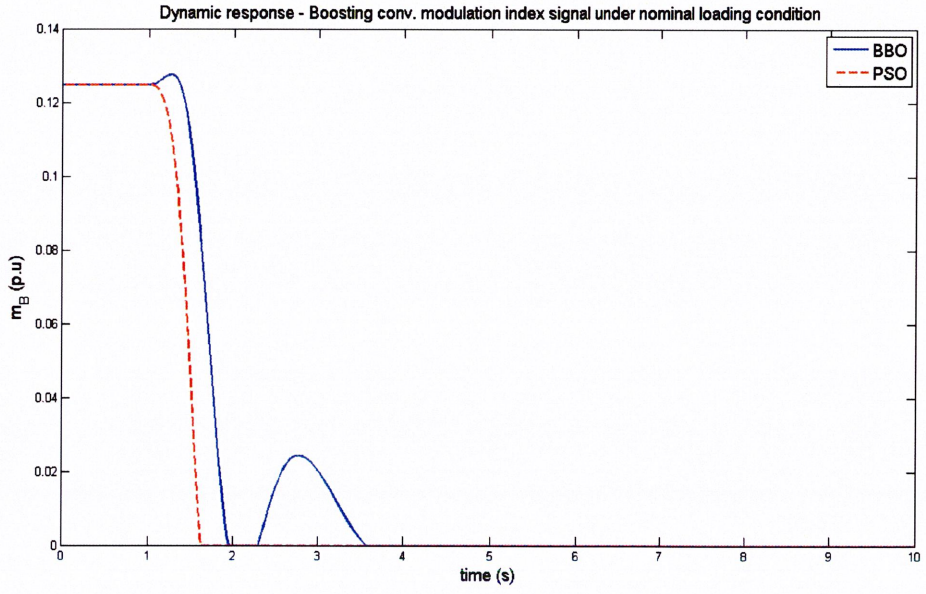


Figure (4.10)
Dynamic response of UPFC MIMO control system - Boosting converter modulation index m_B

Table (4.3)
System eigenvalues for UPFC MIMO control system

	BBO	PSO
System eigenvalues	-76.0770 -17.6464 -17.3556 -10.7422 EM:$-2.3315 \pm j7.1736$ -5.4174 $-1.7260 \pm j3.5746$ -0.2003 -0.6323 $-1.2011 \pm j0.4684$ -1.4453	-32.1477 -19.5078 -17.0007 -13.4112 EM :$-2.6535 \pm j7.2561$ -6.5431 $-1.4914 \pm j3.9534$ $-1.2096 \pm j0.6246$ -0.2003 -0.6282 -1.0373
ζ_{EM}	0.3090	0.3434

From figures 4.4 to 4.10, the dynamic response of the system can be seen for a 10% step change in input mechanical power P_m. It can be seen that the BBO tuned MIMO controller has a better settling time for the damping controller when compared with the PSO tuned MIMO controller, where the settling times are $t_{sBBO} = 2.082$s and $t_{sPSO} = 3.060$s. It can be seen that there is a steady state error in the deviation of the power flow of the compensated line for both controllers, as the boosting modulation index saturates at its low limit in both cases. The settling time for both controllers for the DC voltage regulator is almost the same, but they vary in the settling time of the AC bus voltage regulator. Moreover, the damping of the electromechanical modes for both controllers is given in table 4.3, along with the system eigenvalues. It can be seen that PSO controller provide more damping for those oscillations when compared with BBO controllers.

In order to assess the ability of the control system to track the setpoint given, therefore a step input of 0.1 p.u for the compensated line power flow is given to the system. The figures (4.11) to (4.15), illustrates the system response for the step input disturbance in the power flow:

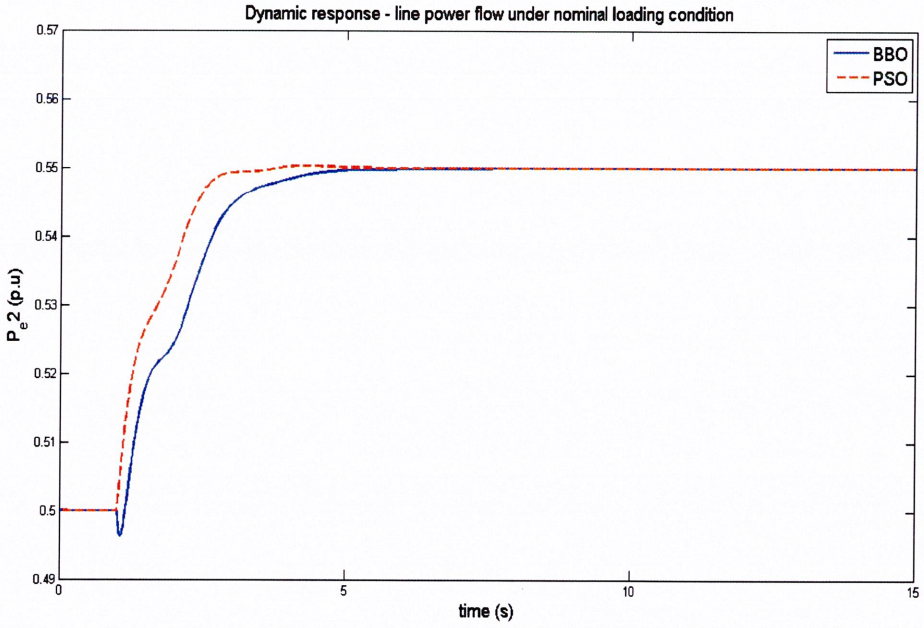


Figure (4.11)
Line power flow P_{e2}

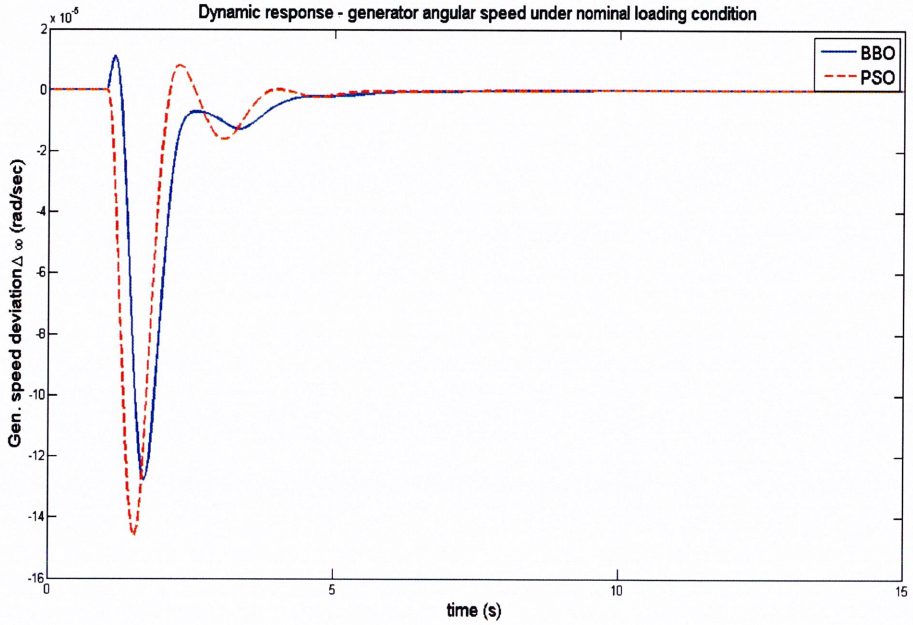


Figure (4.12)
Generator angular speed deviation

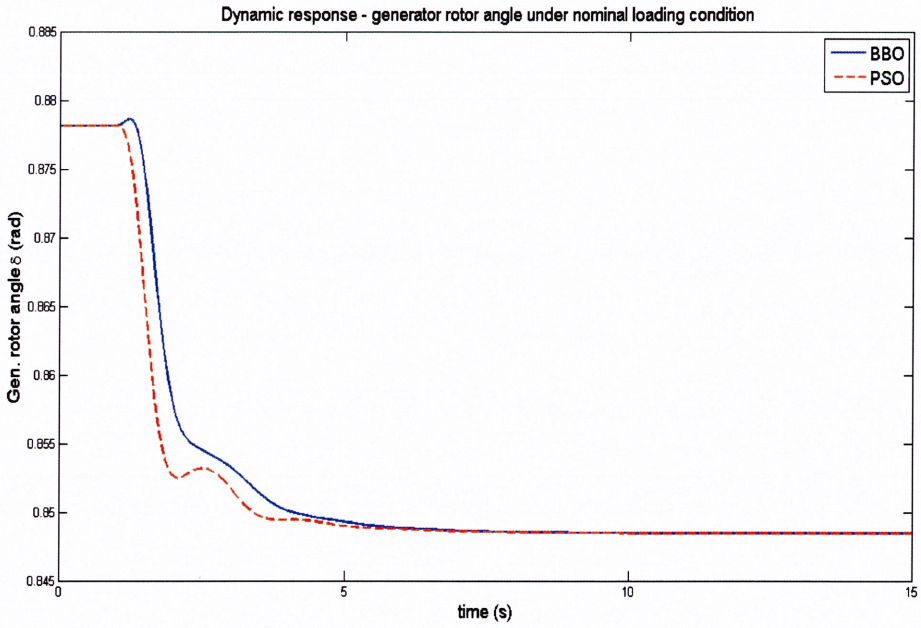


Figure (4.13)
Generator rotor angle

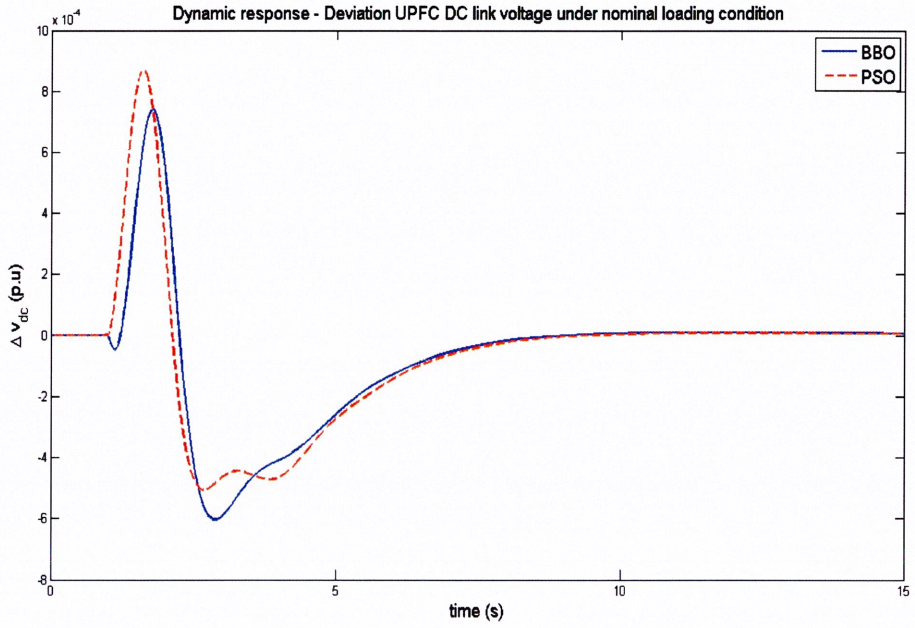


Figure (4.14)
Deviation in UPFC DC link voltage Δv_{dc}

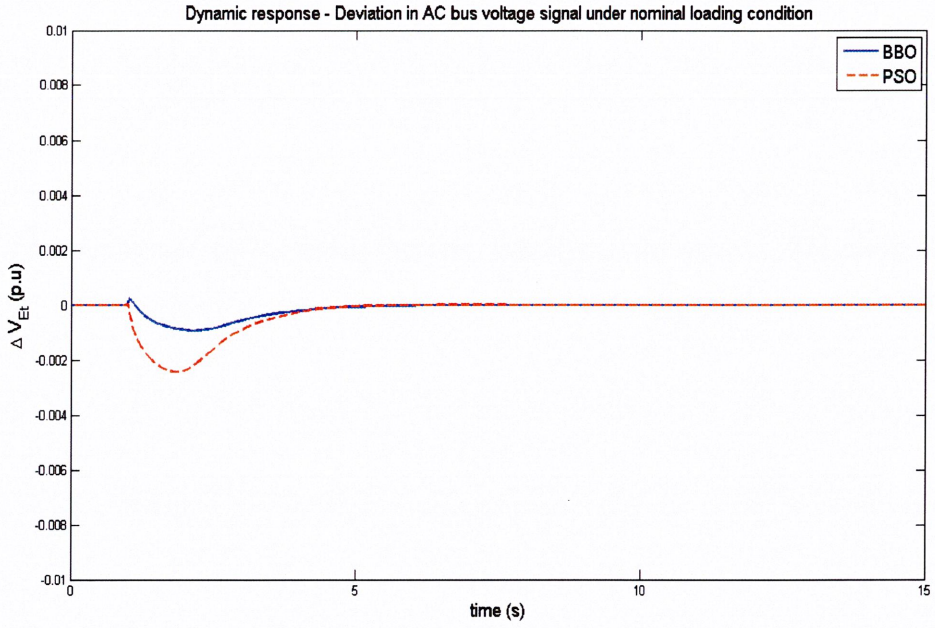


Figure (4.15)
Deviation in AC bus voltage ΔV_{Et}

It can be seen that the system is able to track the setpoint with no steady state error and that is for all of the controlled variables. Moreover, the controller was able to damp the oscillations in the response effectively after the introduction of the disturbance, which can be seen from the $\Delta\omega$ response plot. The settling time of the line power flow is t_s= 2.013 sec for PSO ,while for BBO the settling time is t_s= 3.566 sec. The DC voltage regulator had the highest settling time in all of the responses of $t_s = 7$ sec for both algorithms, in which it returned to its previous value.

Chapter 5

Control System Performance Analysis

- **5.1 Overview**
- **5.2 Response Analysis for Power Oscillation Damping (POD) Controller**
- **5.3 Response Analysis for Multi-Input Multi-Output (MIMO) UPFC Control System**

Chapter 5
Control System Performance Analysis

5.1 Overview

This chapter presents the simulation results and analysis of the controllers designed in chapters 3 and 4. In the first section of this chapter, the controllers that have been designed in chapter 3 will be investigated for a large disturbance introduced at the system at different generator loading conditions with different system uncertainties. The system response will be compared with nominal system conditions - without any system uncertainties, the analysis of the response will be based on:

1. Steady state system response.

2. Transient state system response, and that is by considering the following::

   (a) Robustness.

   (b) Stability.

   (c) Settling time.

   (d) Peak attained.

After that, an investigation on the possibility of system response enhancement through fine tuning of the DC voltage regulator is presented. The response will be analyzed using the above performance criterion.

At the second section of this chapter, the MIMO control systems designed in the previous chapter will be examined and analyzed. The control system will be assessed for different system disturbances at different loading conditions, and they are:

1. Variation in power flow compensation factor: this will investigate the ability of the control system to adhere to the changes in setpoint, which is a common practice in industry as the load changes based on the system requirements.

2. Output disturbance: this will investigate the ability of the control system to maintain the output within the limits following a disturbance to the system. A sudden load change in the second transmission line is going to be considered; where the system will be simulated for a three phase disturbance to ground in the compensated transmission line.

3. Three phase fault at generator bus: this will test the ability of the damping controller to return the system to the pre-fault operating condition, during this test the control system robustness will be examined also as different uncertainties are introduced in the system.

5.2 Response Analysis for Power Oscillation Damping (POD) Controller

5.2.1 Response Analysis under System Uncertainties

In here an analysis for the damping controllers that were designed in chapter 3, based on the ζ objective function and ITAE objective function is performed. The controllers are simulated at four different operating conditions for a 10% step change in mechanical power P_m with four different parameter uncertainties as given in table 5.1:

Table (5.1)
System operating points and its uncertainties

Loading Condition	P_e	Q_e	System Parameter uncertainty
Light Loading	0.30	0.015	30% increase in line reactance x_{t1}
Nominal Loading	1.0	0.015	30% increase in compensated line reactance x_{Bv}
Heavy Loading	1.1	0.4	25% increase in machine inertia M
Leading power factor	0.7	-0.03	30% increase in field time constant T'_{do}

5.2.1.1 Light Loading Condition

Figures (5.1) to (5.4), illustrates the system response for a 10% step change in mechanical input power P_m under light loading condition ($P_e = 0.3$ p.u and $Q_e = 0.015$ p.u). Each figure, contains two system responses, the first (in blue continuous line) represents the response under nominal system conditions, no uncertainties are present, while the second response (in green dashed line) represent the response under system uncertainty, and in this case it is 30% increase in reactance of the uncompensated line x_{t1}.

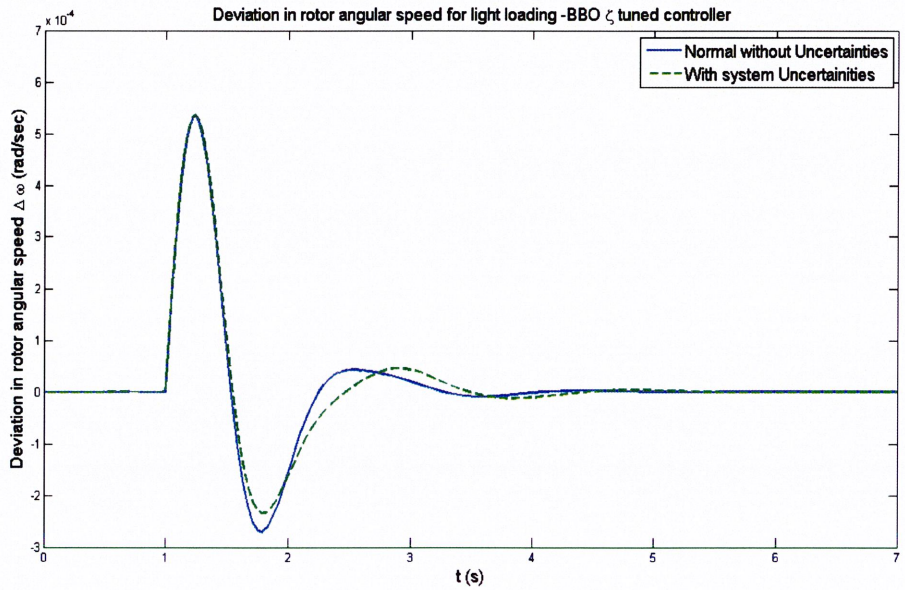


Figure (5.1)
System uncertainty - Dynamic response of POD controller tuned with BBO algorithm for ζ-objective function under light loading condition

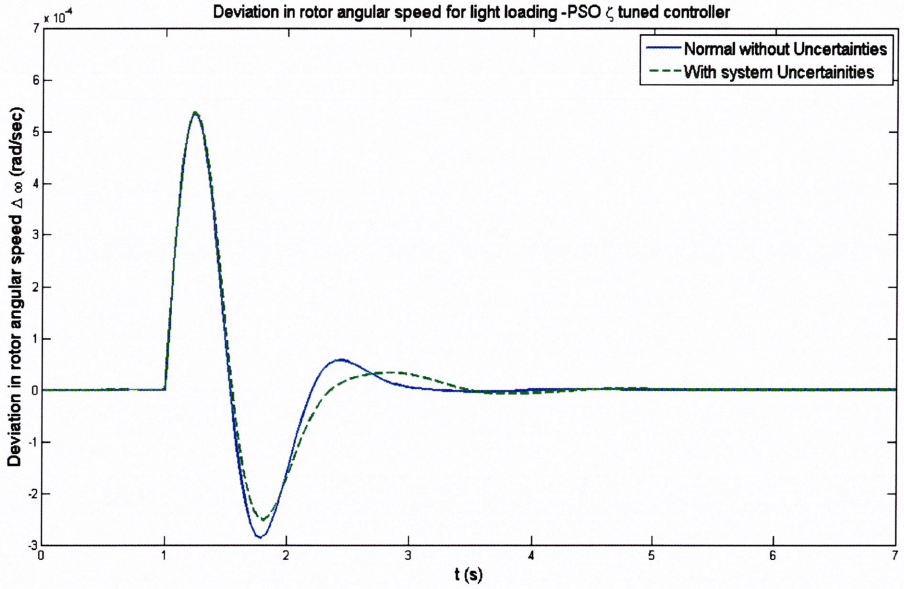


Figure (5.2)
System uncertainty - Dynamic response of POD controller tuned with PSO algorithm for ζ-objective function under light loading condition

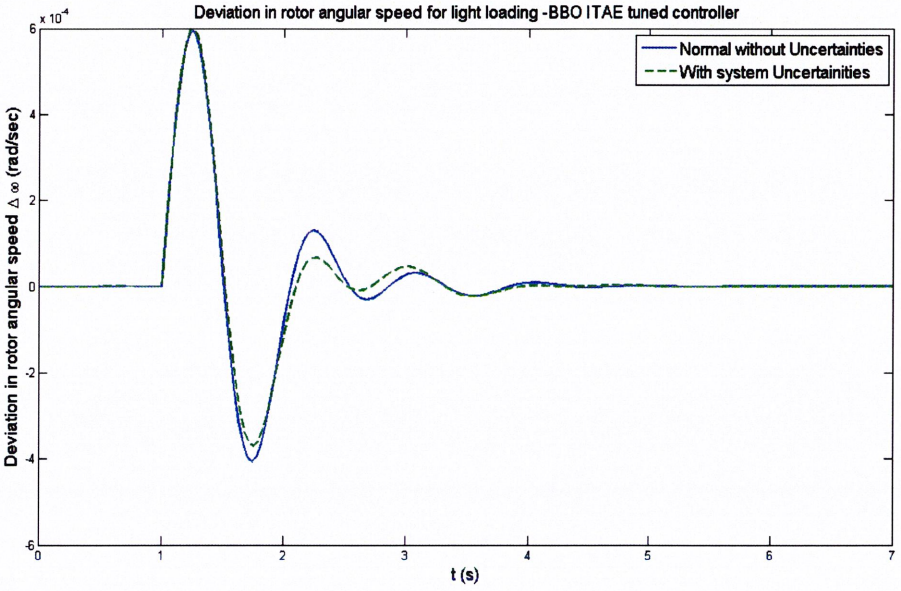


Figure (5.3)
System uncertainty - Dynamic response of POD controller tuned with BBO algorithm for ITAE-objective function under light loading condition

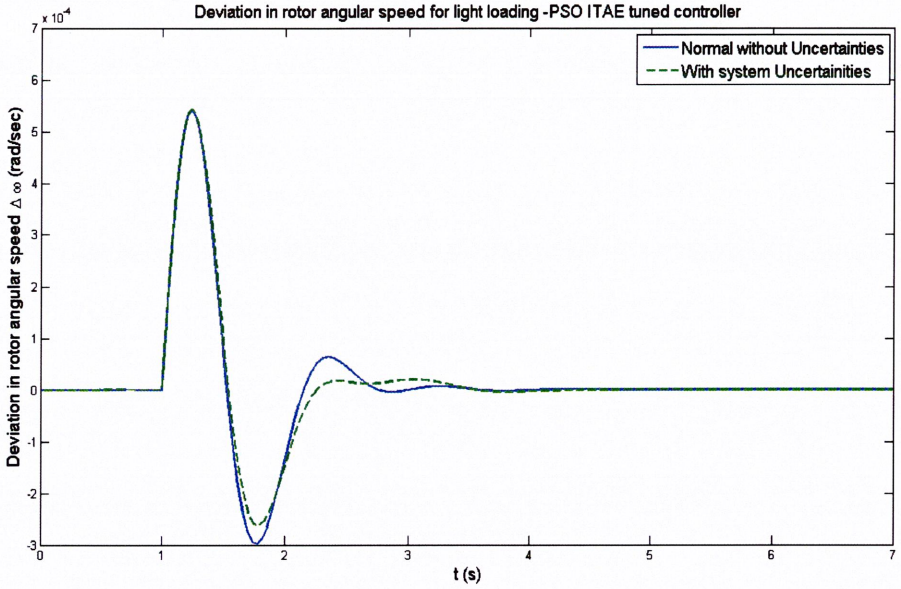


Figure (5.4)
System uncertainty - Dynamic response of POD controller tuned with PSO algorithm for ITAE-objective function under light loading condition

From the figures, it can be seen that the POD controllers in all cases are able to maintain the system stability even in the presence of the uncertainty. The system performance changed from the nominal system conditions and that can be seen in table (5.2):

Table (5.2)
System performance under light loading conditions in the presence of uncertainty for POD controllers

	Settling time t_s		Peak		ζ_{EM}	
	Nominal	Uncertainty	Nominal	Uncertainty	Nominal	Uncertainty
BBO - ζ	1.0992	1.1534	0.0005	0.0005	0.3829	0.3685
PSO - ζ	1.0916	1.1330	0.0005	0.0005	0.3939	0.3861
BBO - ITAE	1.3606	1.0507	0.0006	0.0006	0.2125	0.2178
PSO - ITAE	1.0727	1.0851	0.0005	0.0005	0.3309	0.3410

From this it can be seen that BBO ITAE POD controller, have a better settling time when compared to the other controllers after the uncertainty has been introduced. The problem with the BBO ITAE POD controller is

that it has the greatest peak compared to the other controllers. Moreover the damping of the EM modes it has the lowest damping factor.

5.2.1.2 Nominal Loading Condition

Similarly, figures (5.5) to (5.8) illustrate the system response for the POD controllers under nominal loading conditions, with and without system uncertainties.

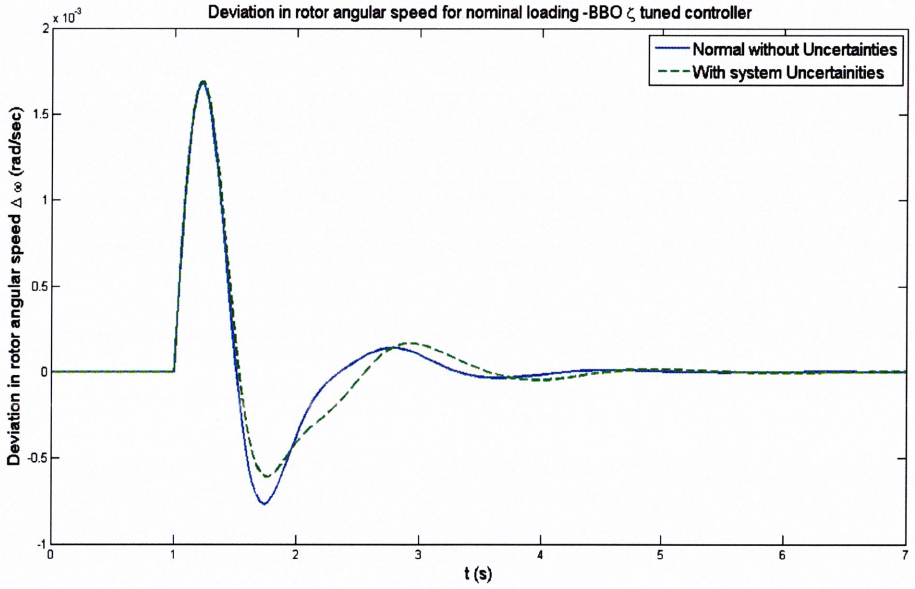


Figure (5.5)
System uncertainty - Dynamic response of POD controller tuned with BBO algorithm for ζ-objective function under nominal loading condition

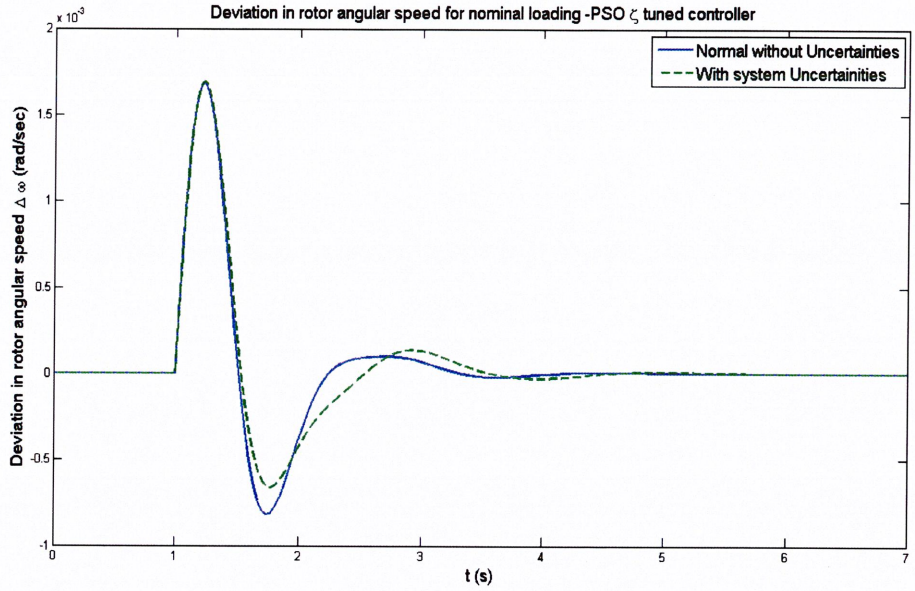


Figure (5.6)
System uncertainty - Dynamic response of POD controller tuned with PSO algorithm for ζ-objective function under nominal loading condition

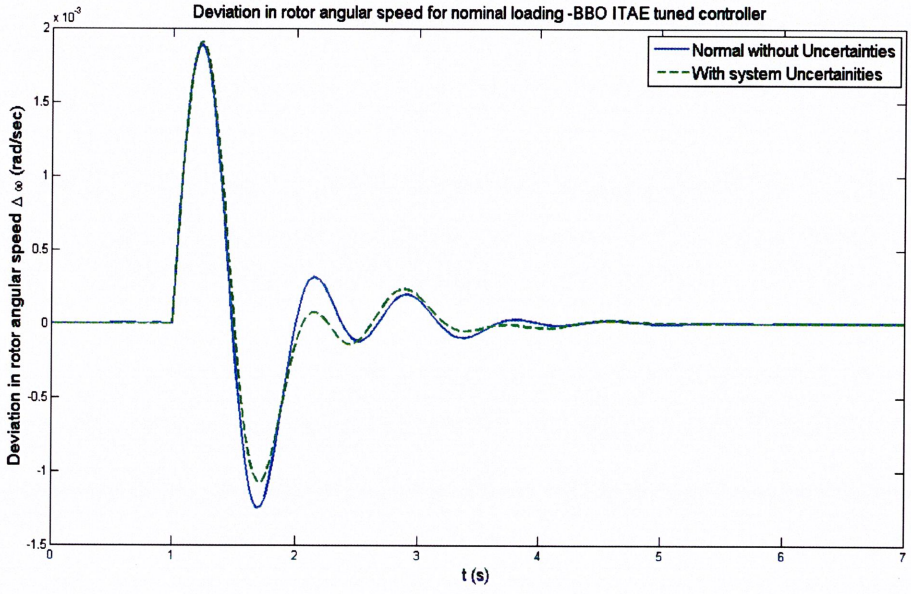


Figure (5.7)
System uncertainty - Dynamic response of POD controller tuned with BBO algorithm for ITAE-objective function under nominal loading condition

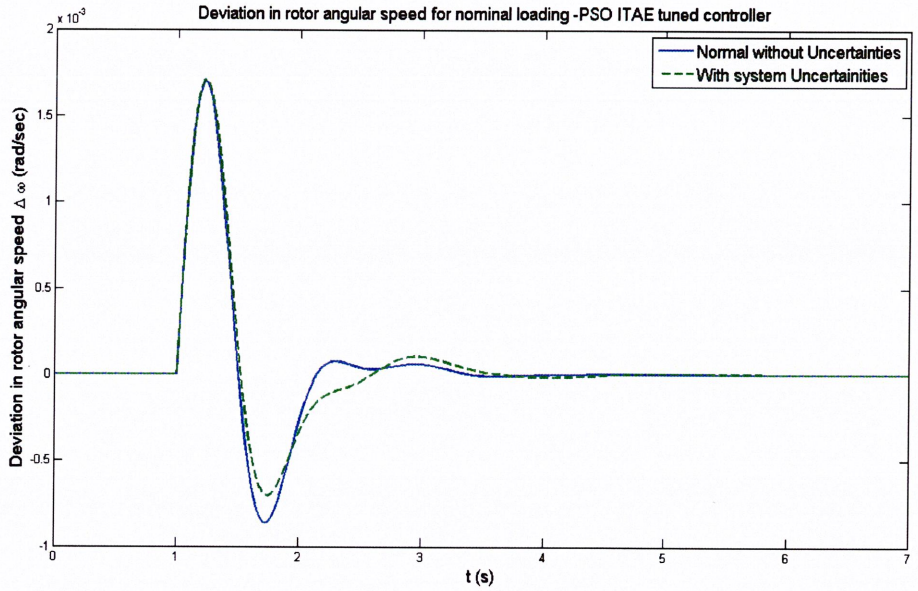


Figure (5.8)
System uncertainty - Dynamic response of POD controller tuned with PSO algorithm for ITAE-objective function under nominal loading condition

The control system is robust, as it was able to maintain the stability of the system in the presence of uncertainty. The degradation of performance can be seen from figures and it is fully given in the following table:

Table (5.3)
System performance under nominal loading conditions in the presence of uncertainty for POD controllers

	Settling time t_s		Peak		ζ_{EM}	
	Nominal	Uncertainty	Nominal	Uncertainty	Nominal	Uncertainty
BBO - ζ	2.0096	2.2776	0.0017	0.0017	0.3608	0.3486
PSO - ζ	1.1670	2.1871	0.0017	0.0017	0.3831	0.3757
BBO - ITAE	2.0905	2.1383	0.0019	0.0019	0.1911	0.2000
PSO - ITAE	1.0862	2.0647	0.0017	0.0017	0.3342	0.3383

5.2.1.3 Heavy Loading Condition

In here the system is simulated under generator loading conditions ($P_e = 1.1$ p.u and $Q_e = 0.4$ p.u). The uncertainty introduced in here, is

a 25% increase in machine inertia M. The figures (5.9) to (5.12) represent the system response for a 10% step change in mechanical input power P_m.

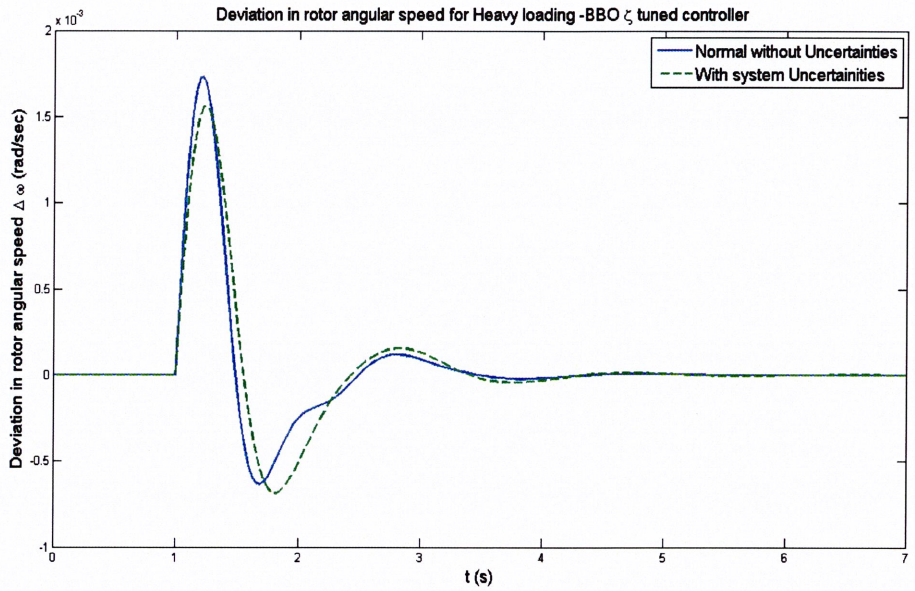


Figure (5.9)
System uncertainty - Dynamic response of POD controller tuned with BBO algorithm for ζ-objective function under heavy loading condition

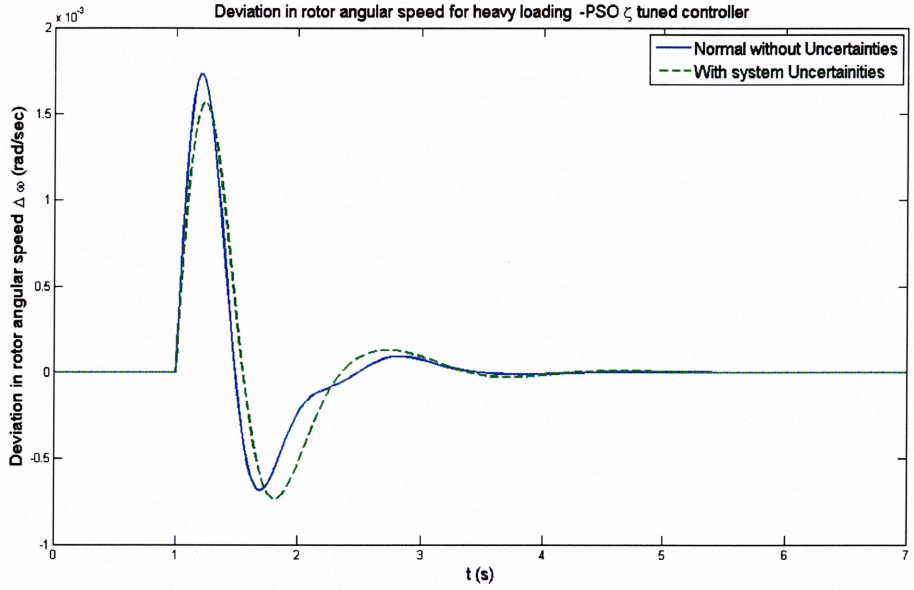


Figure (5.10)
System uncertainty - Dynamic response of POD controller tuned with PSO algorithm for ζ-objective function under heavy loading condition

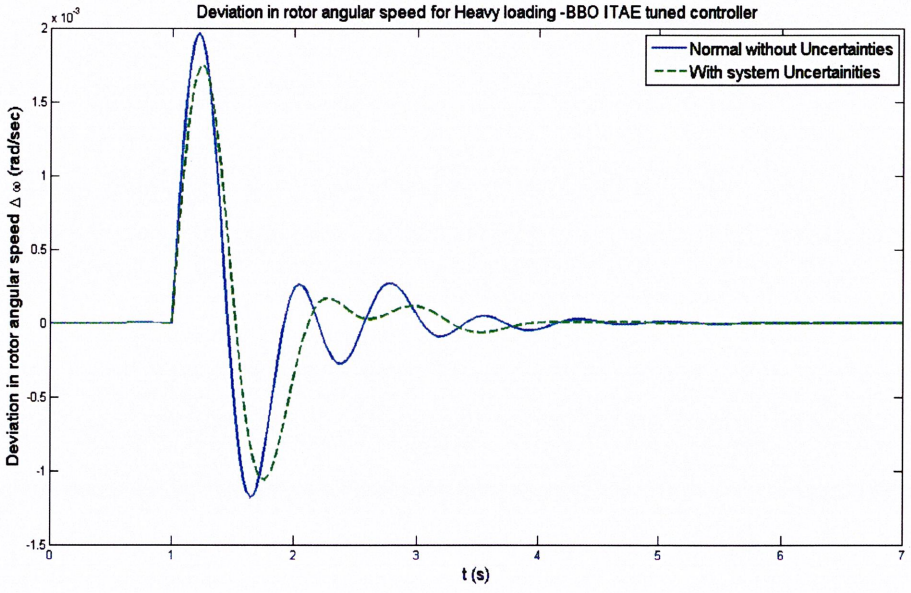


Figure (5.11)
System uncertainty - Dynamic response of POD controller tuned with BBO algorithm for ITAE-objective function under heavy loading condition

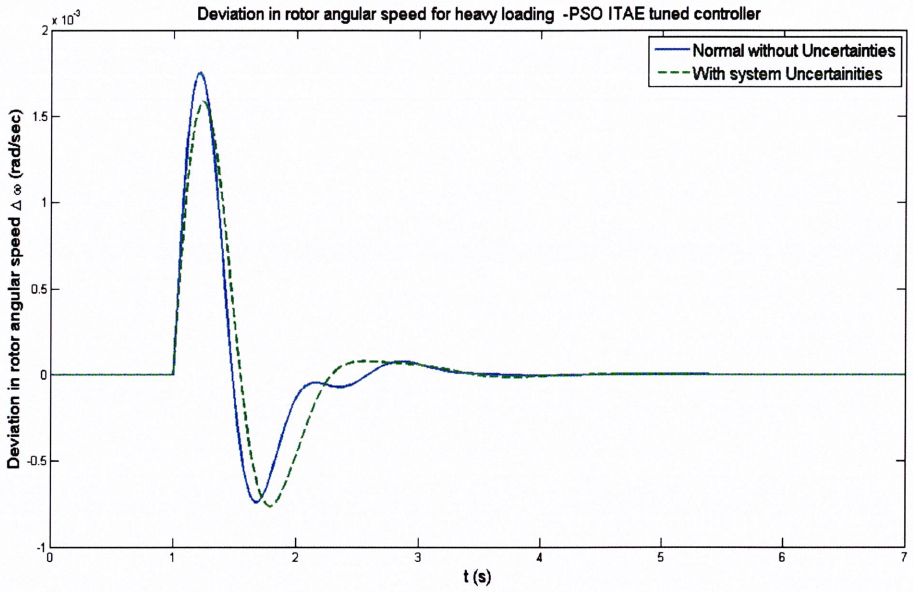


Figure (5.12)
System uncertainty - Dynamic response of POD controller tuned with PSO algorithm for ITAE-objective function under heavy loading condition

As expected, that by increasing the machine inertia it becomes more stable, which in other terms improved the system performance and that can be seen in the figures above. Table (5.4), shows all the performance indices:

Table (5.4)
System performance under heavy loading conditions in the presence of uncertainty for POD controllers

	Settling time t_s		Peak		ζ_{EM}	
	Nominal	Uncertainty	Nominal	Uncertainty	Nominal	Uncertainty
BBO - ζ	2.0117	2.1129	0.0017	0.0016	0.3281	0.3702
PSO - ζ	1.2246	2.0246	0.0017	0.0016	0.3511	0.4279
BBO - ITAE	1.9878	2.1090	0.0020	0.0017	0.1638	0.2403
PSO - ITAE	1.0448	1.2183	0.0018	0.0016	0.3120	0.3823

It can be seen that the damping ratio of the electromechanical modes has increased, but the settling time has increased and that can be seen that due to the increase in peak time of the response, hence the response of nominal system condition attain the value of the output before the response in

case of the uncertainty (in here the settling time is taken once the output is between $\Delta\omega = \pm 1 \times 10^{-4}$)

5.2.1.4 Leading Loading Condition

Leading power factor loading condition of the generator is considered in this test. The system is simulated with and without uncertainty, 30% change in T'_{d0}, for a 10% step change in P_m as have been done in the cased before.

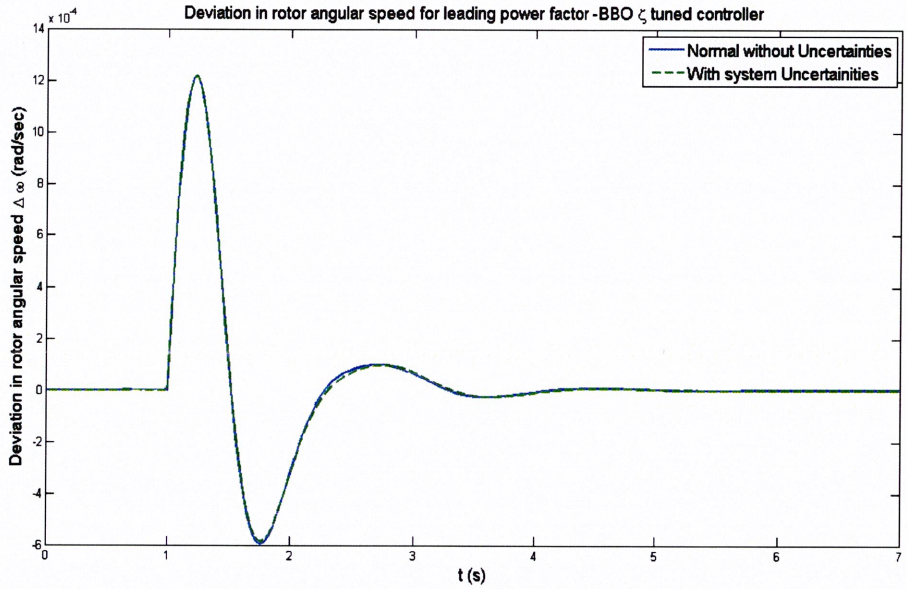


Figure (5.13)
System uncertainty - Dynamic response of POD controller tuned with BBO algorithm for ζ-objective function under leading power factor loading condition

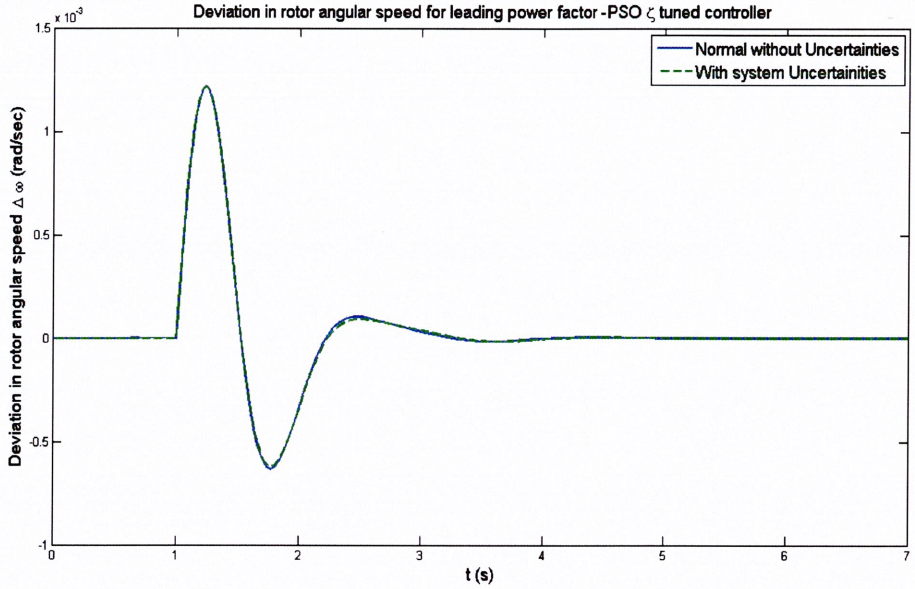


Figure (5.14)
System uncertainty - Dynamic response of POD controller tuned with PSO algorithm for ζ-objective function under leading power factor loading condition

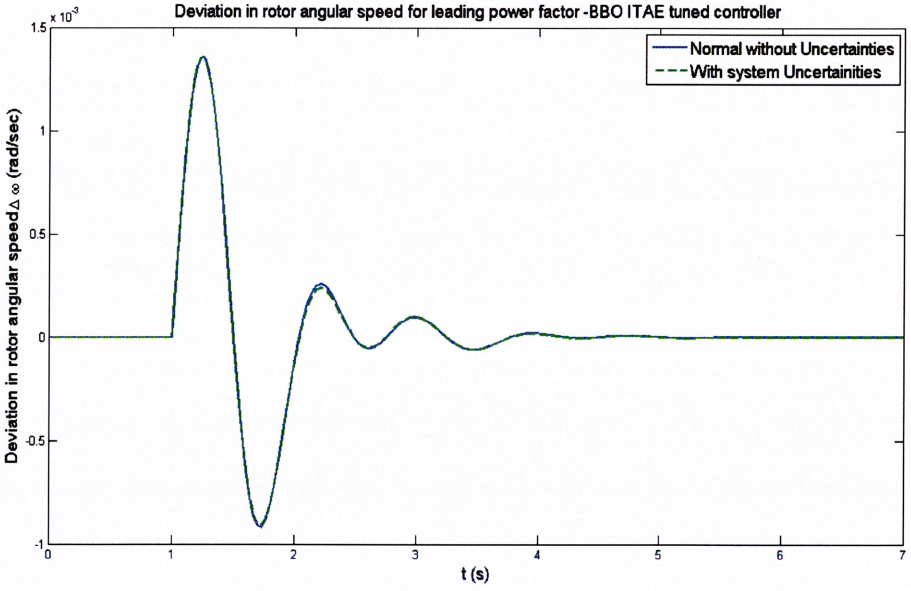


Figure (5.15)
System uncertainty - Dynamic response of POD controller tuned with BBO algorithm for ITAE-objective function under leading power factor loading condition

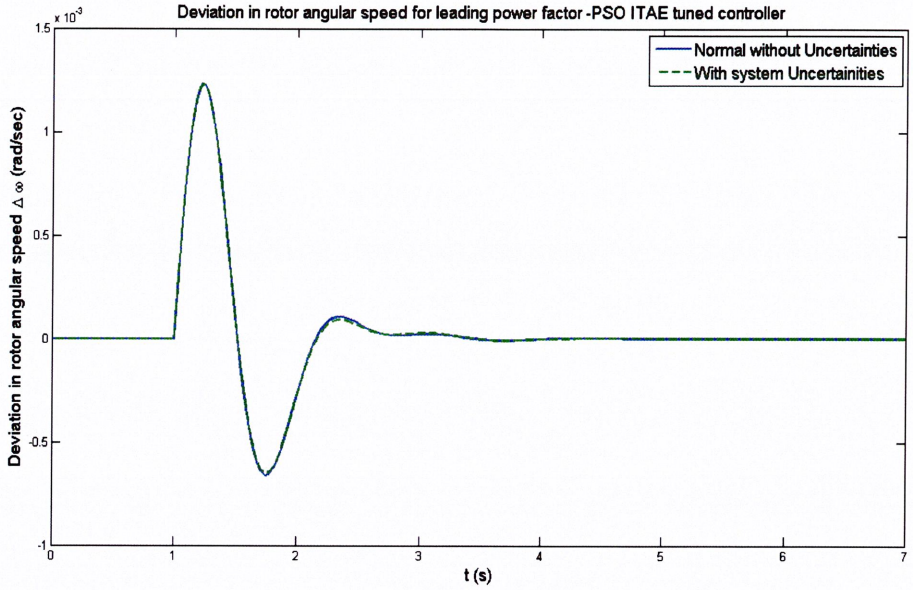


Figure (5.16)
System uncertainty - Dynamic response of POD controller tuned with PSO algorithm for ITAE-objective function under leading power factor loading condition

The system seems not to be affected with such uncertainty, hence it is robust for such degradation in system parameters. The performance of the control system is analyzed in table (5.5):

Table (5.5)
System performance under leading power factor loading conditions in the presence of uncertainty for POD controllers

	Settling time t_s		Peak		ζ- EM	
	Nominal	Uncertainty	Nominal	Uncertainty	Nominal	Uncertainty
BBO - ζ	1.1661	1.2084	0.0012	0.0012	0.3793	0.3769
PSO - ζ	1.5724	1.1883	0.0012	0.0012	0.3992	0.3955
BBO - ITAE	1.4119	1.4130	0.0014	0.0014	0.2084	0.2084
PSO - ITAE	1.4139	1.0977	0.0012	0.0012	0.3423	0.3405

5.2.2 Analysis of Fine tuned system response

In this section the possibility of fine tuning the system response through changing the DC regulator gains (K_{dp} and K_{di}),the system behavior is to be

improved as these algorithms are stochastic process, so there is no guarantee that an optimal solution is obtained. The system is simulated for the same loading conditions and with the uncertainties presented above. The POD controllers are tuned with $K_{dp} = -7.15$ and $K_{di} = -1.15$. Each figure, represents the system before and after fine tuning. The results are discussed and analyzed in the following sections for every loading condition.

5.2.2.1 Light Loading Condition

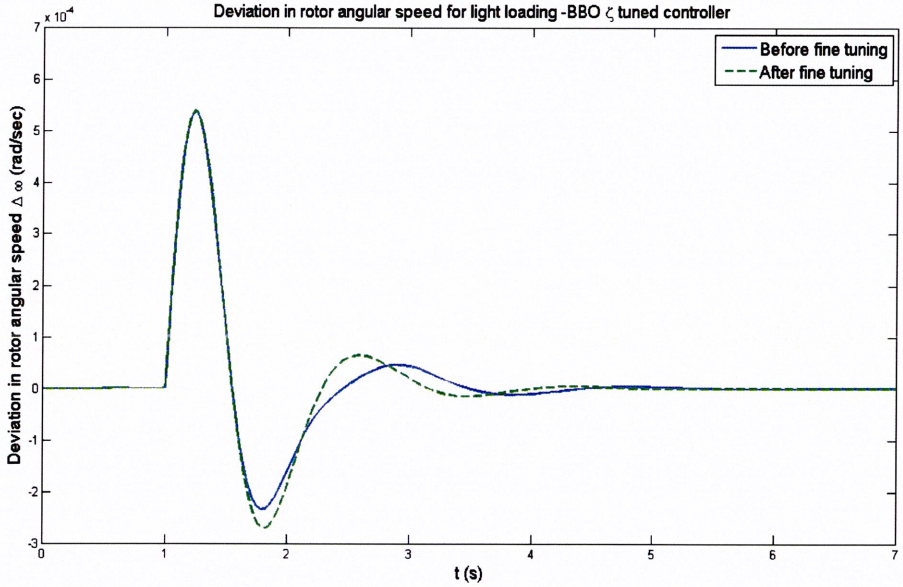


Figure (5.17)
Fine tuning - Dynamic response of POD controller tuned with BBO algorithm for ζ-objective function under light loading condition

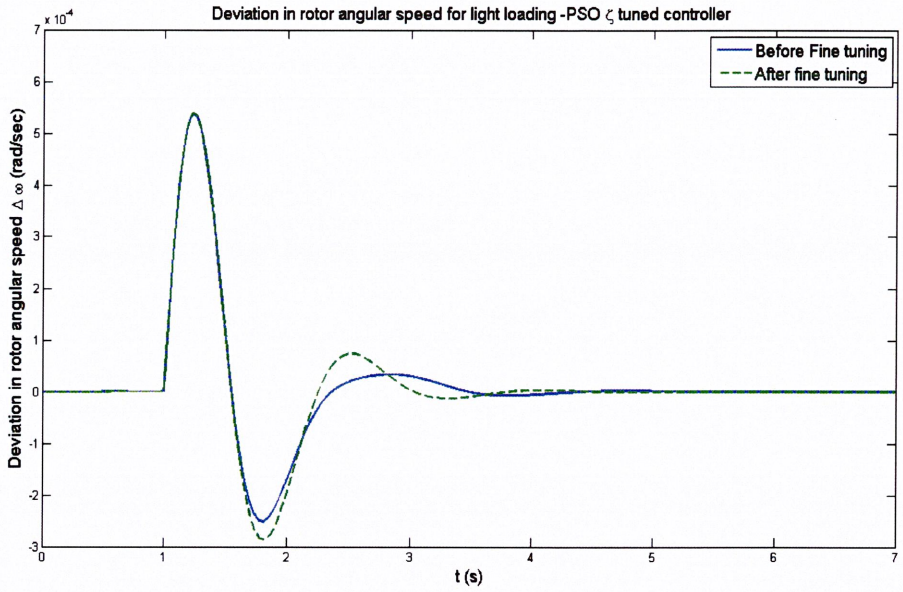


Figure (5.18)
Fine tuning - Dynamic response of POD controller tuned with PSO algorithm for ζ-objective function under light loading condition

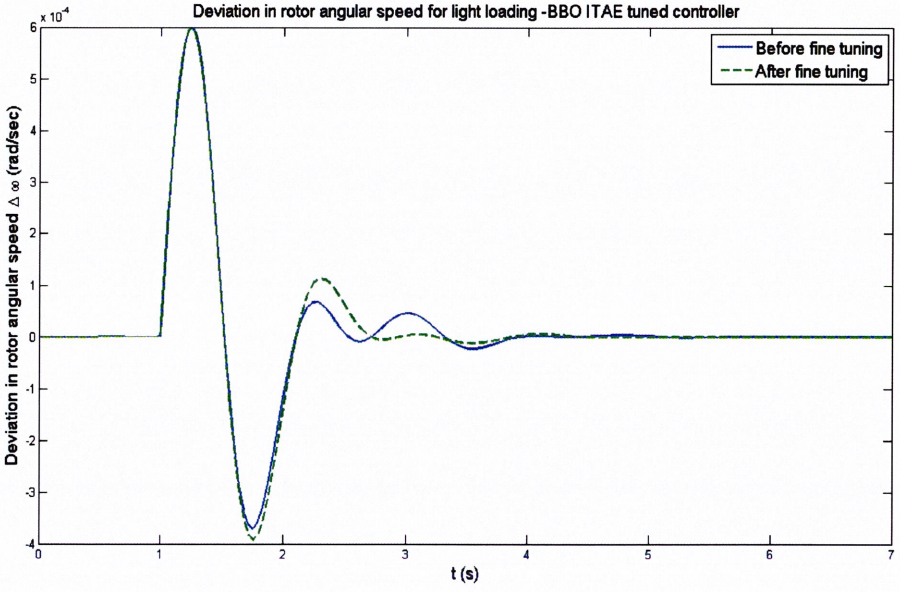


Figure (5.19)
Fine tuning - Dynamic response of POD controller tuned with BBO algorithm for ITAE-objective function under light loading condition

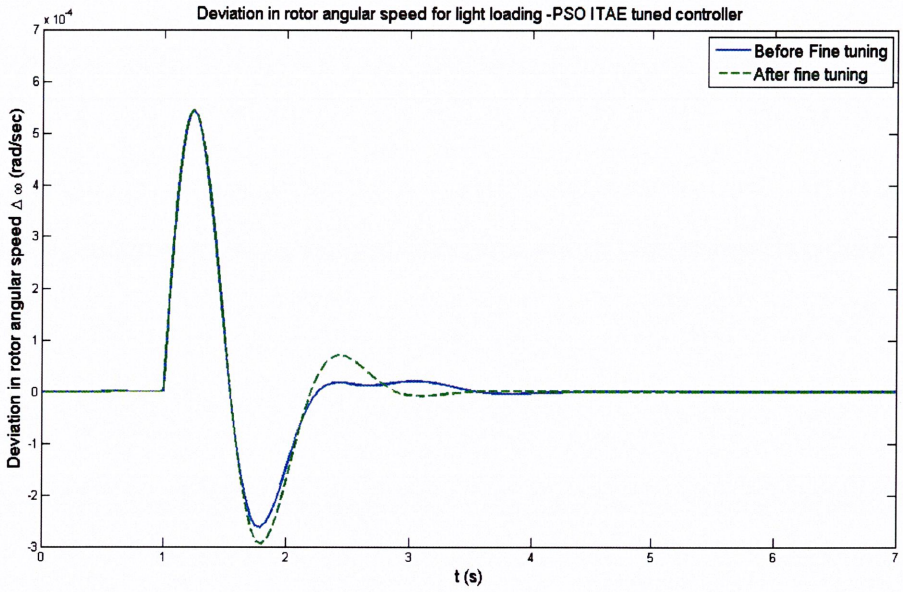


Figure (5.20)
Fine tuning - Dynamic response of POD controller tuned with PSO algorithm for ITAE-objective function under light loading condition

Table (5.6)
System performance before and after fine tuning under light loading conditions for POD controllers

	Settling time t_s		Peak		ζ_{EM}	
	Before	After	Before	After	Before	After
BBO - ζ	1.1534	1.1659	0.0005	0.0005	0.3685	0.3944
PSO - ζ	1.1330	1.1581	0.0005	0.0005	0.3861	0.4500
BBO - ITAE	1.0507	1.4365	0.0006	0.0006	0.2178	0.2657
PSO - ITAE	1.0851	1.1120	0.0005	0.0005	0.3410	0.4223

From figures (5.17) to (5.20) and table (5.6), it can be seen that the system performance has improved through fine tuning the DC regulator. A decrease in the settling time of the response, as well as an increase in the damping ratio of the electromechanical modes for all of the controllers. By comparing the responses it can be seen that the ITAE PSO tuned POD controller has a superior performance compared to the other controllers.

5.2.2.2 Nominal Loading Condition

This section, represents the dynamics response of the system at nominal loading condition after fine tuning. The system responses are given in figures (5.21) to (5.24):

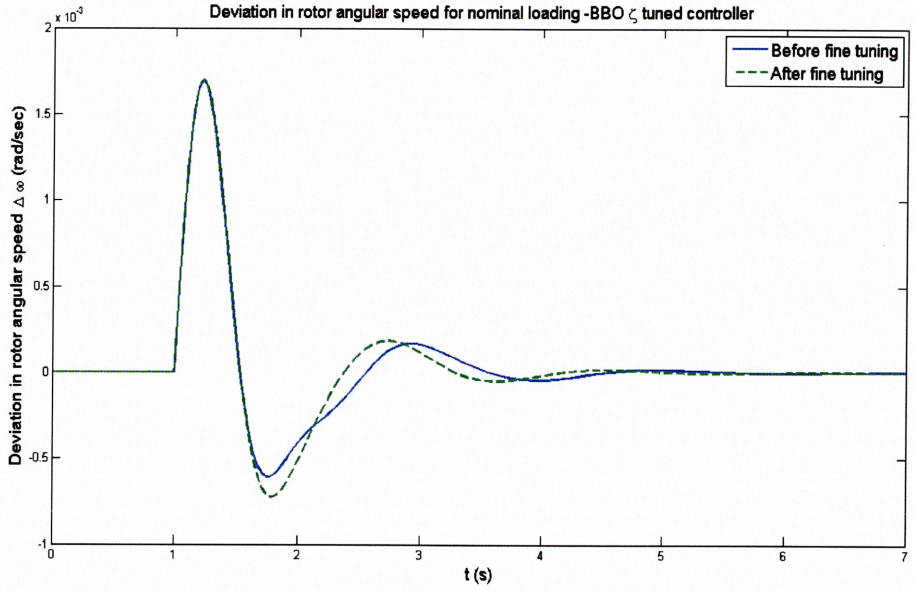


Figure (5.21)
Fine tuning - Dynamic response of POD controller tuned with BBO algorithm for ζ-objective function under nominal loading condition

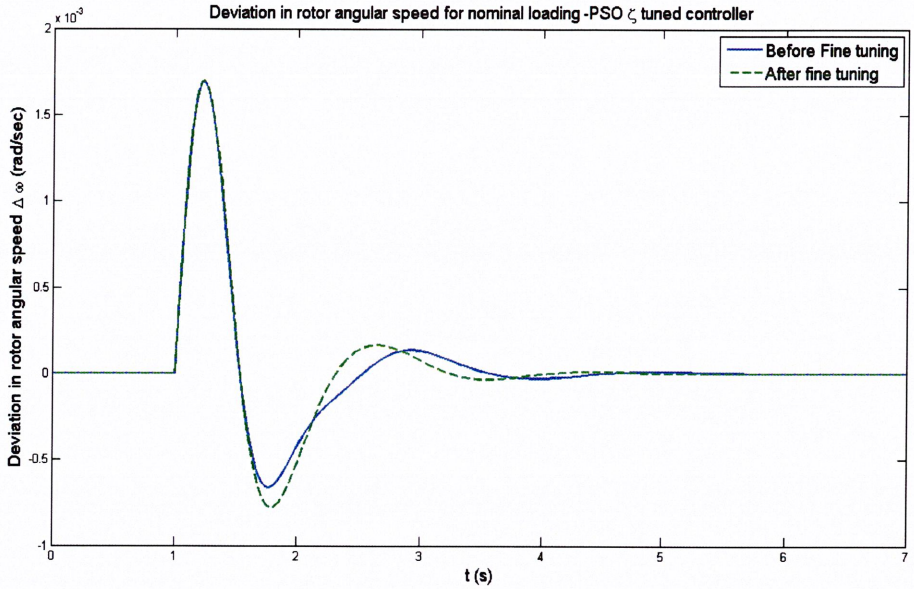


Figure (5.22)
Fine tuning - Dynamic response of POD controller tuned with PSO algorithm for ζ-objective function under nominal loading condition

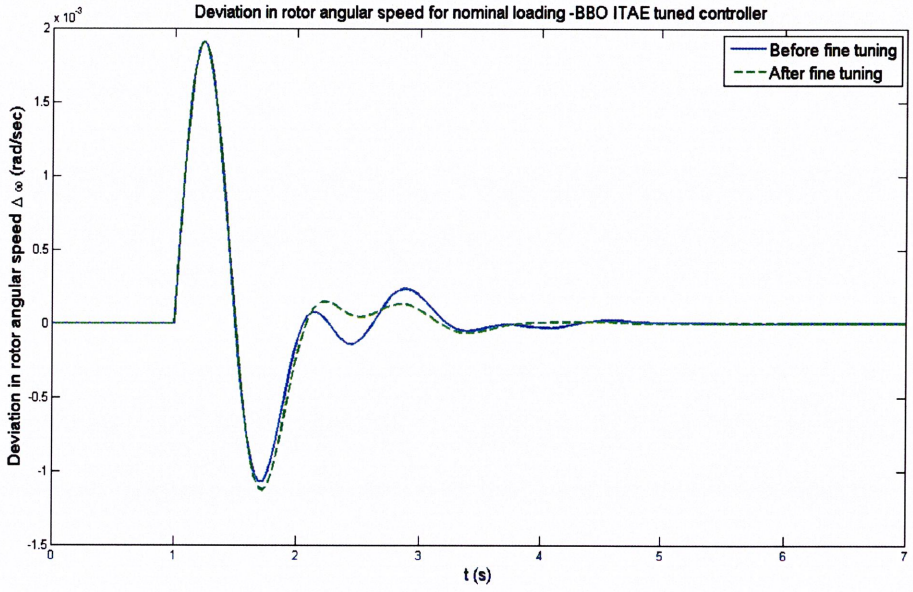


Figure (5.23)
Fine tuning - Dynamic response of POD controller tuned with BBO algorithm for ITAE-objective function under nominal loading condition

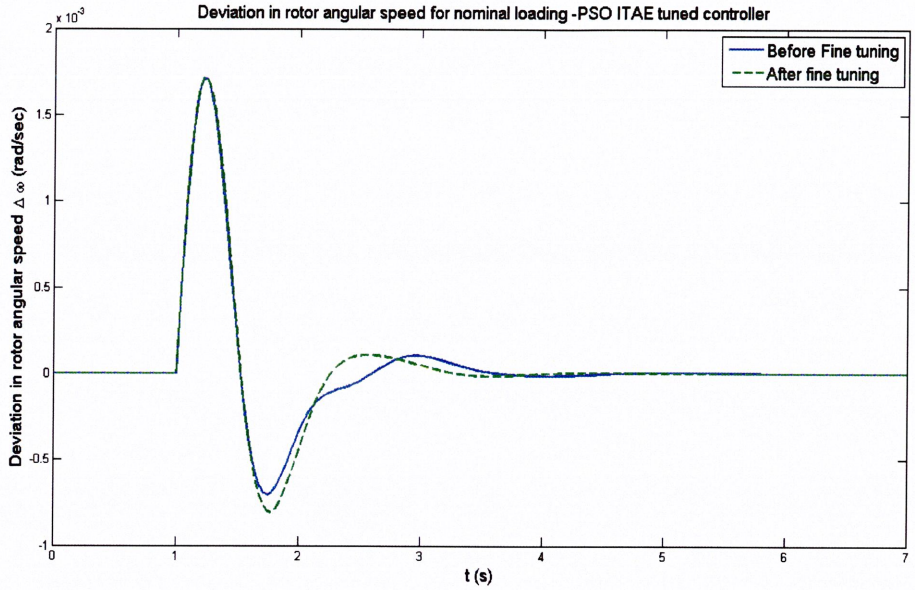


Figure (5.24)
Fine tuning - Dynamic response of POD controller tuned with PSO algorithm for ITAE-objective function under nominal loading condition

Table (5.7)
System performance before and after fine tuning under nominal loading conditions for POD controllers

	Settling time t_s		Peak		ζ_{EM}	
	Before	After	Before	After	Before	After
BBO - ζ	2.2776	2.0684	0.0017	0.0017	0.3486	0.3671
PSO - ζ	2.1871	1.9718	0.0017	0.0017	0.3757	0.4202
BBO - ITAE	2.1383	2.0303	0.0019	0.0019	0.2000	0.2477
PSO - ITAE	2.0647	1.7418	0.0017	0.0017	0.3383	0.4342

Similar to the previous case, the system performance has improved after the fine tuning and this can be seen from table (5.7). Comparing the PSO tuned controllers with the BBO tuned controllers, it can be seen that the PSO exhibits a better performance in terms of damping the oscillations of the system.

5.2.2.3 Heavy Loading Condition

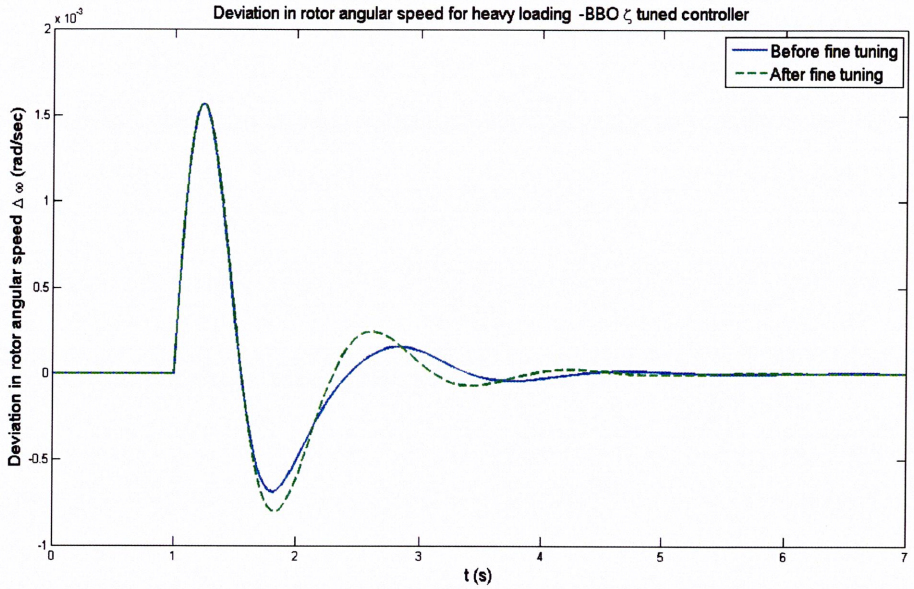


Figure (5.25)
Fine tuning - Dynamic response of POD controller tuned with BBO algorithm for ζ-objective function under heavy loading condition

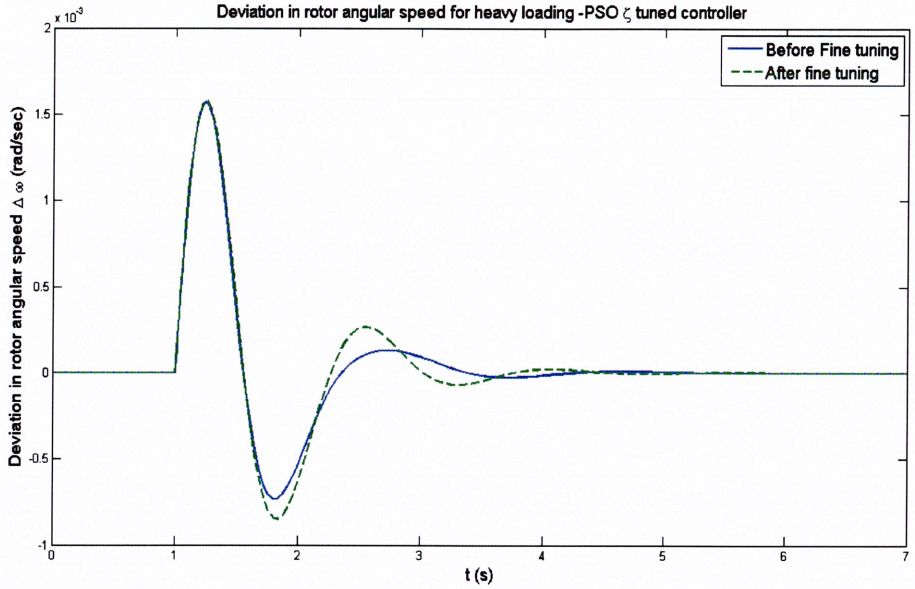


Figure (5.26)
Fine tuning - Dynamic response of POD controller tuned with PSO algorithm for ζ-objective function under heavy loading condition

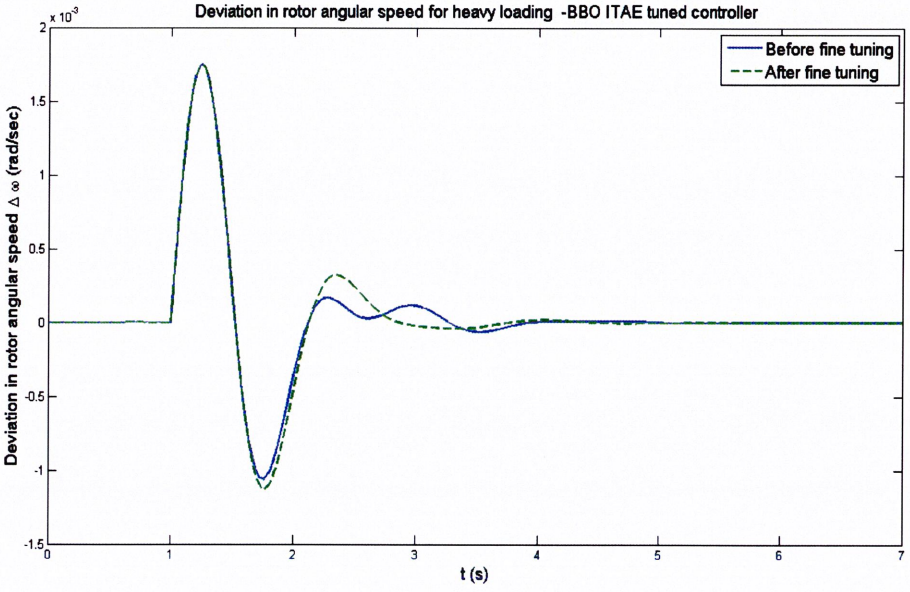


Figure (5.27)
Fine tuning - Dynamic response of POD controller tuned with BBO algorithm for ITAE-objective function under heavy loading condition

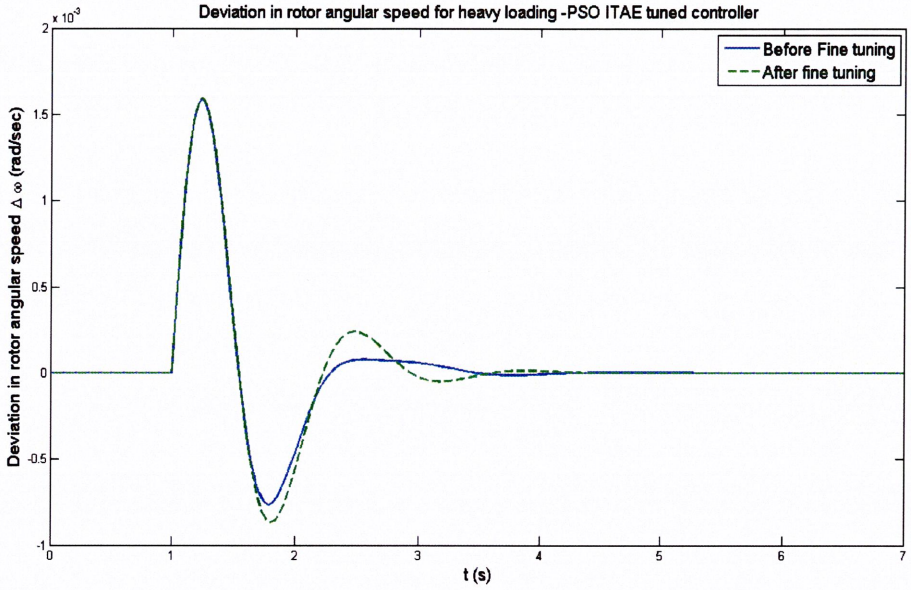


Figure (5.28)
Fine tuning - Dynamic response of POD controller tuned with PSO algorithm for ITAE-objective function under heavy loading condition

Table (5.8)
System performance before and after fine under heavy loading conditions for POD controllers

	Settling time t_s		Peak		ζ_{EM}	
	Before	After	Before	After	Before	After
BBO - ζ	2.1129	2.0043	0.0016	0.0016	0.3702	0.3519
PSO - ζ	2.0246	1.8981	0.0016	0.0016	0.4279	0.3668
BBO - ITAE	2.1090	1.7011	0.0017	0.0017	0.2403	0.3139
PSO - ITAE	1.2183	1.7655	0.0016	0.0016	0.3823	0.4211

From figures (5.25) to (5.28) and table (5.8), it can be seen that the system response after fine tuning has varied between the designed controller, where it can be seen that for the ζ - BBO tuned POD the damping ratio of the EM has decreased by 2% but this did not increase the settling time, but on the contrary it has decreased to 2.8 sec after the disturbance. While for the ITAE - PSO tuned POD controller, it can be seen that the settling time has increased while the EM damping ratio has increased. For the other two

controllers, the ζ - PSO and ITAE - BBO POD controllers the performance has improved through increasing the EM damping ratio and decreasing the settling time t_s.

5.2.2.4 Leading Loading Condition

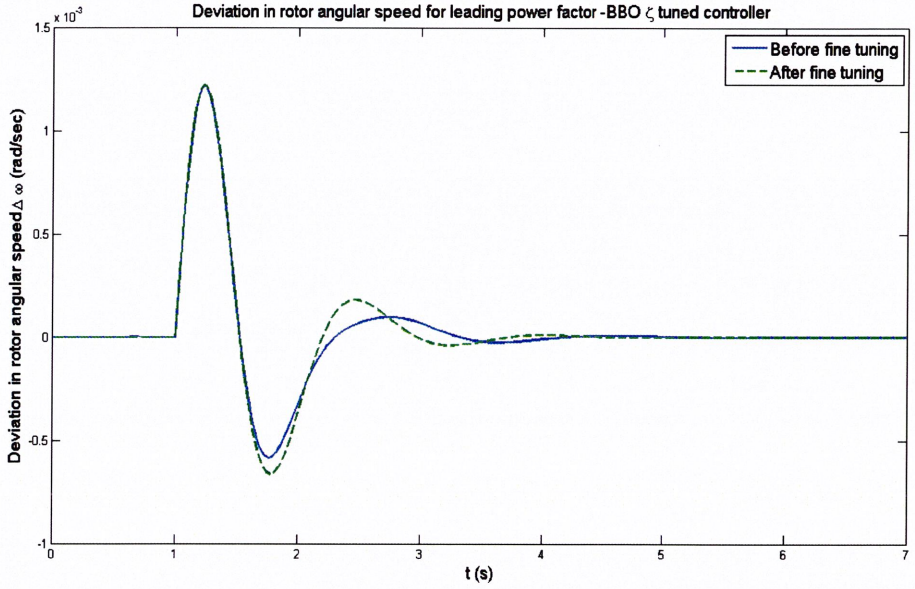


Figure (5.29)
Fine tuning - Dynamic response of POD controller tuned with BBO algorithm for ζ-objective function under leading power factor loading condition

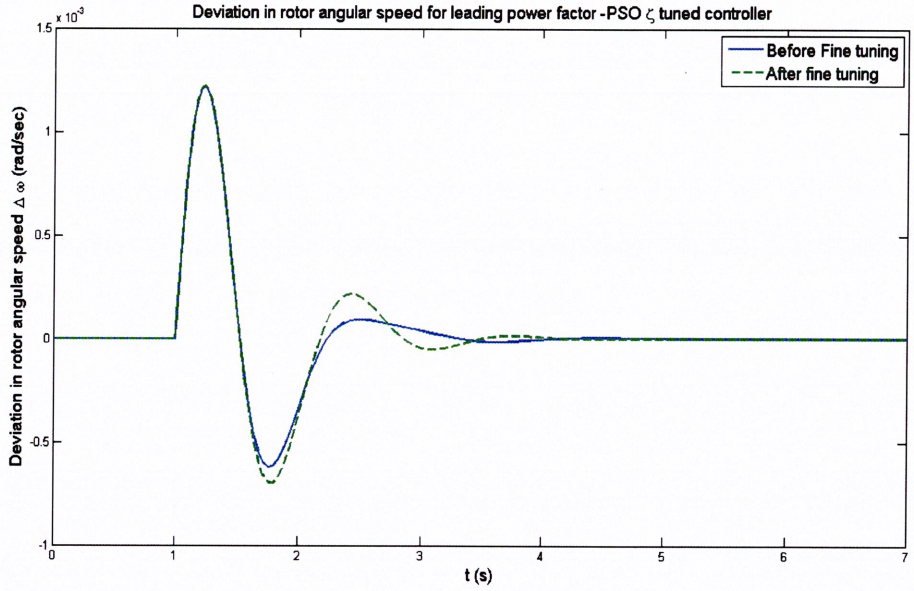


Figure (5.30)
Fine tuning - Dynamic response of POD controller tuned with PSO algorithm for ζ-objective function under leading power factor loading condition

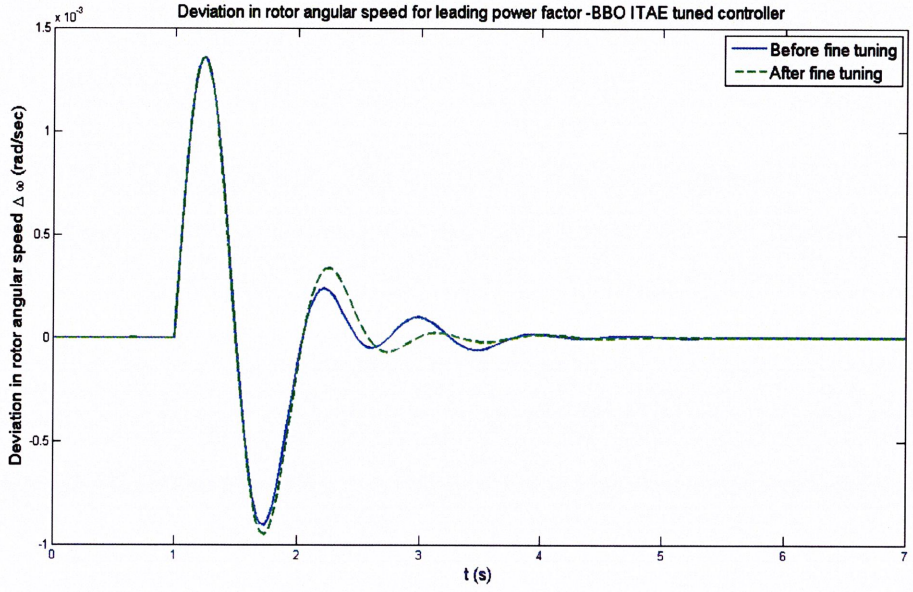


Figure (5.31)
Fine tuning - Dynamic response of POD controller tuned with BBO algorithm for ITAE-objective function under leading power factor loading conditions

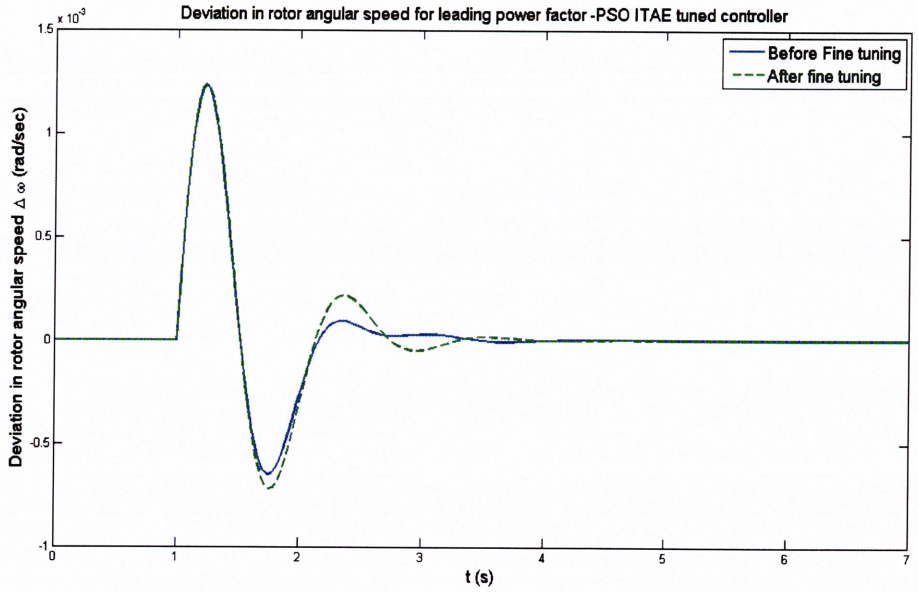


Figure (5.32)
Fine tuning - Dynamic response of POD controller tuned with PSO algorithm for ITAE-objective function under leading power factor loading condition

Table (5.9)
System performance before and after fine tuning under leading power factor loading conditions for POD controllers

	Settling time t_s		Peak		ζ_{EM}	
	Before	After	Before	After	Before	After
BBO - ζ	1.2084	1.7638	0.0012	0.0012	0.3769	0.4004
PSO - ζ	1.1883	1.7139	0.0012	0.0012	0.3955	0.3920
BBO - ITAE	1.4130	1.5061	0.0014	0.0014	0.2084	0.2552
PSO - ITAE	1.0977	1.6363	0.0012	0.0012	0.3405	0.3611

From figure (5.29) to (5.32) and table (5.9), the system performance after fine tuning has varied between the controllers. In case of the ζ - BBO tuned POD controllers, the system performance has degraded as the EM damping ratio has decreased along with an increase in settling time. On the other hand, the settling time t_s of the ITAE-PSO controller has an increase in settling time, while the ζ EM has increased. For the other two, an improvement in both the EM damping ratio with the settling time is noted.

5.3 Response Analysis for Multi-Input Multi-Output (MIMO) UPFC Control System

In this section an analysis of the MIMO UPFC controllers that were designed in chapter 4 is presented. The control system is tested based on its ability to control several variables simultaneously, where in the first case study the active power compensation factor is being varied in order to see the ability of the controllers to cope with the variation in setpoint. The second case study investigates the ability of the controllers to track the setpoint after introduction of a disturbance in the system. In this case study a six cycle three phase fault at the compensated transmission system is simulated. The third case study, investigates the ability of the controllers to damp power system oscillations after the system being disturbed under different system loading conditions.

5.3.1 Setpoint Variation

In this case study the control systems will be tested for their ability to track different setpoint values. Varying the active power setpoint between (-15% to +15%) compensation under nominal system loading, while analyzing the system outputs in order to see the effect of setpoint variation on the ability of the system to track the setpoint without steady state errors.

The system responses for the setpoint variation for the BBO tuned MIMO controller are given in figures (5.33) to (5.37):

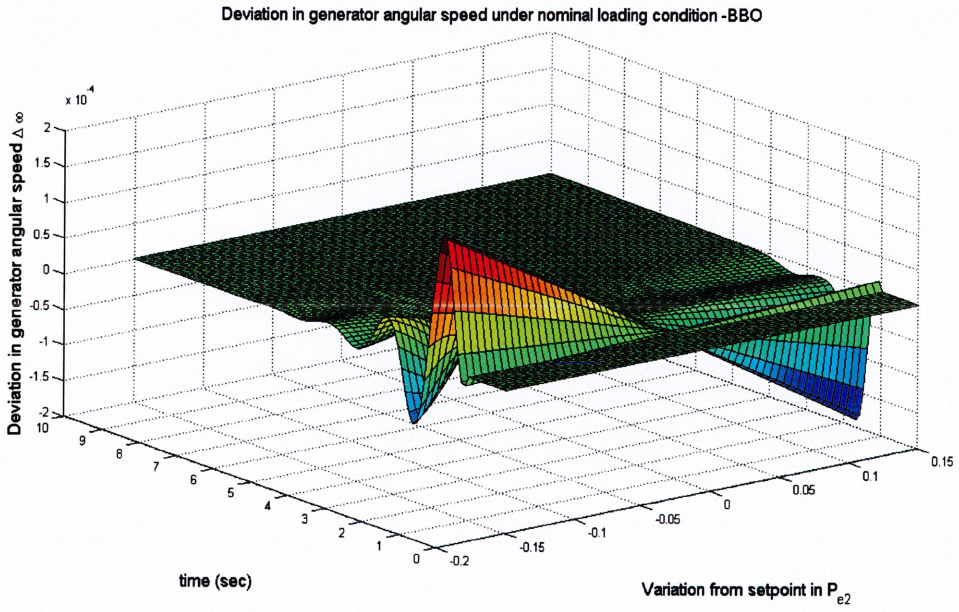


Figure (5.33)
Dynamic response - Generator angular speed deviation $\Delta\omega$ for BBO tuned MIMO control system under variation of power flow setpoint

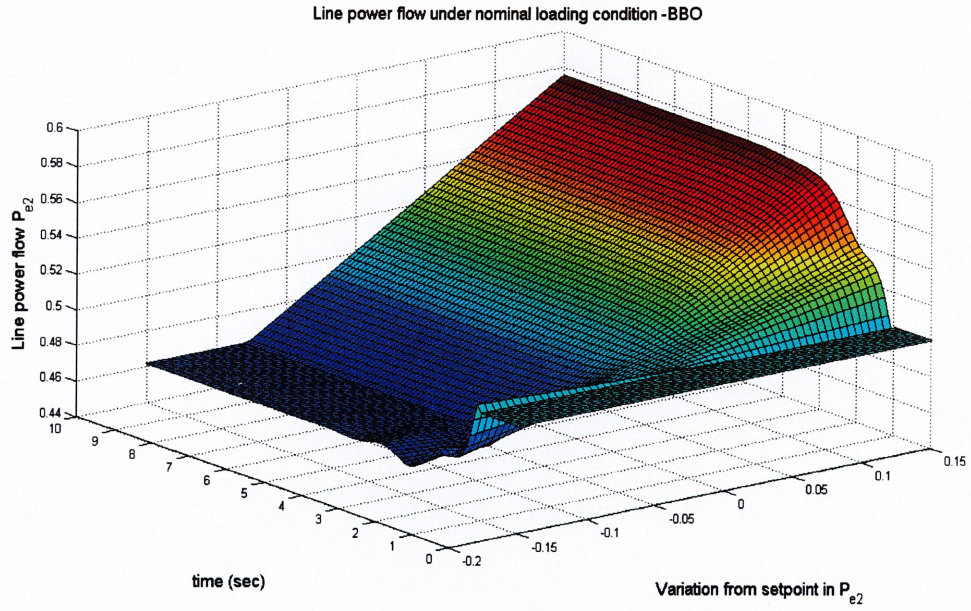


Figure (5.34)
Dynamic response - Line power flow P_{e2} for BBO tuned MIMO control system under variation of power flow setpoint

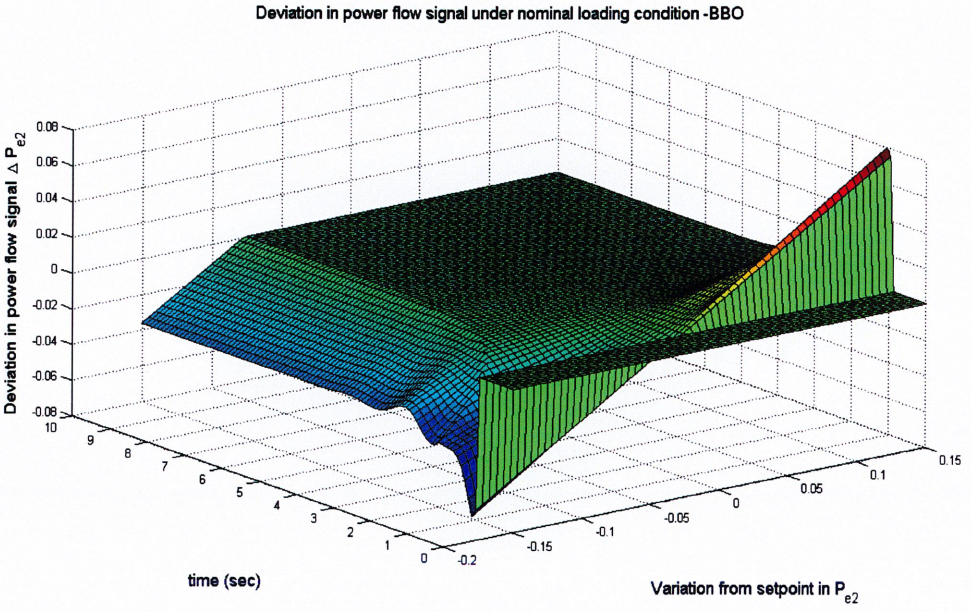


Figure (5.35)
Dynamic response - Deviation in line power flow ΔP_{e2} BBO tuned MIMO control system under variation of power flow setpoint

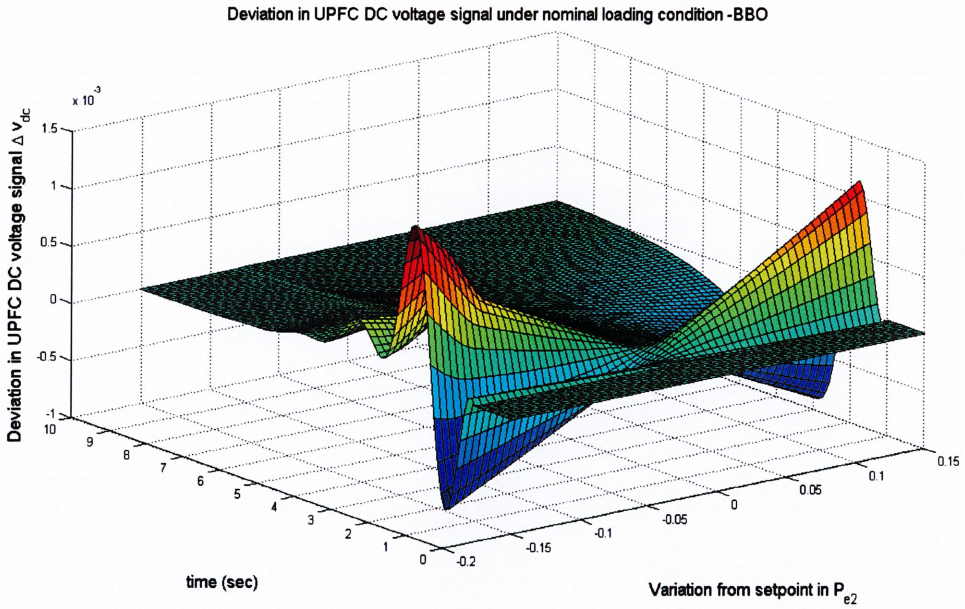


Figure (5.36)
Dynamic response - Deviation in UPFC DC link voltage Δv_{dc} for BBO tuned MIMO control system under variation of power flow setpoint

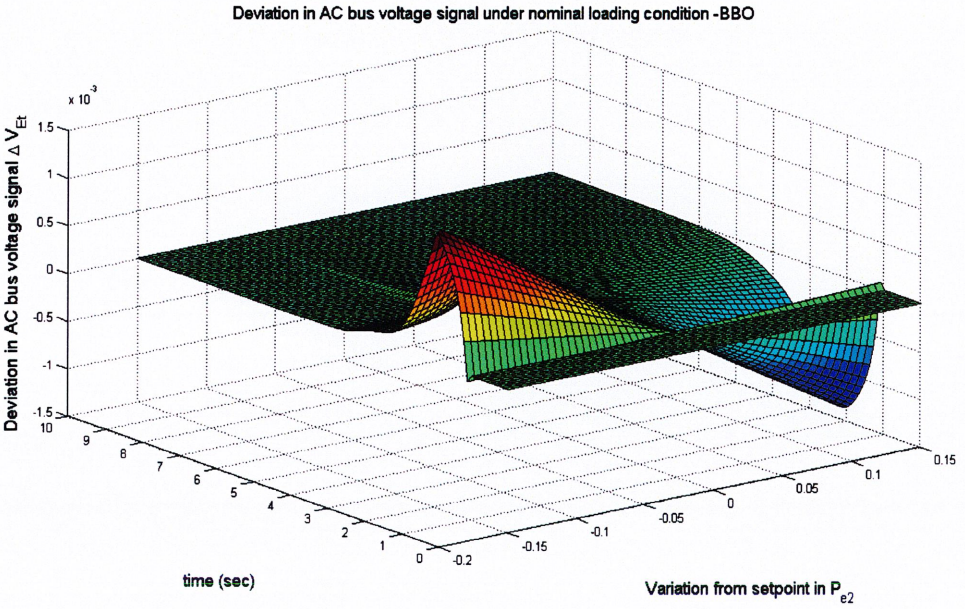


Figure (5.37)
Dynamic response - Deviation in AC bus voltage ΔV_{Et} for BBO tuned MIMO control system under variation of power flow setpoint

The system response for PSO tuned MIMO controller is shown in figures (5.38) to (5.42):

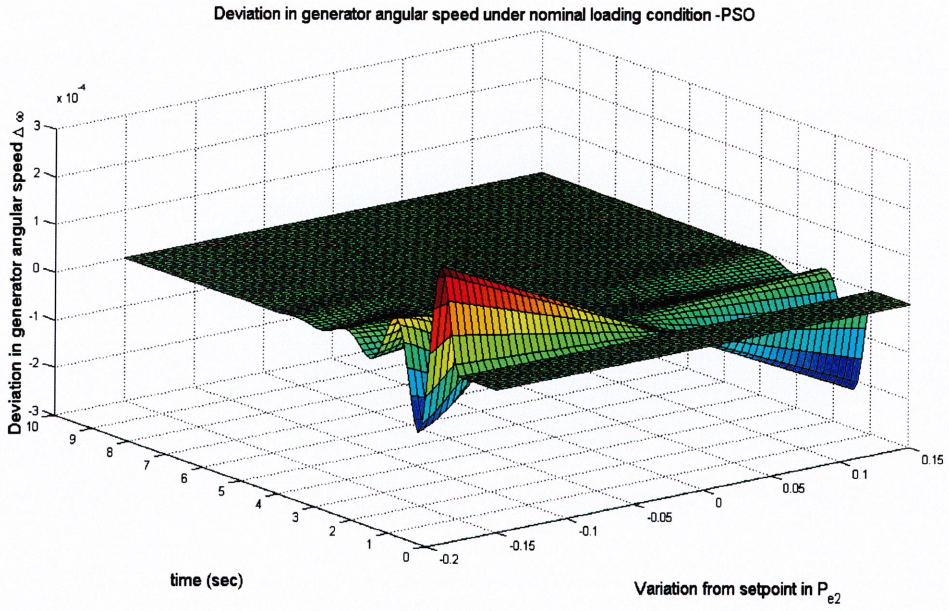


Figure (5.38)
Dynamic response - Generator angular speed deviation $\Delta\omega$ for PSO tuned MIMO control system under variation of power flow setpoint

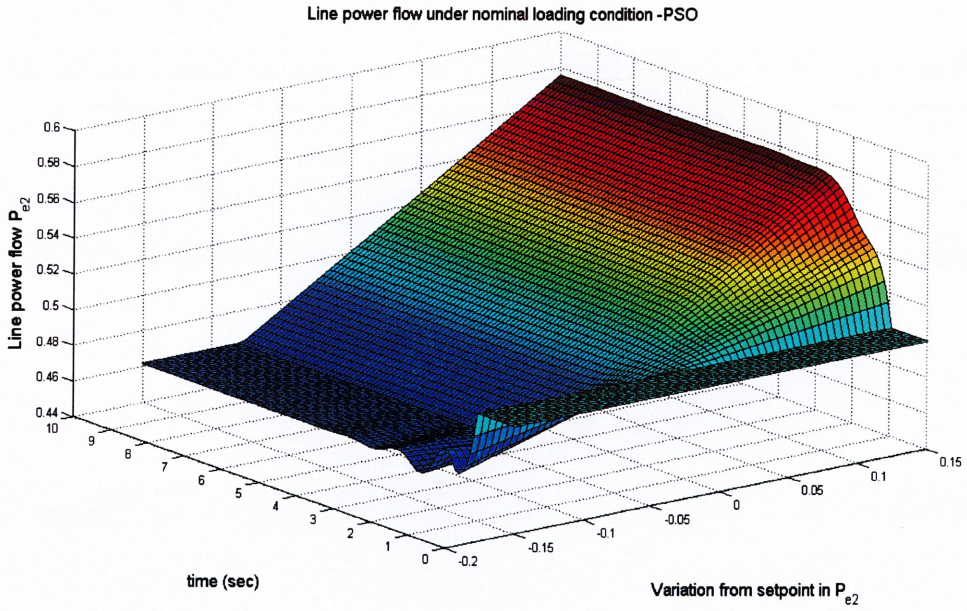


Figure (5.39)
Dynamic response - Line power flow P_{e2} for PSO tuned MIMO control system under variation of power flow setpoint

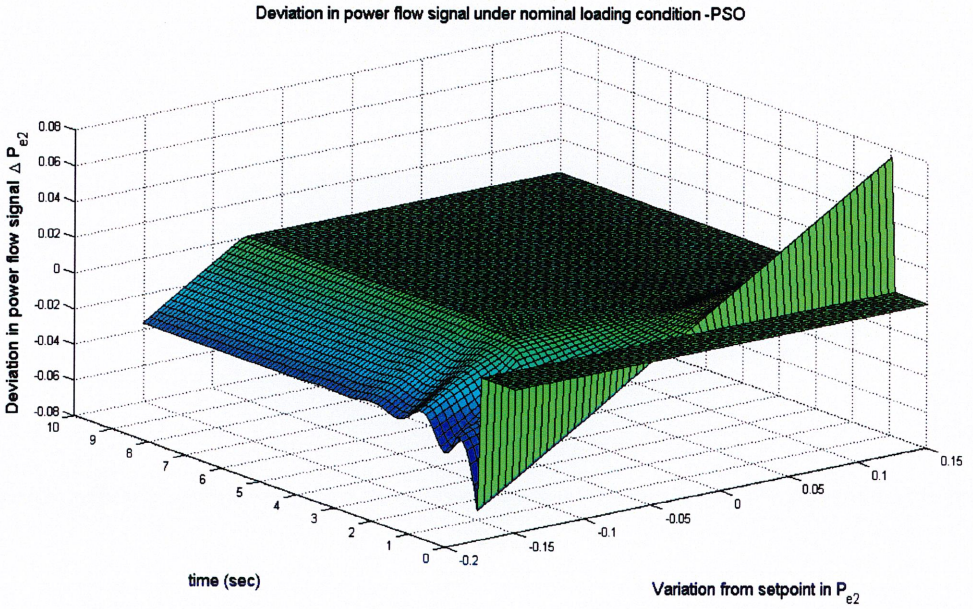


Figure (5.40)
Dynamic response - Deviation in line power flow ΔP_{e2} PSO tuned MIMO control system under variation of power flow setpoint

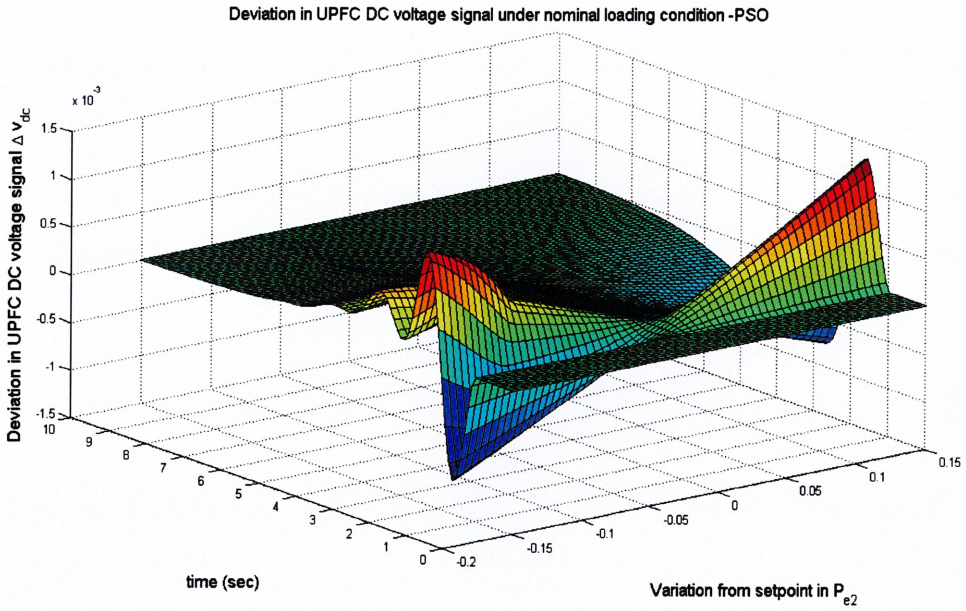


Figure (5.41)
Dynamic response - Deviation in UPFC DC link voltage Δv_{dc} for PSO tuned MIMO control system under variation of power flow setpoint

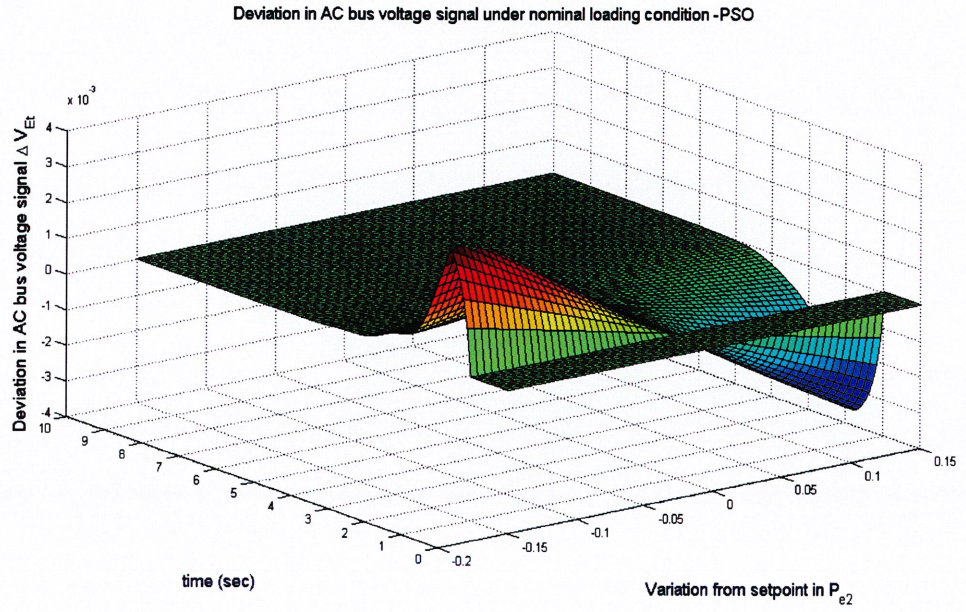


Figure (5.42)
Dynamic response - Deviation in AC bus voltage ΔV_{Et} for PSO tuned MIMO control system under variation of power flow setpoint

It can be seen that for negative setpoints (from -15% to -7.5% decrease in setpoint value), the system saturates for both MIMO controllers, and hence a steady state error is found between these setpoint values. The response of both controllers is similar in terms of tracking of setpoint, with different response parameters at each setpoint.

5.3.2 System Disturbance Rejection

In this section the MIMO controllers will be tested for the ability to reject load disturbance, thus a three phase six cycle fault at the compensated transmission line occurs at t = 8 s. The controllers will be tested under system nominal loading conditions. Figures (5.43) to (5.46), illustrates the system response for the load disturbance:

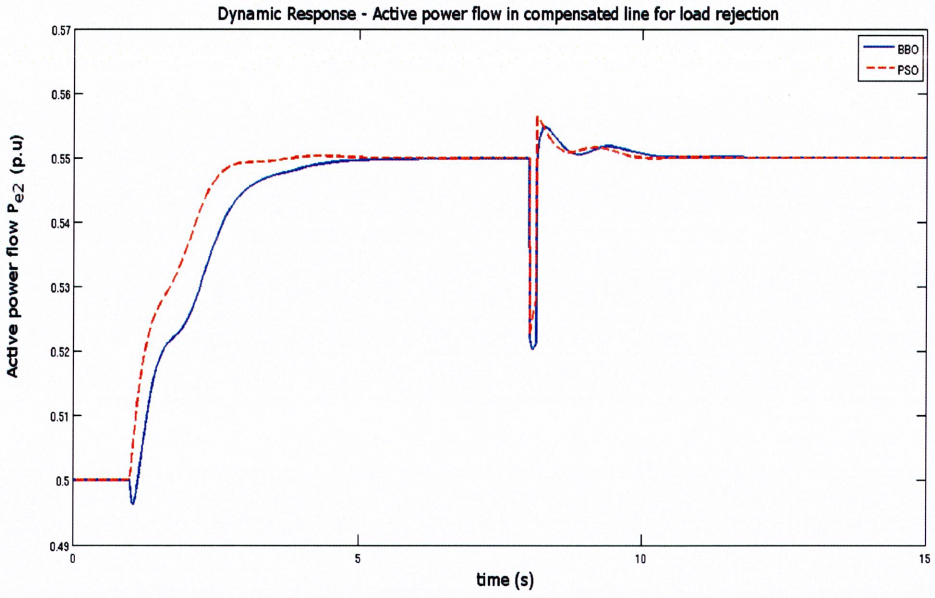


Figure (5.43)
Dynamic response - Line power flow P_{e2} after load disturbance in line 2

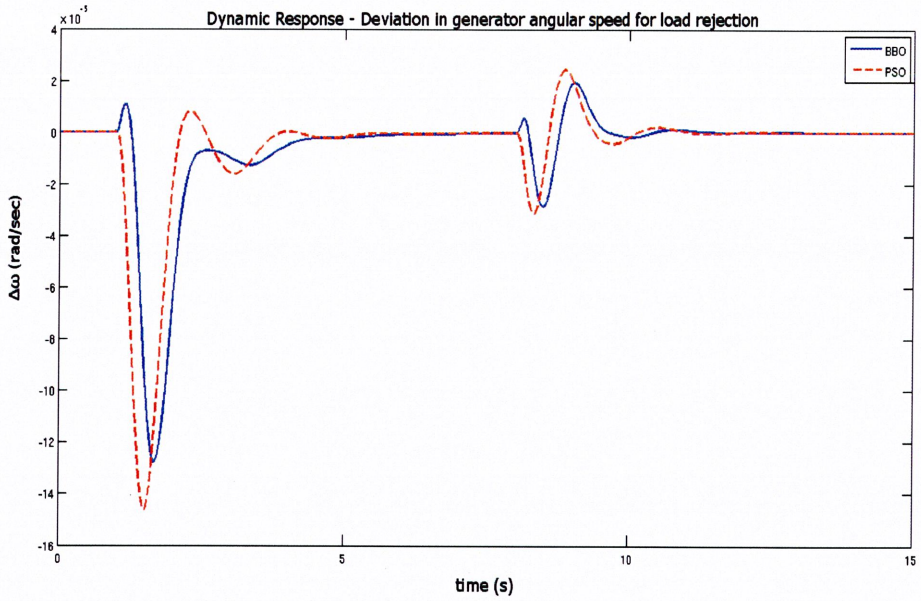


Figure (5.44)
Dynamic Response - Generator angular speed Deviation$\Delta\omega$ after load disturbance in line 2

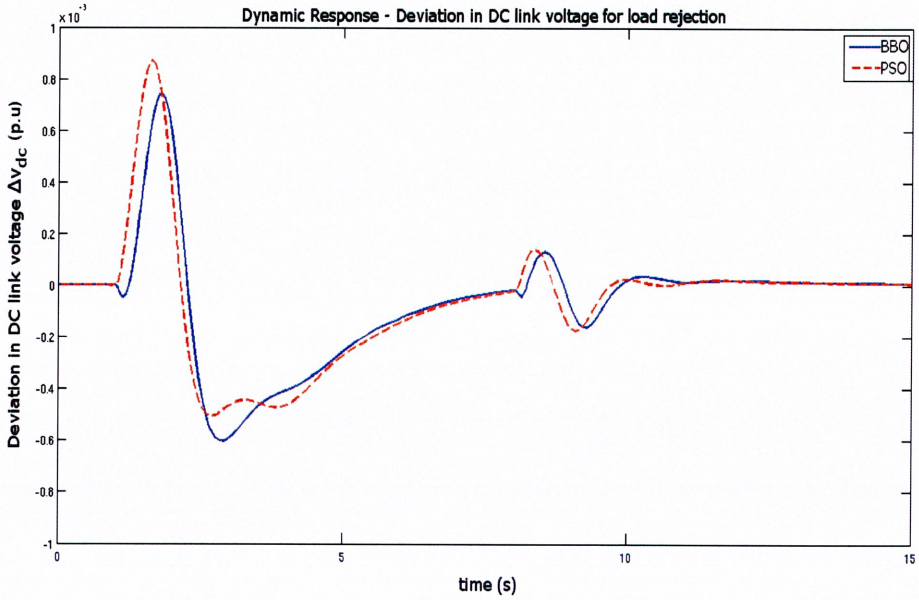


Figure (5.45)
Dynamic response - Deviation in UPFC DC line voltage Δv_{dc} after load disturbance in line 2

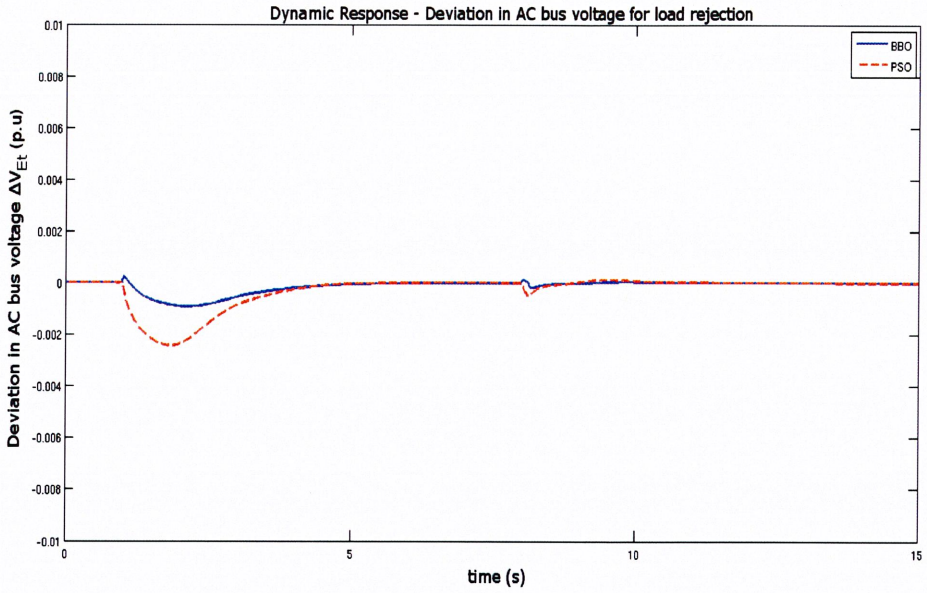


Figure (5.46)
Dynamic response - Deviation in AC bus voltage ΔV_{Et} after load disturbance in line 2

It can be seen that both controllers where able to reject the disturbance and maintain output at its prespecified value. The system responses are almost identical in terms of the ability to reject disturbances, and that can be shown from the responses.

5.3.3 Damping Power System Oscillations

This section analyzes the ability of the MIMO controllers to damp power system oscillation. Therefore, a three phase six cycles fault at the generator bus will be introduced. The system will simulated and analyzed at different generator loading (light,nominal,heavy, and leading power factor) conditions.

5.3.3.1 Light Loading Condition

In here the system is being light loaded at $P_e = 0.3$ p.u and $Q_e = 0.015$ p.u, at $t = 1$ s the a three phase six cycle fault is introduced to the system. The figures (5.47) to (5.50), illustrates the system response for this fault condition

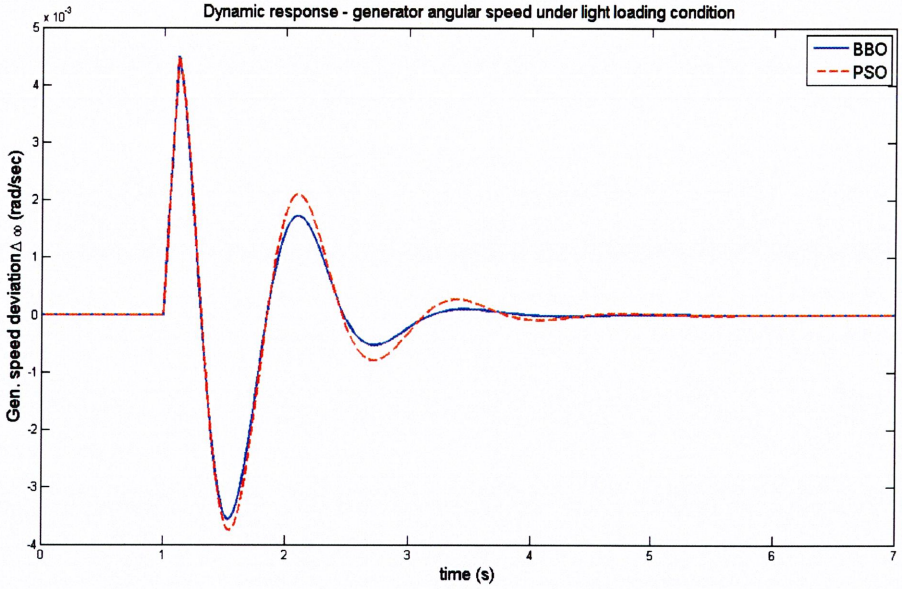


Figure (5.47)
Dynamic response - Generator angular speed deviation $\Delta\omega$ after three six cycle fault for light loading condition

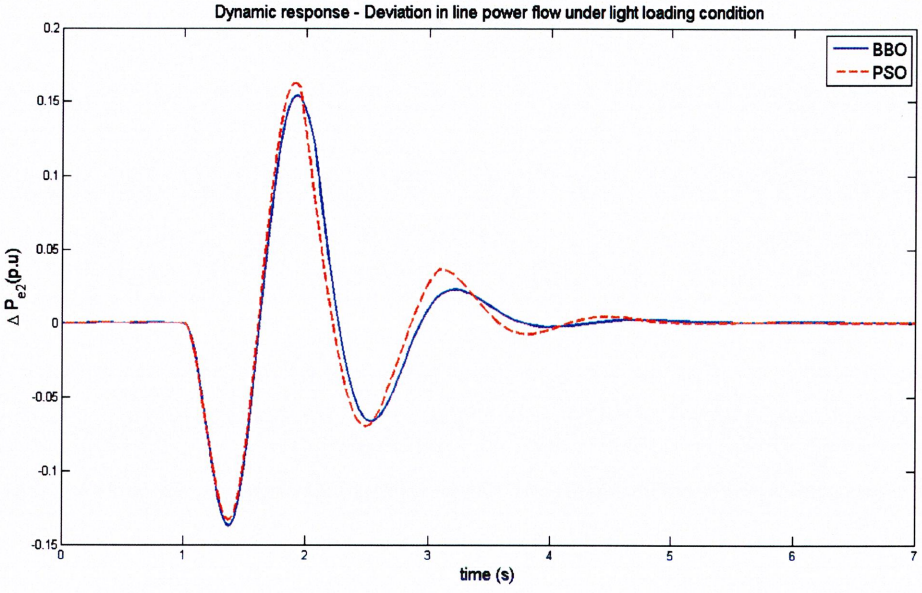


Figure (5.48)
Dynamic response - Line power flow deviation ΔP_{e2} after three six cycle fault for light loading condition

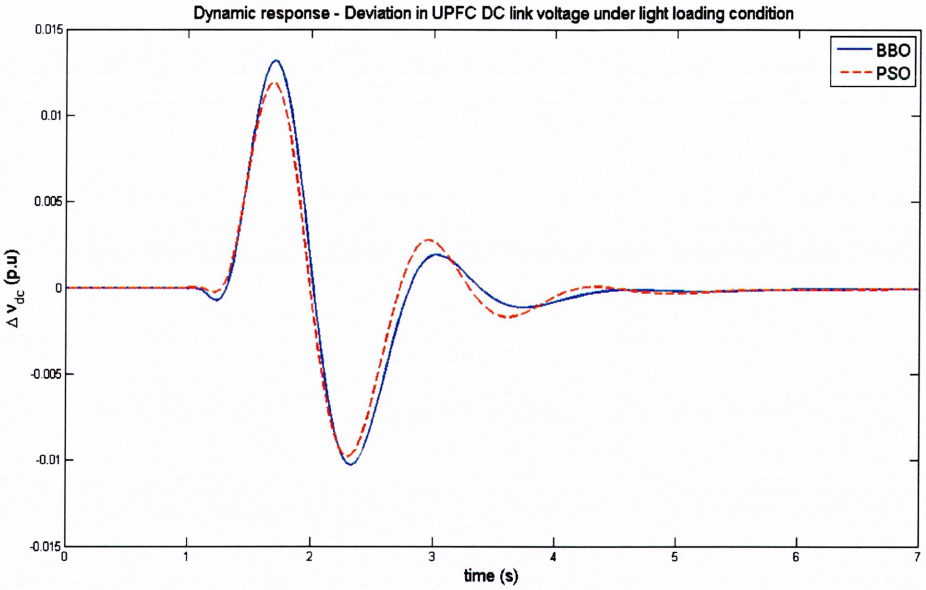


Figure (5.49)
Dynamic response - UPFC DC link voltage deviation Δv_{dc} after three six cycle fault for light loading condition

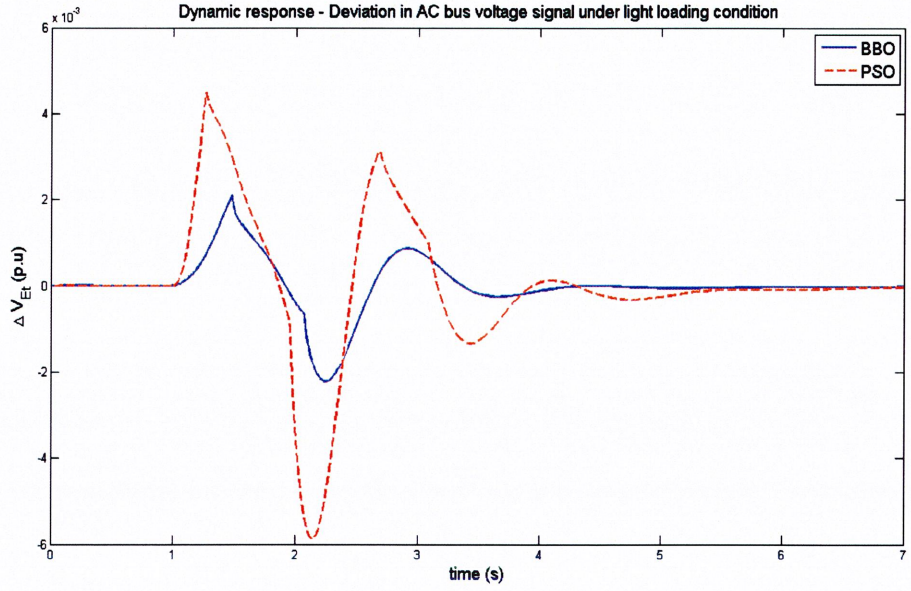


Figure (5.50)
Dynamic response - AC bus voltage deviation ΔV_{Et} after three six cycle fault for light loading condition

From the figures, it can be seen that the controllers where able to maintain the system stability. The eigenvalus anf EM damping ratio are given in table (5.10), however it can be seen that BBO tuned MIMO controller has a better performance in terms of damping oscillations compared to the PSO tuned controller, where the settling time for BBO is $t_{sBBO} = 2.024$ sec while for the PSO it is $t_{sPSO} = 2.575$ sec.

Table (5.10)
System eigenvalues and EM damping ratios at light loaded conditions for MIMO controllers

	BBO	PSO
System eigenvalues	-74.9832 -18.2478 -16.9008 -11.9308 EM:$-2.4341 \pm j6.2959$ $-1.7840 \pm j4.1157$ -4.6698 -0.2003 -0.5832 -1.0245 -1.4750 -1.2553	-31.7558 -19.6524 -16.5931 -13.3797 EM:$-2.8050 \pm j6.2378$ -5.9148 $-1.6587 \pm j4.4153$ -0.2003 $-1.1833 \pm j0.4265$ -0.6218 -1.0156
ζ_{EM}	0.3606	0.4104

5.3.3.2 Nominal Loading Condition

For nominal loading condition with the fault defined earlier, the system response is depicted in figures (5.51) to (5.54):

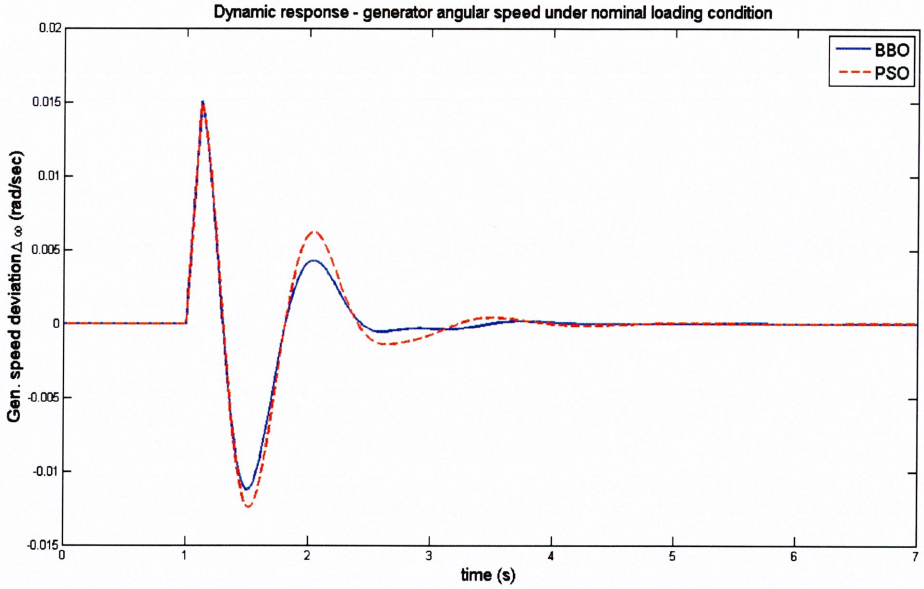


Figure (5.51)
Dynamic response - Generator angular speed deviation $\Delta\omega$ after three six cycle fault for Nominal loading condition

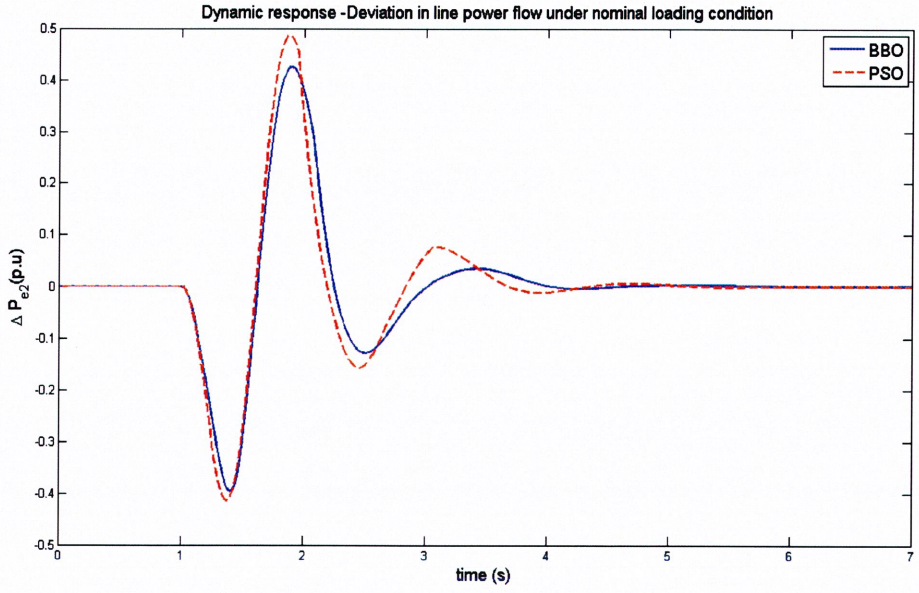


Figure (5.52)
Dynamic response - Line power flow deviation ΔP_{e2} after three six cycle fault for nominal loading condition

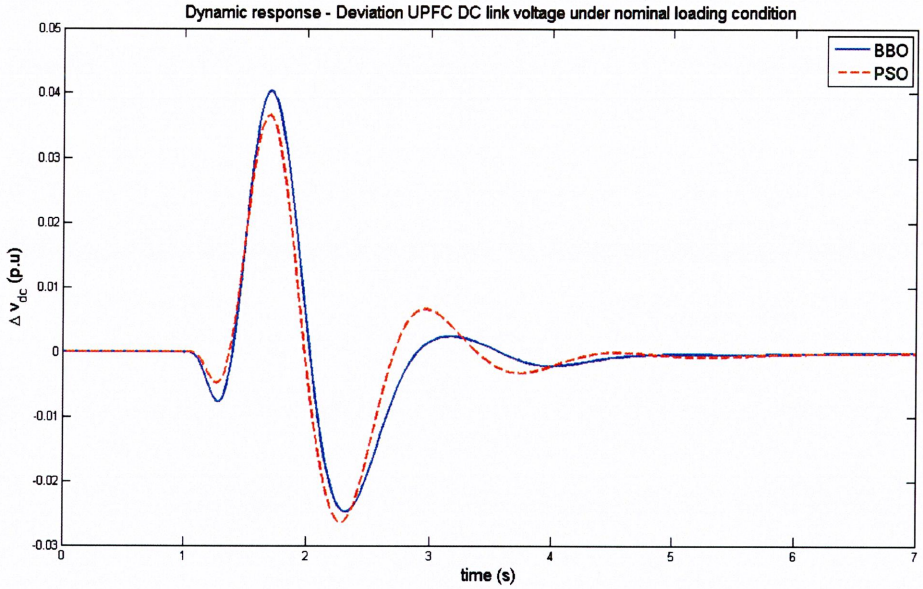


Figure (5.53)
Dynamic response - UPFC DC link voltage deviation Δv_{dc} after three six cycle fault for nominal loading condition

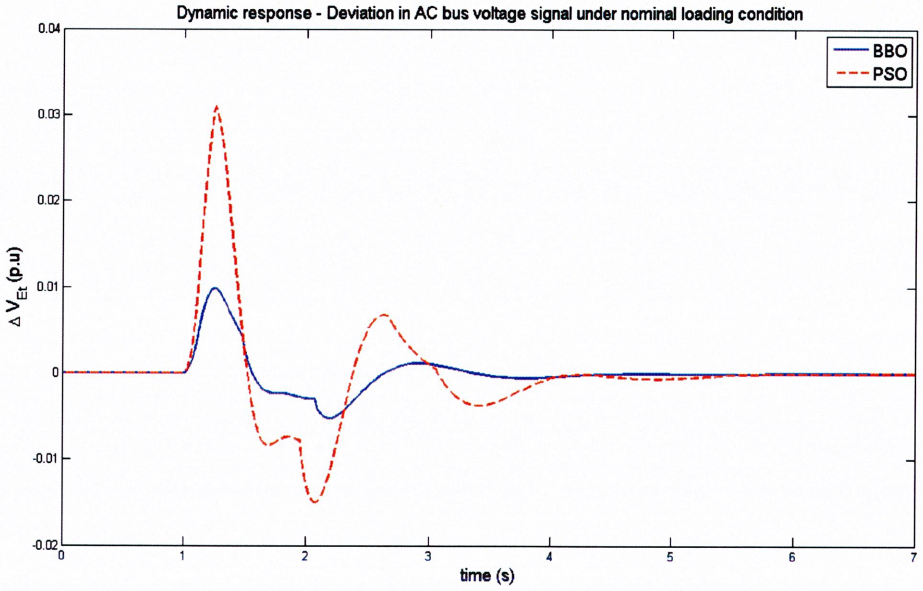


Figure (5.54)
Dynamic response - AC bus voltage deviation ΔV_{Et} after three six cycle fault for nominal loading condition

From the responses it can be seen that BBO has a superior capability in damping oscillation compared to PSO. The EM damping ratio was given in table (4.3).

5.3.3.3 Heavy Loading Condition

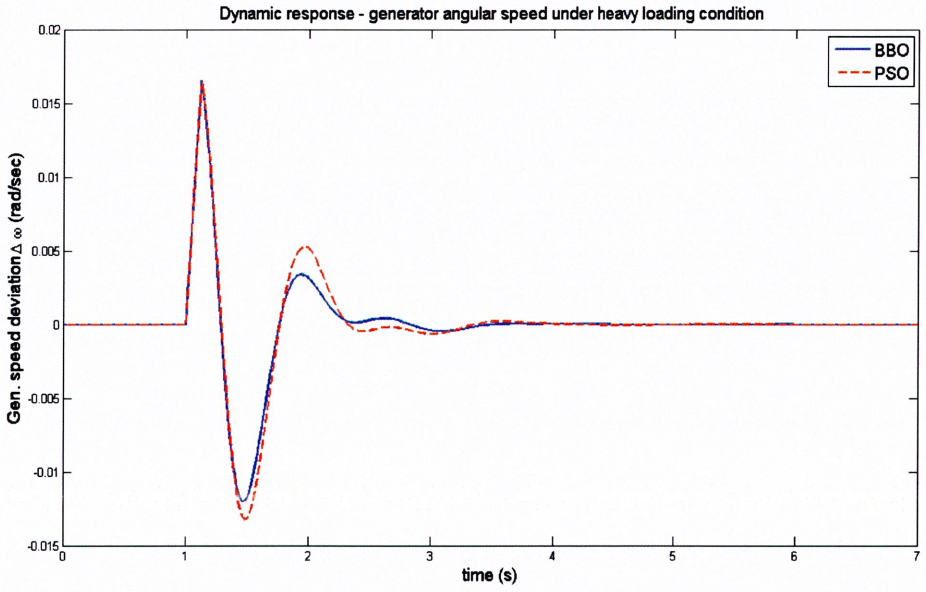


Figure (5.55)
Dynamic response - Generator angular speed deviation $\Delta\omega$ after three six cycle fault for heavy loading condition

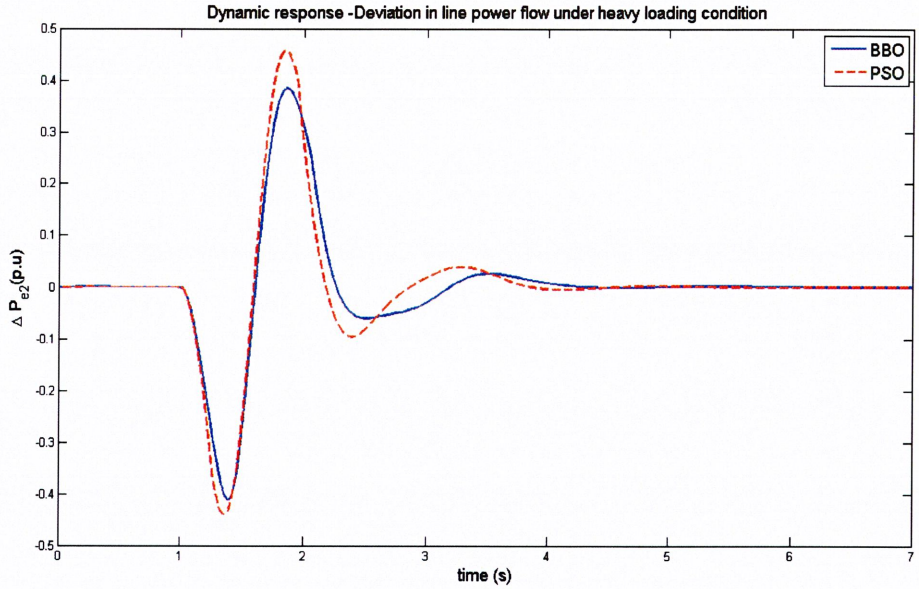


Figure (5.56)
Dynamic response - Line power flow deviation ΔP_{e2} after three six cycle fault for heavy loading condition

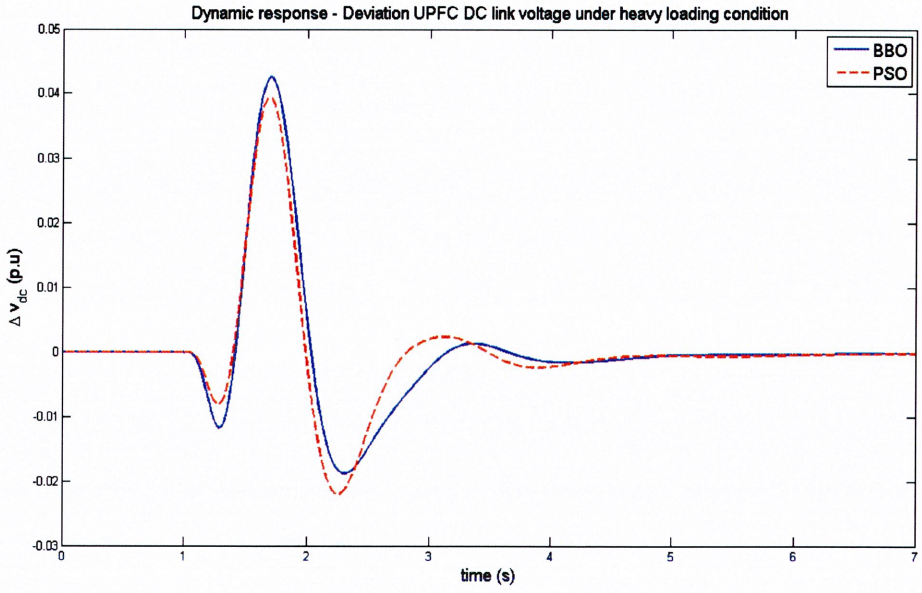


Figure (5.57)
Dynamic response - UPFC DC link voltage deviation Δv_{dc} after three six cycle fault for heavy loading condition

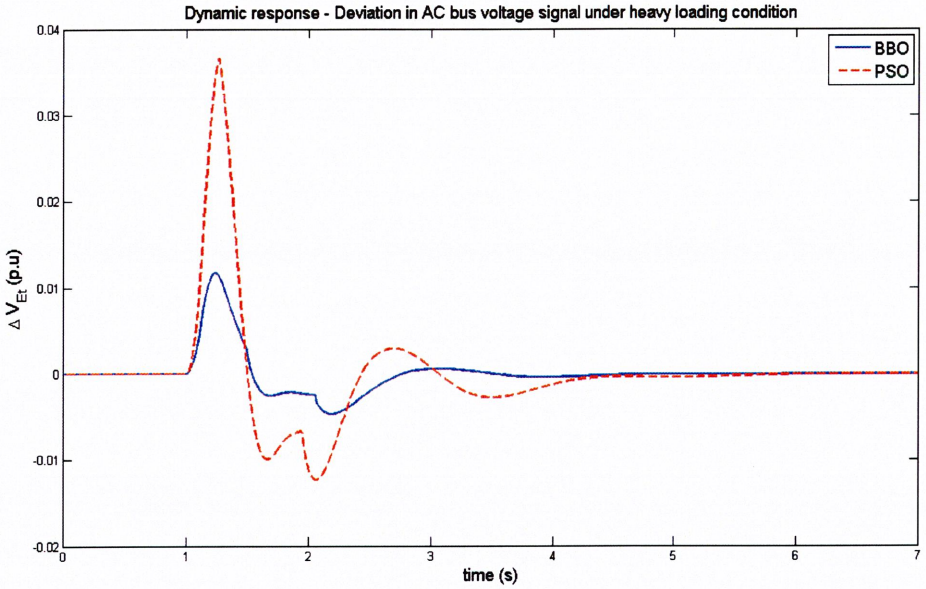


Figure (5.58)
Dynamic response - AC bus voltage deviation ΔV_{Et} after three six cycle fault for heavy loading condition

The system response for a step change in mechanical power P_m under heavy loading conditions is depicted in figures (5.55) to (5.58). In this case the settling time for BBO is given as $t_{sBBO} = 2.347$ sec and for PSO tuned controller is $t_{sPSO} = 2.692$ sec. The system eigenvalues and EM damping ratios for each controller is presented in table (5.11):

Table (5.11)
System eigenvalues and EM damping ratios at heavy loaded conditions for MIMO controllers

	BBO	PSO
System eigenvalues	-75.8424 -17.6070 -17.2593 -11.4875 EM:$-2.2617 \pm j7.9630$ -5.1057 $-1.6802 \pm j3.3662$ -0.2003 -0.6285 $-1.2483 \pm j0.3871$ -1.4561	-32.0854 -19.5194 -16.8664 -13.7137 EM:$-2.4860 \pm j8.0423$ -6.3230 $-1.5629 \pm j3.6709i$ $-1.2918 \pm j0.5671$ -0.2003 -0.6273 -1.0360
ζ_{EM}	0.2732	0.2953

It can be seen that even though the PSO tuned controller have a higher EM damping ratio its settling time is greater than the BBO tuned controller, and that can explained because that the response is not purely governed by EM rather it can be a combination of other modes interacting with each other.

5.3.3.4 Leading Power Factor Loading Condition

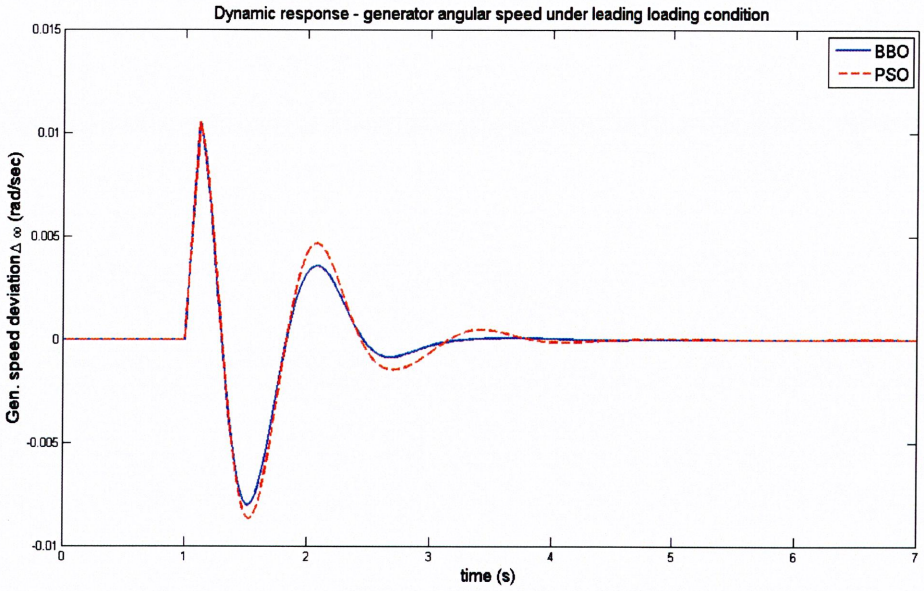


Figure (5.59)
Dynamic response - Generator angular speed deviation $\Delta\omega$ after three six cycle fault for leading power factor condition

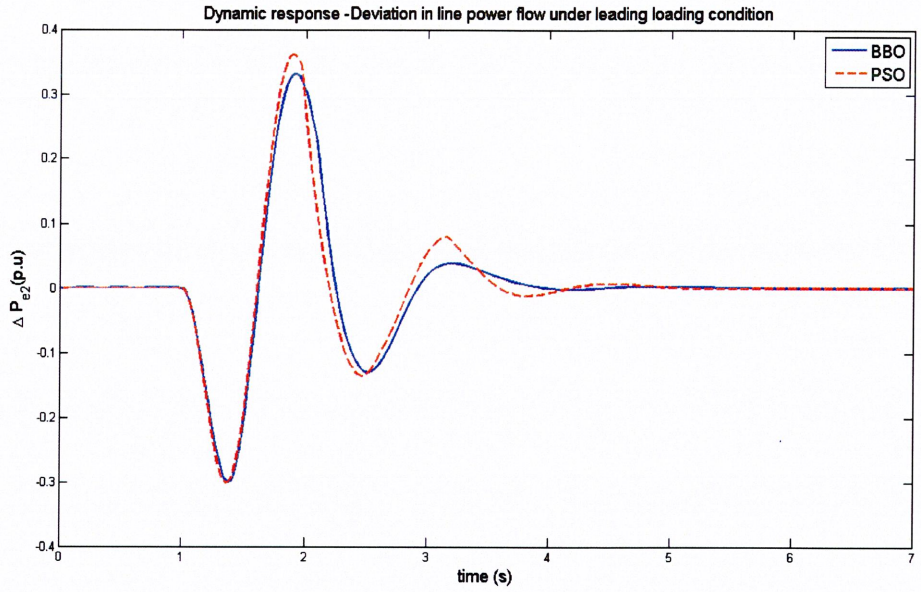


Figure (5.60)
Dynamic response - Line power flow deviation ΔP_{e2} after three six cycle fault for leading power factor condition

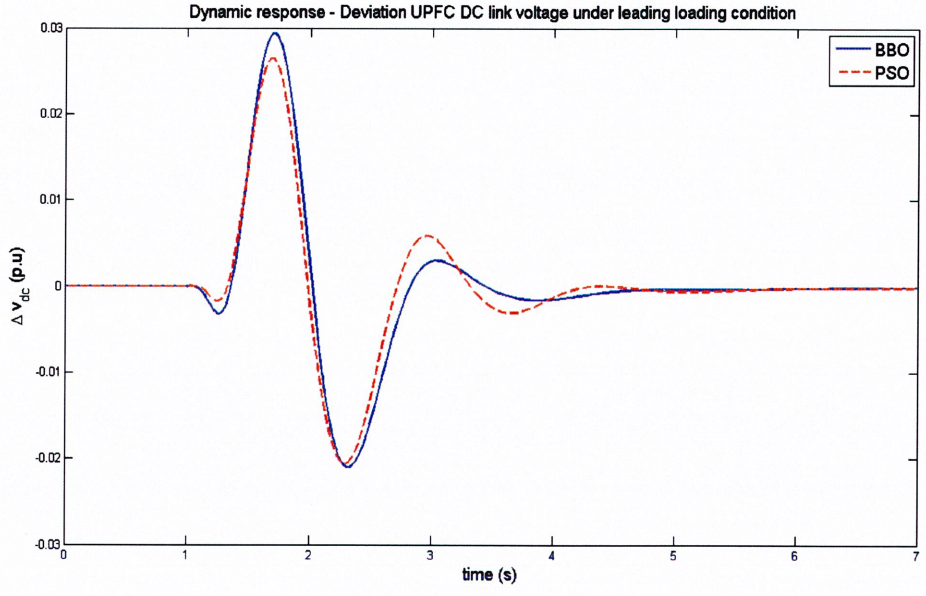


Figure (5.61)
Dynamic response - UPFC DC link voltage deviation Δv_{dc} after three six cycle fault for leading power factor condition

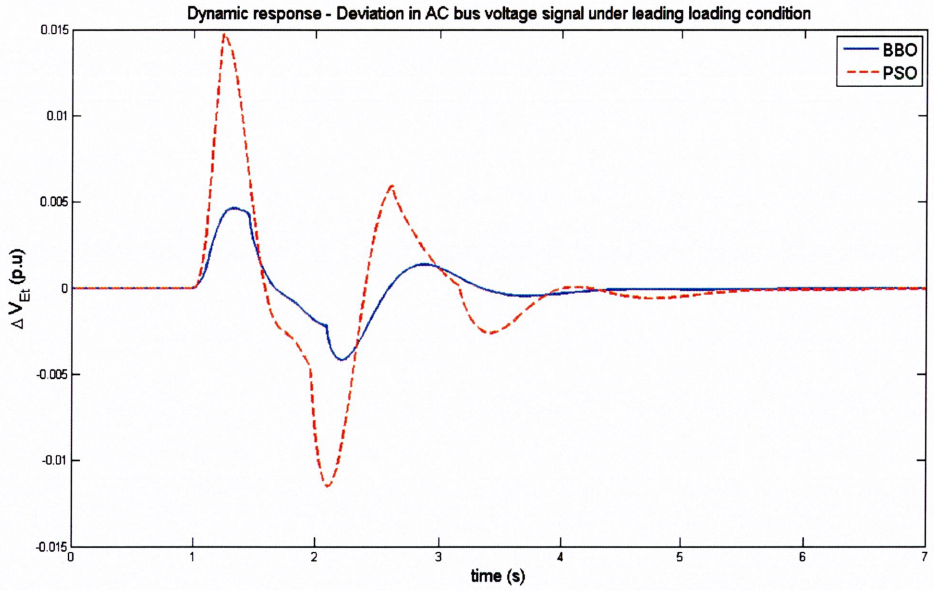


Figure (5.62)
Dynamic response - AC bus voltage deviation ΔV_{Et} after three six cycle fault for leading power factor condition

Table (5.12)
System eigenvalues and EM damping ratios at leading power factor loading conditions for MIMO controllers

	BBO	PSO
System eigenvalues	-75.5594 -17.7807 -17.0910 -9.6246 EM:$-2.3121 \pm j6.6038$ -5.7890 $-2.0142 \pm j3.7115$ -0.2003 -0.6449 $-1.2657 \pm j0.4249$ -1.4524	-31.9599 -19.4927 -16.8229 -13.0312 EM:$-2.6988 \pm j6.7162$ -6.6883 $-1.6339 \pm j4.0470$ $-1.3026 \pm j0.5743$ -0.2003 -0.6366 -1.0339
ζ_{EM}	0.3304	0.3728

The figures (5.59) to (5.62), shown above illustrate the system response under leading power factor loading conditions ($P_e = 0.7$ p.u and $Q_e =$

-0.03 p.u). From the figures and table(5.12), it can be seen that the damping controllers were able to keep the system operating in a stable equilibrium point, between the two algorithms it can be seen that BBO has a smaller settling time compared to PSO, $t_{sBBO} = 2.089$ sec and $t_{sPSO} = 2.693$ sec, even though that PSO has higher performance on the objective function as was shown in chapter 4. This as explained earlier, is due to the interaction of modes of the system, for this the objective function can be improved to reflect the actual performance of the system from all aspects, for instance including the figure of demerit as was done in Shayeghi et al. (2009). Or the use of a multiobjective optimization can be used.

Chapter 6
Conclusion and Future Work

- **6.1 Conclusion**
- **6.2 Suggestions for Future Work**

Chapter 6
Conclusion and Future Work

6.1 Conclusion

The rapid demand for electrical power results in an extended use of transmission system, hence driving it near to its stability limit. This created the need for an intelligent grid that is able to control its parameters. An innovative solution was presented by Electric Power Research Institute (EPRI) with Flexible AC Transmission Systems (FACTS). These devices allow the control of the transmission system parameters (impedance ,voltage, and phase angle). Hence FACTS devices introduced the intelligence in transmission system. UPFC being the most versatile FACTS controller that can control all the transmission system parameters. Therefore, a smart grid can be achieved through the introduction of such device that will control the parameters based on the need of the system. On the other hand, evolutionary optimization algorithms has emerged in the research fields as a solution to many problems. This research study combines these two promising research fields in order to find a smart controller for the UPFC based on the evolutionary optimization algorithms.

The focus on the modeling of the UPFC has been addressed in chapter 2, and it was shown that the decoupled UPFC load flow model presents a simple and effective model for load flow studies. The decoupled model takes the solution in two different iterative procedures. A MATLAB code was developed in order to obtain the test system operating conditions. Furthermore, it was evident that the PWM base UPFC model introduced by Nabavi-Niaki & Iravani (1996), was superior to the other model presented, due to its practicality and explicitness of the control signals.

A power oscillation damping (POD) controller based UPFC was designed by using the Biogeography Based Optimization (BBO) algorithm and Particle Swarm Optimization (PSO) algorithm. Different approaches

for the tuning process was investigated by trying different objective functions in order to design a robust controller. It was seen that based on the objective function, the performance of the algorithm varies.

A multi-input multi-output (MIMO) control system was introduced in chapter 4. This control system was intended to utilize all the UPFC functionality by controlling line power flow, regulating bus voltage, damping power system oscillation, and more importantly regulate the DC voltage in UPFC DC link to ensure stable UPFC operation. The MIMO control system was tuned with the same algorithms introduced in chapter 3. The system was simulated for two different disturbances the first was a 10% step increase in generator mechanical power P_m, were the second was a 10% step increase in active power flow control stepoint P_{e2}. The control system suffered the from a steady state error in the active power flow control in the first case, due to the interaction between the system controlled variables. This has degraded the performance of the system and introduced the steady state error in the active power flow.

The fifth chapter analyzed all of the controllers that were designed in the chapters 4 and 5, it analyzed the system robustness, disturbance rejection, tracking capability, and the fine tuning of the controllers to enhance the system response. The chapter concluded that the performance of the algorithms on the objective function does not give a clear indication of the superiority of an algorithm over the other, where it was shown that the performance varies in different cases that were considered. A modification to the controller design and a measurement to the algorithm strength can be done with the use of a multiobjective optimization in order to enhance the design capabilities.

6.2 Suggestions for Future Work

1. Implement the system on ATP-EMTP simulation software to compare the results with ones obtained from MATLAB.

2. Implement the study for a multi-machine power system to assess the UPFC capability to damp the oscillations in such systems.

3. Furthre research work to design a BBO base artificial neural network controller or robust controller based on H_∞ and compare the results with obtained ones.

4. Implement the same study for a different FACTS controller such as Hybrid Flow Controller (HFC) or interline power flow controller (IPFC) and compare the results with UPFC.

5. Use different Optimization algorithms such as ant colony or bee colony and compare the result with the obtained from BBO and PSO

6. Further work should be carried out on the POD controller to using eigenvalue based objective functions and compare the results with the obtained ones.

List of References

Abido, M. (2005). Analysis and assessment of STATCOM-based damping stabilizers for power system stability enhancement. *Electric Power Systems Research*, *73*(2), 177–185.

Abido, M. (2009). Power system stability enhancement using facts controllers: A review. *Arabian Journal for Science & Engineering (Springer Science & Business Media BV)*, *34*.

Abido, M. A., Al-Awami, A., & Abdel-Magid, Y. (2006, July). Analysis and Design of UPFC Damping Stabilizers for Power System Stability Enhancement. In *Industrial electronics, 2006 ieee international symposium on* (Vol. 3, p. 2040-2045). doi: 10.1109/ISIE.2006.295887

Ajami, A., & Gholizadeh, R. (2012). Optimal design of UPFC-based damping controller using imperialist competitive algorithm. *Turkish Journal of Electrical Engineering & Computer Sciences*, *20*(Sup. 1), 1109–1122.

Al-Awami, A. T., Abdel-Magid, Y., & Abido, M. (2007). A particle-swarm-based approach of power system stability enhancement with unified power flow controller. *International Journal of Electrical Power & Energy Systems*, *29*(3), 251–259.

Al-Awami, A. T., Abido, M. A., & Abdel-Magid, Y. L. (n.d.). Application of PSO to design UPFC-based stabilizers.

Clerc, M., & Kennedy, J. (2002). The particle swarm-explosion, stability, and convergence in a multidimensional complex space. *Evolutionary Computation, IEEE Transactions on*, *6*(1), 58–73.

Darwin, C., & Bynum, W. F. (2009). *The origin of species by means of natural selection: or, the preservation of favored races in the struggle for life*. AL Burt.

Eberhart, R. C., & Shi, Y. (2000). Comparing inertia weights and constriction factors in particle swarm optimization. In *Evolutionary computation, 2000. proceedings of the 2000 congress on* (Vol. 1, pp. 84–88).

El-Sadek, M. Z., Ahmed, A., & Zidan, H. E. (2006, Dec). Comparison of unified power flow controller models for power flow studies. In *Power systems conference, 2006. mepcon 2006. eleventh international middle east* (Vol. 1, p. 189-196).

Fang, Y., & Macdonald, D. (1998). Dynamic quadrature booster as an aid to system stability.

Fuerte-Esquivel, C., Acha, E., & Ambriz-Perez, H. (2000, Feb). A comprehensive Newton-Raphson UPFC model for the quadratic power flow solution of practical power networks. *Power Systems, IEEE Transactions on*, *15*(1), 102-109. doi: 10.1109/59.852107

Gyugyi, L. (1992). Unified power-flow control concept for flexible AC transmission systems. In *Iee proceedings c (generation, transmission and distribution)* (Vol. 139, pp. 323–331).

Hingorani, N. G., Gyugyi, L., & El-Hawary, M. (2000). *Understanding FACTS: concepts and technology of flexible AC transmission systems* (Vol. 1). IEEE press New York.

Homans, G. C. (1958). Social behavior as exchange. *American journal of sociology*, 597–606.

Kennedy, J., Eberhart, R., et al. (1995). Particle swarm optimization. In *Proceedings of ieee international conference on neural networks* (Vol. 4, pp. 1942–1948).

Kennedy, J. F., Kennedy, J., & Eberhart, R. C. (2001). *Swarm intelligence*. Morgan Kaufmann.

MacArthur, R. H. (1967). *The theory of island biogeography* (Vol. 1). Princeton University Press.

Monroe, E. G. (1948). *The geographical distribution of butterflies in the west indies*. Cornell University.

Nabavi-Niaki, A., & Iravani, M. (1996, Nov). Steady-state and dynamic models of unified power flow controller (UPFC) for power system studies. *Power Systems, IEEE Transactions on, 11*(4), 1937-1943. doi: 10.1109/59.544667

Noroozian, M. (1998). Application of shunt and series compensators for damping of electromechanical oscillations.

Oonsivilai, A., & Marungsri, B. (2008). Stability Enhancement for Multi-machine Power System by Optimal PID Tuning of Power System Stabilizer using Particle Swarm Optimization. *WSEAS transactions on power systems, 3*(6), 465–474.

Padiyar, K. (2007). *FACTS controllers in power transmission and distribution*. New Age International.

Padiyar, K. (2008). *Power system dynamics*. BS publications.

Padiyar, K. R., & Kulkarni, A. (1998, Oct). Control design and simulation of unified power flow controller. *Power Delivery, IEEE Transactions on, 13*(4), 1348-1354. doi: 10.1109/61.714507

Panda, S., & Padhy, N. P. (2007). MATLAB/SIMULINK Based Model of Single-Machine Infinite-Bus with TCSC for Stability Studies and Tuning Employing GA. *International Journal of Computer Science & Engineering, 1*(1).

Rahim, A., & Nassimi, S. (1996). Synchronous generator damping enhancement through coordinated control of exciter and SVC. *IEE Proceedings-Generation, Transmission and Distribution, 143*(2), 211–218.

Rakitianskaia, A. (2011). *Using particle swarm optimisation to train feed-forward neural networks in dynamic environments.* Unpublished doctoral dissertation, University of Pretoria.

Rogers, G. (2000). *Power system oscillations.* Kluwer Academic Boston.

Seborg, D., Edgar, T. F., & Mellichamp, D. (2006). *Process dynamics & control.* John Wiley & Sons.

Shayeghi, H., Shayanfar, H., Jalilzadeh, S., & Safari, A. (2009). Design of output feedback UPFC controller for damping of electromechanical oscillations using PSO. *Energy Conversion and Management, 50*(10), 2554–2561.

Simon, D. (2008). Biogeography-based optimization. *Evolutionary Computation, IEEE Transactions on, 12*(6), 702–713.

Simon, D. (2013). *Evolutionary optimization algorithms.* John Wiley & Sons.

Smith, K., Ran, L., & Penman, J. (1997, Jan). Dynamic modelling of a unified power flow controller. *Generation, Transmission and Distribution, IEE Proceedings-, 144*(1), 7-12. doi: 10.1049/ip-gtd:19970680

Son, K. M., & Lasseter, R. H. (2004). A Newton-type current injection model of UPFC for studying low-frequency oscillations. *Power Delivery, IEEE Transactions on, 19*(2), 694–701.

Taher, S. A., Akbari, S., Abdolalipour, A., & Hematti, R. (2010). Robust decentralized controller design for UPFC using μ-synthesis. *Communications in Nonlinear Science and Numerical Simulation, 15*(8), 2149–2161.

Taher, S. A., Hemmati, R., Abdolalipour, A., & Akbari, S. (2012). Comparison of different robust control methods in design of decentralized {UPFC} controllers. *International Journal of Electrical Power & Energy Systems*, *43*(1), 173 - 184. Retrieved from http://www.sciencedirect.com/science/article/pii/S0142061512001524 doi: http://dx.doi.org/10.1016/j.ijepes.2012.04.026

Vural, A., & Tumay, M. (2003). Steady state analysis of unified power flow controller: mathematical modeling and simulation studies. In *Power tech conference proceedings, 2003 ieee bologna* (Vol. 4, pp. 6–pp).

Wallace, A. R. (2011). *The geographical distribution of animals: with a study of the relations of living and extinct faunas as elucidating the past changes of the earth's surface* (Vol. 1). Cambridge University Press.

Wang, H. (2000, Jul). A unified model for the analysis of FACTS devices in damping power system oscillations. III. Unified power flow controller. *Power Delivery, IEEE Transactions on*, *15*(3), 978-983. doi: 10.1109/61.871362

Wang, H. (2002). Interactions and multivariable design of multiple control functions of a unified power flow controller. *International journal of electrical power & energy systems*, *24*(7), 591–600.

Yam, C., & Haque, M. (2004). A {SVD} based controller of {UPFC} for power flow control. *Electric Power Systems Research*, *70*(1), 76 - 84. Retrieved from http://www.sciencedirect.com/science/article/pii/S0378779603002931 doi: http://dx.doi.org/10.1016/j.epsr.2003.11.014

Yang, X.-S. (2010). *Engineering optimization: an introduction with metaheuristic applications*. John Wiley & Sons.

Appendix A
System Data

Synchronous generator parameters	M =8.0 MJ/MVA, D =0,T'_{d0} =5.044s, x_d =1 p.u., x'_d =0.3 p.u., x_q =0.6 p.u., x_t =0.1 p.u., f_B =50 Hz
Excitation system parameters	$K_A = 50$ T_A =0.05s
Transmission system	x_{t1} =0.6 p.u., x_{BV} =0.6 p.u.
UPFC parameters	$x_B = 0.1$ p.u., x_E =0.1 p.u., C_{dc} =3 p.u., V_{dc} =2 p.u., K_s =1, and T_s =0.05s
Infinite bus	V_b =1 p.u. and $\delta_b = 0°$

Table (A.1)
System Data

Appendix B
Single Machine Infinite Bus with UPFC

B.1 Network Current Derivation

Consider figure (2.25), in which a generator is connected to an infinite bus through a double line transmission circuit. In order to model the system it is required to find the expression of the currents in terms of the system state variables. First, consider the current through x_t:

$$\mathbf{I_t} = \frac{\mathbf{V_t} - \mathbf{V_{Et}}}{j\, x_t}$$

The equation can be rewritten as:

$$j\, x_t\, \mathbf{I_t} = \mathbf{V_t} - \mathbf{V_{Et}}$$

Transforming the equation to the dq-reference frame:

$$j\, x_t\, (i_q - j\, i_d)\, e^{j\delta} = (v_q - j\, v_d)\, e^{j\delta} - (v_{Etq} - j\, v_{Etd})\, e^{j\delta}$$

$$v_{Etq} = v_q - x_t i_d$$
$$v_{Etd} = v_d + x_t i_q$$

Using equations 2.60 and 2.61, the above equations can be rewritten as
:

$$v_{Etq} = E'_q - x_{dt} i_d \qquad \text{(B.1)}$$
$$v_{Etd} = x_{qt} i_q \qquad \text{(B.2)}$$

where

$x_{dt} = x'_d + x_t$

$x_{qt} = x_q + x_t$

The current in the upper uncompensated transmission line can be found as:

$$\mathbf{I_1} = \frac{\mathbf{V_{Et}} - \mathbf{V_b}}{j\, x_{t1}}$$

Rewriting the equation in the dq-reference frame:

$$(i_{1q} - j\, i_{1d}) = \frac{1}{j\, x_{t1}} (v_{Etq} - j\, v_{Etd} - V_b \cos\delta + j\, V_b \sin\delta)$$

Hence

$$i_{1q} = -\frac{1}{x_{t1}} (v_{Etd} - V_b \sin\delta) \tag{B.3}$$

$$i_{1d} = \frac{1}{x_{t1}} (v_{Etq} - V_b \cos\delta) \tag{B.4}$$

Similarly for the compensated line:

$$\mathbf{I_B} = \frac{\mathbf{V_{Et}} - \mathbf{V_B} - \mathbf{V_b}}{j\, x_{BB}}$$

where

$x_{BB} = x_{Bv} + x_B$

Rewriting it in dq-reference frame:

$$\begin{aligned}(i_{Bq} - j\, i_{Bd}) \;=\; & \frac{1}{j\, x_{BB}} \Big(v_{Etq} - j\, v_{Etq} - \frac{m_B v_{dc}}{2} (\sin\delta_B - j\, \cos\delta_B) \\ & -V_b (\cos\delta - j\, \sin\delta) \Big)\end{aligned}$$

The dq currents of the compensated line are found as:

$$i_{Bq} = -\frac{1}{x_{BB}}\left(v_{Etd} - \frac{m_B v_{dc}}{2}\cos\delta_B - V_b \sin\delta\right) \tag{B.5}$$

$$i_{Bd} = \frac{1}{x_{BB}}\left(v_{Etq} - \frac{m_B v_{dc}}{2}\sin\delta_B - V_b \cos\delta\right) \tag{B.6}$$

The current through the shunt branch can be found as:

$$\mathbf{I_E} = \frac{\mathbf{V_{Et}} - \mathbf{V_E}}{j\, x_E}$$

Transforming the equation to the dq frame:

$$(i_{Eq} - j\, i_{Ed}) = \frac{1}{j\, x_E}\left(v_{Etq} - j\, v_{Etd} - \frac{m_E v_{dc}}{2}(\sin\delta_E - j\, \cos\delta_E)\right) \tag{B.7}$$

The bus voltage dq components can be found as:

$$v_{Etq} = x_E i_{Ed} + \frac{m_E v_{dc}}{2}\sin\delta_E \tag{B.8}$$

$$v_{Etd} = -x_E i_{Eq} + \frac{m_E v_{dc}}{2}\cos\delta_E \tag{B.9}$$

Applying K.C.L at the UPFC sending bus:

$$i_d = i_{Ed} + i_{1d} + i_{Bd} \tag{B.10}$$

$$i_q = i_{Eq} + i_{1q} + i_{Bq} \tag{B.11}$$

Substituting the value of $v_{Etq}$and v_{Etd} to rewrite the current components in terms of i_{Ed} and i_{Eq}:

$$i_{1d} = \frac{1}{x_{t1}}\left(x_E i_{Ed} + \frac{m_E v_{dc}}{2}\sin\delta_E - V_b\cos\delta\right) \tag{B.12}$$

$$i_{1q} = -\frac{1}{x_{t1}}\left(-x_E i_{Eq} + \frac{m_E v_{dc}}{2}\cos\delta_E - V_b\sin\delta\right) \tag{B.13}$$

$$i_{Bd} = \frac{1}{x_{BB}}\left(x_E i_{Ed} + \frac{m_E v_{dc}}{2}\sin\delta_E - \frac{m_B v_{dc}}{2}\sin\delta_B - V_b\cos\delta\right) \tag{B.14}$$

$$i_{Bq} = -\frac{1}{x_{BB}}\left(-x_E i_{Eq} + \frac{m_E v_{dc}}{2}\cos\delta_E - \frac{m_B v_{dc}}{2}\cos\delta_B - V_b\sin\delta\right) \tag{B.15}$$

Substituting the currents in the i_d and i_q:

$$i_d = C_1 i_{Ed} + C_2\frac{m_E v_{dc}}{2}\sin\delta_E - C_3\frac{m_B v_{dc}}{2}\sin\delta_B - C_2 V_b\cos\delta \tag{B.16}$$

$$i_q = C_1 i_{Eq} - C_2\frac{m_E v_{dc}}{2}\cos\delta_E + C_3\frac{m_B v_{dc}}{2}\cos\delta_B + C_2 V_b\sin\delta \tag{B.17}$$

where

$C_1 = 1 + \frac{x_E}{x_{BB}} + \frac{x_E}{x_{t1}}$

$C_2 = \frac{x_{BB}+x_{t1}}{x_{BB}x_{t1}}$

$C_3 = \frac{x_{t1}}{x_{BB}x_{t1}}$

Substituting i_d and i_q in B.1 and B.2:

$$v_{Etq} = E'_q - x_{dt}C_1 i_{Ed} - x_{dt}C_2\frac{m_E v_{dc}}{2}\sin\delta_E + x_{dt}C_3\frac{m_B v_{dc}}{2}\sin\delta_B + x_{dt}C_2 V_b\cos\delta$$

$$v_{Etd} = x_{qt}C_1 i_{Eq} - x_{qt}C_2\frac{m_E v_{dc}}{2}\cos\delta_E + x_{qt}C_3\frac{m_B v_{dc}}{2}\cos\delta_B + x_{qt}C_2 V_b\sin\delta$$

$$\because\quad i_{Ed} = \frac{1}{x_E}\left(v_{Etq} - \frac{m_E v_{dc}}{2}\sin\delta_E\right)$$

$$i_{Eq} = -\frac{1}{x_E}\left(v_{Etd} - \frac{m_E v_{dc}}{2}\cos\delta_E\right)$$

By substituting the values of v_{Etq} and v_{Etd} in i_{Ed} and i_{Eq}, this results

in:

$$i_{Ed} = \frac{x_{Bt}}{x_{d\Sigma}} E'_q - \frac{x_{d1}}{x_{d\Sigma}} \frac{m_E v_{dc}}{2} \sin\delta_E + \frac{x_{d2}}{x_{d\Sigma}} \frac{m_B v_{dc}}{2} \sin\delta_B + \frac{x_{d3}}{x_{d\Sigma}} V_b \cos\delta \tag{B.18}$$

$$i_{Eq} = \frac{x_{q1}}{x_{q\Sigma}} \frac{m_E v_{dc}}{2} \cos\delta_E - \frac{x_{q2}}{x_{q\Sigma}} \frac{m_B v_{dc}}{2} \cos\delta_B - \frac{x_{q3}}{x_{q\Sigma}} V_b \sin\delta \tag{B.19}$$

where

$$x_{Bt} = x_{BB} x_{t1}$$

$$x_{d\Sigma} = x_{BB} x_{t1} (x_E + x_{dt}) + x_{dt} x_E (x_{BB} + x_{t1})$$

$$x_{d1} = x_{BB} x_{t1} + x_{dt} (x_{BB} + x_{t1})$$

$$x_{d2} = x_{dt} x_{t1}$$

$$x_{d3} = x_{dt} (x_{BB} + x_{t1})$$

$$x_{q\Sigma} = x_{BB} x_{t1} (x_E + x_{qt}) + x_{qt} x_E (x_{BB} + x_{t1})$$

$$x_{q1} = x_{BB} x_{t1} + x_{qt} (x_{BB} + x_{t1})$$

$$x_{q2} = x_{qt} x_{t1}$$

$$x_{q3} = x_{qt} (x_{BB} + x_{t1})$$

By substituting the obtained expression of i_{Ed} and i_{Eq} into equations B.14 to B.17:

$$i_{Bd} = \frac{x_{Et}}{x_{d\Sigma}} E'_q + \frac{x_{d2}}{x_{d\Sigma}} \frac{m_E v_{dc}}{2} \sin\delta_E - \frac{x_{d4}}{x_{d\Sigma}} \frac{m_B v_{dc}}{2} \sin\delta_B - \frac{x_{d5}}{x_{d\Sigma}} V_b \cos\delta \tag{B.20}$$

$$i_{Bq} = \frac{x_{q2}}{x_{q\Sigma}} \frac{m_E v_{dc}}{2} \cos\delta_E - \frac{x_{q4}}{x_{q\Sigma}} \frac{m_B v_{dc}}{2} \cos\delta_B - \frac{x_{q5}}{x_{q\Sigma}} V_b \sin\delta \tag{B.21}$$

$$i_d = \frac{x_{c1}}{x_{d\Sigma}} E'_q - \frac{x_{Bt}}{x_{d\Sigma}} \frac{m_E v_{dc}}{2} \sin\delta_E + \frac{x_{Et}}{x_{d\Sigma}} \frac{m_B v_{dc}}{2} \sin\delta_B - \frac{x_{c2}}{x_{d\Sigma}} V_b \cos\delta \tag{B.22}$$

$$i_q = \frac{x_{Bt}}{x_{q\Sigma}} \frac{m_E v_{dc}}{2} \cos\delta_E - \frac{x_{Et}}{x_{q\Sigma}} \frac{m_B v_{dc}}{2} \cos\delta_B + \frac{x_{c2}}{x_{q\Sigma}} V_b \sin\delta \tag{B.23}$$

where

$$x_{Et} = x_E x_{t1}$$

$$x_{d4} = x_{t1} (x_E + x_{dt}) + x_{dt} x_E$$

$$x_{d5} = x_{t1} (x_E + x_{dt})$$

$$x_{q4} = x_{t1} (x_E + x_{qt})$$

$$x_{q5} = x_{t1} (x_E + x_{qt})$$

$$x_{c1} = x_{BB} x_{t1} + x_E (x_{BB} + x_{t1})$$

$$x_{c2} = x_E \left(x_{BB} + x_{t1} \right)$$

B.2 System Linearization

In order to evaluate the system stability, a linear model is to be developed. In this research the linear model is used solely to find the eigenvalues of the system in order to assess the stability and to calculate the electromechanical modes of the system. Linearization is done based on the Taylor series expansion around the operating point.

Consider 2.54:

$$\frac{d\delta}{dt} = \omega_B \omega_r$$

through linearization:

$$\frac{d\Delta\delta}{dt} = \omega_B \Delta\omega_r \tag{B.24}$$

The rotor speed dynamics described in equation 2.55 as:

$$\frac{d\omega_r}{dt} = \frac{1}{M} \left(-D\,\omega_r + P_m - P_e \right)$$

where

$$P_e = E'_q\, i_q - \left(x'_d - x_q \right) i_q i_d$$

Linearizing power equation:

$$\begin{aligned} \Delta P_e = {} & \Delta E'_q i_{q0} + \left(E'_{q0} - \left(x'_d - x_q \right) i_{d0} \right) \Delta i_q \\ & - \left(x'_d - x_q \right) i_{q0} \Delta i_d \end{aligned} \tag{B.25}$$

To linearize this equation it is required to find the linear counter parts of the dq currents defined in B.22 and B.23, Δi_d and Δi_q are found as:

$$\Delta i_d = C_{1d}\Delta\delta + C_{2d}\Delta E'_q + C_{3d}\Delta v_{dc} + C_{4d}\Delta m_E + C_{5d}\Delta\delta_E + C_{6d}\Delta m_B + C_{7d}\Delta\delta_B \quad \text{(B.26)}$$

$$\Delta i_q = C_{1q}\Delta\delta + C_{2q}\Delta v_{dc} + C_{3q}\Delta m_E + C_{4q}\Delta\delta_E + C_{5q}\Delta m_B + C_{6q}\Delta\delta_B \quad \text{(B.27)}$$

where

$C_{1d} = \frac{x_{c2}}{x_{d\Sigma}} V_b \sin\delta_0$; $C_{2d} = \frac{x_{c1}}{x_{d\Sigma}}$; $C_{3d} = -\frac{x_{Bt}}{x_{d\Sigma}}\frac{m_{E0}}{2}\sin\delta_{E0} + \frac{x_{Et}}{x_{d\Sigma}}\frac{m_{B0}}{2}\sin\delta_{B0}$

$C_{4d} = -\frac{x_{Bt}}{x_{d\Sigma}}\frac{v_{dc0}}{2}\sin\delta_{E0}$; $C_{5d} = -\frac{x_{Bt}}{x_{d\Sigma}}\frac{m_{E0}v_{dc0}}{2}\cos\delta_{E0}$; $C_{6d} = \frac{x_{Et}}{x_{d\Sigma}}\frac{v_{dc0}}{2}\sin\delta_{B0}$

$C_{7d} = \frac{x_{Et}}{x_{d\Sigma}}\frac{m_{B0}v_{dc0}}{2}\cos\delta_{B0}$

$C_{1q} = \frac{x_{c2}}{x_{q\Sigma}} V_b \cos\delta_0$; $C_{2q} = \frac{x_{Bt}}{x_{q\Sigma}}\frac{m_{E0}}{2}\cos\delta_{E0} - \frac{x_{Et}}{x_{q\Sigma}}\frac{m_{B0}}{2}\cos\delta_{B0}$

$C_{4q} = \frac{x_{Bt}}{x_{q\Sigma}}\frac{v_{dc0}}{2}\cos\delta_{E0}$; $C_{5q} = -\frac{x_{Bt}}{x_{q\Sigma}}\frac{m_{E0}v_{dc0}}{2}\sin\delta_{E0}$; $C_{6q} = -\frac{x_{Et}}{x_{d\Sigma}}\frac{v_{dc0}}{2}\cos\delta_{B0}$

$C_{7q} = \frac{x_{Et}}{x_{d\Sigma}}\frac{m_{B0}v_{dc0}}{2}\sin\delta_{B0}$

Substitute Δi_d and Δi_q in B.25:

$$\Delta P_e = K_1\Delta\delta + K_2\Delta E'_q + K_{pd}\Delta v_{dc} + K_{pe}\Delta m_E + K_{p\delta e}\Delta\delta_E + K_{pb}\Delta m_B + K_{p\delta b}\Delta\delta_B \quad \text{(B.28)}$$

$K_1 = C_{1d}\left(-\left(x'_d - x_q\right) i_{q0}\right) + C_{1q}\left(E'_{q0} - \left(x'_d - x_q\right) i_{d0}\right)$

$K_2 = C_{2d}\left(-\left(x'_d - x_q\right) i_{q0}\right) + i_{q0}$

$K_{pd} = C_{3d}\left(-\left(x'_d - x_q\right) i_{q0}\right) + C_{3q}\left(E'_{q0} + \left(x'_d - x_q\right) i_{d0}\right)$

$K_{pe} = C_{4d}\left(-\left(x'_d - x_q\right) i_{q0}\right) + C_{4q}\left(E'_{q0} + \left(x'_d - x_q\right) i_{d0}\right)$

$K_{p\delta e} = C_{5d}\left(-\left(x'_d - x_q\right) i_{q0}\right) + C_{5q}\left(E'_{q0} + \left(x'_d - x_q\right) i_{d0}\right)$

$K_{pb} = C_{6d}\left(-\left(x'_d - x_q\right) i_{q0}\right) + C_{6q}\left(E'_{q0} + \left(x'_d - x_q\right) i_{d0}\right)$

$K_{p\delta b} = C_{7d}\left(-\left(x'_d - x'_q\right) i_{q0}\right) + C_{7q}\left(E'_{q0} + \left(x'_d - x_q\right) i_{d0}\right)$

Hence linear speed dynamics equations is:

$$\frac{d\Delta\omega}{dt} = -\frac{K_1}{M}\Delta\delta - \frac{D}{M}\Delta\omega_r - \frac{K_2}{M}\Delta E'_q - \frac{K_{pd}}{M}\Delta v_{dc} - \frac{K_{pe}}{M}\Delta m_E - \frac{K_{p\delta e}}{M}\Delta\delta_E - \frac{K_{pb}}{M}\Delta m_B - \frac{K_{p\delta b}}{M}\Delta\delta_B \quad \text{(B.29)}$$

Consider 2.56:

$$\frac{dE'_q}{dt} = \frac{1}{T'_{d0}}\left(E_{fd} - E'_q - \left(x_d - x'_d\right) i_d\right)$$

Through the linearization of the above equation and using equation B.26:

$$\begin{aligned}\frac{d\Delta E'_q}{dt} = &\frac{K_4}{T'_{d0}}\Delta\delta - \frac{K_3}{T'_{d0}}\Delta E'_q + \frac{1}{T'_{d0}}\Delta E_{fd} + \frac{K_{qd}}{T'_{d0}}\Delta v_{dc} + \frac{K_{qe}}{T'_{d0}}\Delta m_E \\ &+ \frac{K_{q\delta e}}{T'_{d0}}\Delta\delta_E + \frac{K_{qb}}{T'_{d0}}\Delta m_B + \frac{K_{q\delta b}}{T'_{d0}}\Delta\delta_B \end{aligned} \tag{B.30}$$

where

$K_4 = C_{1d}\left(x_d - x'_d\right)$

$K_3 = -C_{2d}\left(x_d - x'_d\right) + 1$

$K_{qd} = C_{3d}\left(x_d - x'_d\right)$

$K_{qe} = C_{4d}\left(x_d - x'_d\right)$

$K_{q\delta e} = C_{5d}\left(x_d - x'_d\right)$

$K_{qb} = C_{6d}\left(x_d - x'_d\right)$

$K_{q\delta b} = C_{7d}\left(x_d - x'_d\right)$

The dynamics of the excitation system is described as:

$$\frac{dE_{fd}}{dt} = \frac{1}{T_A}\left(-E_{fd} + K_A\left(V_{ref} - V_t\right)\right)$$

where

$$V_t = \sqrt{v_q^2 + v_d^2}$$

$$v_q = E'_q - x'_d i_d$$

$$v_d = x'_q i_q$$

$$\because V_t^2 = v_q^2 + v_d^2$$
$$\therefore 2V_{t0}\Delta V_t = 2v_{q0}\Delta v_q + 2v_{d0}\Delta v_d$$

$$\Delta V_t = \left(\frac{v_{q0}}{V_{t0}}\right)\Delta v_q + \left(\frac{v_{d0}}{V_{t0}}\right)\Delta v_d \tag{B.31}$$

In order to find ΔV_t , v_q and v_d defined in 2.60 and 2.61 are linearized::

$$\Delta v_q = \Delta E'_q - x'_d\left(C_{1d}\Delta\delta + C_{2d}\Delta E'_q + C_{3d}\Delta v_{dc} + C_{4d}\Delta m_E + C_{5d}\Delta\delta_E + C_{6d}\Delta m_B + C_{7d}\Delta\delta_B\right)$$
$$\Delta v_d = x'_q\left(C_{1q}\Delta\delta + C_{2q}\Delta v_{dc} + C_{3q}\Delta m_E + C_{4q}\Delta\delta_E + C_{5q}\Delta m_B + C_{6q}\Delta\delta_B\right)$$

Substituting this in ΔV_t results in:

$$\Delta V_t = K_5\Delta\delta + K_6\Delta E'_q + K_{vd}\Delta v_{dc} + K_{ve}\Delta m_E + K_{v\delta e}\Delta\delta_E + K_{vb}\Delta m_B + K_{v\delta b}\Delta\delta_B \tag{B.32}$$

where

$$K_5 = -\left(\frac{v_{q0}}{V_{t0}}\right)x'_d C_{1d} + \left(\frac{v_{d0}}{V_{t0}}\right)x'_q C_{1q}$$
$$K_4 = \left(\frac{v_{q0}}{V_{t0}}\right)(-x'_d C_{2d} + 1)$$
$$K_{vd} = -\left(\frac{v_{q0}}{V_{t0}}\right)x'_d C_{3d} + \left(\frac{v_{d0}}{V_{t0}}\right)x'_q C_{3q}$$
$$K_{ve} = -\left(\frac{v_{q0}}{V_{t0}}\right)x'_d C_{4d} + \left(\frac{v_{d0}}{V_{t0}}\right)x'_q C_{4q}$$
$$K_{v\delta e} = -\left(\frac{v_{q0}}{V_{t0}}\right)x'_d C_{5d} + \left(\frac{v_{d0}}{V_{t0}}\right)x'_q C_{5q}$$
$$K_{vb} = -\left(\frac{v_{q0}}{V_{t0}}\right)x'_d C_{6d} + \left(\frac{v_{d0}}{V_{t0}}\right)x'_q C_{6q}$$
$$K_{v\delta b} = -\left(\frac{v_{q0}}{V_{t0}}\right)x'_d C_{7d} + \left(\frac{v_{d0}}{V_{t0}}\right)x'_q C_{7q}$$

Hence the linearized excitation model is:

$$\frac{d\Delta E_{fd}}{dt} = -\frac{K_A K_5}{T_A}\Delta\delta - \frac{K_A K_6}{T_A}\Delta E'_q - \frac{1}{T_A}\Delta E_{fd} - \frac{K_A K_{vd}}{T_A}\Delta v_{dc} - \frac{K_A K_{ve}}{T_A}\Delta m_E - \frac{K_A K_{v\delta e}}{T_A}\Delta\delta_E - \frac{K_A K_{vb}}{T_A}\Delta m_B - \frac{K_A K_{v\delta b}}{T_A}\Delta\delta_B \quad \text{(B.33)}$$

In order to linearize the UPFC DC link dynamics Δi_{Ed}, Δi_{Eq}, Δi_{Bd}, and Δi_{Bq} should be found:

$$\Delta i_{Ed} = C_{1Ed}\Delta\delta + C_{2Ed}\Delta E'_q + C_{3Ed}\Delta v_{dc} + C_{4Ed}\Delta m_E + C_{5Ed}\Delta\delta_E + C_{6Ed}\Delta m_B + C_{7Ed}\Delta\delta_B \quad \text{(B.34)}$$

where

$C_{1Ed} = -\frac{x_{d3}}{x_{d\Sigma}} V_b \sin\delta_0$, $C_{2Ed} = \frac{x_{Bt}}{x_{d\Sigma}}$,

$C_{3Ed} = -\frac{x_{d1}}{x_{d\Sigma}}\frac{m_{E0}}{2}\sin\delta_{E0} + \frac{x_{d2}}{x_{d\Sigma}}\frac{m_{B0}}{2}\sin\delta_{B0}$,

$C_{4Ed} = -\frac{x_{d1}}{x_{d\Sigma}}\frac{v_{dc0}}{2}\sin\delta_{E0}$, $C_{5Ed} = -\frac{x_{d1}}{x_{d\Sigma}}\frac{m_{E0}v_{dc0}}{2}\cos\delta_{E0}$,

$C_{6Ed} = \frac{x_{d2}}{x_{d\Sigma}}\frac{v_{dc0}}{2}\sin\delta_{B0}$,

$C_{7Ed} = \frac{x_{d2}}{x_{d\Sigma}}\frac{m_{B0}v_{dc0}}{2}\cos\delta_{B0}$

$$\Delta i_{Eq} = C_{1Eq}\Delta\delta + C_{2Eq}\Delta v_{dc} + C_{3Eq}\Delta m_E + C_{4Eq}\Delta\delta_E + C_{5Eq}\Delta m_B + C_{6Eq}\Delta\delta_B \quad \text{(B.35)}$$

where

$C_{1Eq} = \frac{x_{q3}}{x_{q\Sigma}} V_b \cos\delta_0$, $C_{2Eq} = \frac{x_{q1}}{x_{q\Sigma}}\frac{m_{E0}}{2}\cos\delta_{E0} - \frac{x_{q2}}{x_{q\Sigma}}\frac{m_{B0}}{2}\cos\delta_{B0}$,

$C_{3Eq} = \frac{x_{q1}}{x_{q\Sigma}}\frac{v_{dc0}}{2}\cos\delta_{E0}$, $C_{4Eq} = -\frac{x_{q1}}{x_{q\Sigma}}\frac{m_{E0}v_{dc0}}{2}\sin\delta_{E0}$,

$C_{5Eq} = -\frac{x_{q2}}{x_{q\Sigma}}\frac{v_{dc0}}{2}\cos\delta_{B0}$,

$C_{6Eq} = \frac{x_{q2}}{x_{q\Sigma}}\frac{m_{B0}v_{dc0}}{2}\sin\delta_{B0}$

$$\Delta i_{Bd} = C_{1Bd}\Delta\delta + C_{2Bd}\Delta E'_q + C_{3Bd}\Delta v_{dc} + C_{4Bd}\Delta m_E + C_{5Bd}\Delta\delta_E + C_{6Bd}\Delta m_B + C_{7Bd}\Delta\delta_B \quad \text{(B.36)}$$

where

$C_{1Bd} = \frac{x_{d5}}{x_{d\Sigma}} V_b \sin\delta_0$, $C_{2Bd} = \frac{x_{Et}}{x_{d\Sigma}}$,

$C_{3Bd} = \frac{x_{d2}}{x_{d\Sigma}} \frac{m_{E0}}{2} \sin\delta_{E0} - \frac{x_{d4}}{x_{d\Sigma}} \frac{m_{B0}}{2} \sin\delta_{B0}$,

$C_{4Bd} = \frac{x_{d2}}{x_{d\Sigma}} \frac{v_{dc0}}{2} \sin\delta_{E0}$, $C_{5Bd} = \frac{x_{d2}}{x_{d\Sigma}} \frac{m_{E0} v_{dc0}}{2} \cos\delta_{E0}$,

$C_{6Bd} = -\frac{x_{d4}}{x_{d\Sigma}} \frac{v_{dc0}}{2} \sin\delta_{B0}$,

$C_{7Bd} = -\frac{x_{d4}}{x_{d\Sigma}} \frac{m_{B0} v_{dc0}}{2} \cos\delta_{B0}$

$$\Delta i_{Bq} = C_{1Bq}\Delta\delta + C_{2Bq}\Delta v_{dc} + C_{3Bq}\Delta m_E + C_{4Bq}\Delta\delta_E + C_{5Bq}\Delta m_B + C_{6Bq}\Delta\delta_B \quad \text{(B.37)}$$

where

$C_{1Bq} = -\frac{x_{q3}}{x_{q\Sigma}} V_b \cos\delta_0$,

$C_{2Bq} = \frac{x_{q2}}{x_{q\Sigma}} \frac{m_{E0}}{2} \cos\delta_{E0} - \frac{x_{q4}}{x_{q\Sigma}} \frac{m_{B0}}{2} \cos\delta_{B0}$,

$C_{3Bq} = \frac{x_{q2}}{x_{q\Sigma}} \frac{v_{dc0}}{2} \cos\delta_{E0}$, $C_{4Bq} = -\frac{x_{q2}}{x_{q\Sigma}} \frac{m_{E0} v_{dc0}}{2} \sin\delta_{E0}$,

$C_{5Bq} = -\frac{x_{q4}}{x_{q\Sigma}} \frac{v_{dc0}}{2} \cos\delta_{B0}$,

$C_{6Bq} = \frac{x_{q4}}{x_{q\Sigma}} \frac{m_{B0} v_{dc0}}{2} \sin\delta_{B0}$

Linearizing the DC link voltage equation (2.53), we obtain:

$$\begin{aligned}
\frac{d\Delta v_{dc}}{dt} &= \frac{3}{4C_{dc}} \left(\cos\delta_{E0} i_{Ed0} + \sin\delta_{E0} i_{Eq0}\right) \Delta m_E \\
&+ \frac{3m_{E0}}{4C_{dc}} \left(-\sin\delta_{E0} i_{Ed0} + \cos\delta_{E0} i_{Eq0}\right) \Delta\delta_E + \frac{3}{4C_{dc}} \left(\cos\delta_{B0} i_{Bd0} + \sin\delta_{B0} i_{Bq0}\right) \Delta m_B \\
&+ \frac{3m_{B0}}{4C_{dc}} \left(-\sin\delta_{B0} i_{Bd0} + \cos\delta_{B0} i_{Bq0}\right) \Delta\delta_B + \frac{3m_{E0}}{4C_{dc}} \cos\delta_{E0} \Delta i_{Ed} + \frac{3m_{E0}}{4C_{dc}} \sin\delta_{E0} \Delta i_{Eq} \\
&+ \frac{3m_{B0}}{4C_{dc}} \cos\delta_{B0} \Delta i_{Bd0} + \frac{3m_{B0}}{4C_{dc}} \sin\delta_{B0} \Delta i_{Bq}
\end{aligned} \quad \text{(B.38)}$$

By substituting the values of Δi_{Ed}, Δi_{Eq}, Δi_{Bd}, and Δi_{Bq} in the above equation:

$$\frac{d\Delta v_{dc}}{dt} = K_7\Delta\delta + K_8\Delta E'_q - K_9\Delta v_{dc} + K_{ce}\Delta m_E + K_{c\delta e}\Delta\delta_E + K_{cb}\Delta m_B + K_{c\delta b}\Delta\delta_B \quad \text{(B.39)}$$

where

$K_7 = \frac{3m_{E0}}{4C_{dc}}\cos\delta_{E0}C_{1Ed} + \frac{3m_{E0}}{4C_{dc}}\sin\delta_{E0}C_{1Eq} + \frac{3m_{B0}}{4C_{dc}}\cos\delta_{B0}C_{1Bd} + \frac{3m_{B0}}{4C_{dc}}\sin\delta_{B0}C_{1Bq}$,

$K_8 = \frac{3m_{E0}}{4C_{dc}}\cos\delta_{E0}C_{2Ed} - \frac{3m_{B0}}{4C_{dc}}\cos\delta_{B0}C_{2Bd}$

$K_9 = -\left[\frac{3m_{E0}}{4C_{dc}}\cos\delta_{E0}C_{3Ed} + \frac{3m_{E0}}{4C_{dc}}\sin\delta_{E0}C_{3Eq} + \frac{3m_{B0}}{4C_{dc}}\cos\delta_{B0}C_{3Bd} + \frac{3m_{B0}}{4C_{dc}}\sin\delta_{B0}C_{3Bq}\right]$,

$K_{ce} = \frac{3}{4C_{dc}}(\cos\delta_{E0}i_{Ed0} + \sin\delta_{E0}i_{Eq0}) + \frac{3m_{E0}}{4C_{dc}}\cos\delta_{E0}C_{4Ed} + \frac{3m_{E0}}{4C_{dc}}\sin\delta_{E0}C_{4Eq} + \frac{3m_{B0}}{4C_{dc}}\cos\delta_{B0}C_{4Bd} + \frac{3m_{B0}}{4C_{dc}}\sin\delta_{B0}C_{4Bq}$,

$K_{c\delta e} = \frac{3m_{E0}}{4C_{dc}}(-\sin\delta_{E0}i_{Ed0} + \cos\delta_{E0}i_{Eq0}) + \frac{3m_{E0}}{4C_{dc}}\cos\delta_{E0}C_{5Ed} + \frac{3m_{E0}}{4C_{dc}}\sin\delta_{E0}C_{5Eq} + 3m_{B0}\cos\delta_{B0}C_{5Bd} + \frac{3m_{B0}}{4C_{dc}}\sin\delta_{B0}C_{5Bq}$,

$K_{cb} = -\frac{3}{4C_{dc}}(\cos\delta_{B0}i_{Bd0} + \sin\delta_{B0}i_{Bq0}) + \frac{3m_{E0}}{4C_{dc}}\cos\delta_{E0}C_{6Ed} + \frac{3m_{E0}}{4C_{dc}}\sin\delta_{E0}C_{6Eq} + \frac{3m_{B0}}{4C_{dc}}\cos\delta_{B0}C_{6Bd} + \frac{3m_{B0}}{4C_{dc}}\sin\delta_{B0}C_{6Bq}$,

$K_{c\delta b} = -\frac{3m_{E0}}{4C_{dc}}(-\sin\delta_{B0}i_{Bd0} + \cos\delta_{B0}i_{Bq0}) + \frac{3m_{E0}}{4C_{dc}}\cos\delta_{E0}C_{7Ed} + \frac{3m_{E0}}{4C_{dc}}\sin\delta_{E0}C_{7Eq} + \frac{3m_{B0}}{4C_{dc}}\cos\delta_{B0}C_{7Bd} + \frac{3m_{B0}}{4C_{dc}}\sin\delta_{B0}C_{7Bq}$.

The state space representation of the system is:

$$\begin{vmatrix} \Delta\dot{\delta} \\ \Delta\dot{\omega}_r \\ \Delta\dot{E}'_q \\ \Delta\dot{E}_{fd} \\ \Delta\dot{v}_{dc} \end{vmatrix} = \begin{vmatrix} 0 & \omega_B & 0 & 0 & 0 \\ -\frac{K_1}{M} & -\frac{D}{M} & -\frac{K_2}{M} & 0 & -\frac{K_{pd}}{M} \\ \frac{K_4}{T'_{d0}} & 0 & -\frac{K_3}{T'_{d0}} & \frac{1}{T'_{d0}} & \frac{K_{qd}}{T'_{d0}} \\ -\frac{K_AK_5}{T_A} & 0 & -\frac{K_AK_6}{T_A} & -\frac{1}{T_A} & -\frac{K_AK_{vd}}{T_A} \\ K_7 & 0 & K_8 & 0 & -K_9 \end{vmatrix} \begin{vmatrix} \Delta\delta \\ \Delta\omega_r \\ \Delta E'_q \\ \Delta E_{fd} \\ \Delta v_{dc} \end{vmatrix} + \begin{vmatrix} 0 & 0 & 0 & 0 \\ \frac{K_{pe}}{M} & \frac{K_{p\delta e}}{M} & \frac{K_{pb}}{M} & \frac{K_{p\delta b}}{M} \\ \frac{K_{qe}}{T'_{d0}} & \frac{K_{q\delta e}}{T'_{d0}} & \frac{K_{qb}}{T'_{d0}} & \frac{K_{q\delta b}}{T'_{d0}} \\ \frac{K_AK_{ve}}{T_A} & \frac{K_AK_{v\delta e}}{T_A} & \frac{K_AK_{vb}}{T_A} & \frac{K_AK_{v\delta b}}{T_A} \\ K_{ce} & K_{c\delta e} & K_{cb} & K_{c\delta b} \end{vmatrix} \begin{vmatrix} \Delta m_E \\ \Delta\delta_E \\ \Delta m_B \\ \Delta\delta_B \end{vmatrix} \quad \text{(B.40)}$$

الملخص

في العقدين الأخيرين شهدت منظومة الطاقة الكهربائية توسعاً كبيراً و مطرداً ،وذلك بسبب الطلب المتزايد على الطاقة .أدى هذا التوسع إلى خلق عدة مشاكل في منظومة الطاقة الكهربائية حيث يتم تشغيل خطوط النقل الكهربائي إلى حدود سعتها الكهربائية ،بالإضافة إلى ازدياد الترابط بين الشبكات ،ومع أن منظومة نقل الكهرباء محدودة في التوسع بسبب شح الموارد مع وجود عوائق بيئية صارمة. فإنه تم تشغيل الشبكة الكهربائية وهو ما يؤدي بدوره إلى فقدان الإنتاج بسبب حصول خلخلات في تردد الشبكة.وعليه طرح معهد الطاقة الكهربائية للأبحاث حلاً يكمن في استخدام الدوائر الإلكترونية عالية القدرة ،حيث يتم التحكم بمتغيرات الشبكة باستخدامها.وعُرفّت هذه الدوائر الإلكترونية بالمتحكمات المرنة لأنظمة خطوط نقل التيار المتناوب .

يتناول هذا البحث موضوع تصميم وحدات تحكم ذكية لموحد تدفق الطاقة الكهربائية ،حيث يعتبر أكثر المتحكمات المرنة تعدداً في الاستعمالات ،وذلك بسبب قدرته في التحكم بجميع متغيرات الشبكة في آنٍ واحد.

هذا البحث مقسم على ستة فصول ،يتناول الفصل الأول منه مقدمة في المتحكمات المرنة وتصنيفاتها تبعاً لتكنولوجيا التصنيع و المتغيرات التي يتم التحكم بها ،ثم يطرح مقدمةً لكيفية عمل موحد تدفق الطاقة الكهربائية والمتغيرات المتحكم بها في كل حالة تشغيل .

يطرح الفصل الثاني النموذج الرياضي لموحد الطاقة الكهربائية ويبدأ القسم الأول بمناقشة النماذج الرياضية المستخدمة لإيجاد متغيرات الشبكة في حال الثبات المطروحة في الدراسات السابقة. و بناءً على النتيجة المستحصلة من طرح النماذج ،يذهب هذا القسم لمناقشة تأثير مكان التركيب على إشارات التحكم لموحد الطاقة .وفي القسم الثاني من هذا الفصل يتم طرح النماذج الديناميكية التابعة لموحد التدفق المستخدمة في الأبحاث السابقة ،حيث يتم عرض مقارنة من حيث بناء وحدات التحكم لموحد التدفق لكل من هذه النماذج .

يستعرض الفصل الثالث خوارزميتين متطورتين ،ويناقش كيفية عملهما لإيجاد الحل الأمثل للمسائل الرياضية. ويتناول القسم الأول خوارزمية الجغرافيا الإحيائية والتي تستخدم النموذج الرياضي المستوحى من التوزيع الأمثل للأحياء على مجموعة من المناطق الجغرافية ،ومن ثم يقدم خوارزمية حركة الأسراب ،التي تستخدم النموذج الرياضي لحركة الأسراب في إيجاد الحلول المثلى للمعادلات الرياضية. وثم ينتقل هذا الفصل لمناقشة كيفية تصميم وحدات التحكم لموحد تدفق الطاقة الكهربائية لتثبيط الخلخلات الكهربائية ذات الترددات المنخفضة و الناتجة عن ترابط الشبكات باستخدام هذه الخوارزميات. وتُستعرَض في هذا الفصل أيضاً الدوال الهدفية المستخدمة لإيجاد متغيرات وحدات التحكم للحصول على الاستجابة المثلى من النظام.

يتطرق البحث في الفصل الرابع لمشكلة تصميم وحدات التحكم ذات المتغيرات المتعددة لموحد تدفق الطاقة الكهربائية ،حيث يتم تصميم وحدات التحكم بصورة متأينة باستخدام الخوارزميات التي تم طرحها مسبقاً. تقوم وحدة التحكم ذات المتغيرات المتعددة بالتحكم في تدفق الطاقة الكهربائية في خط النقل ،وينظم فرق الجهد في البسبار الكهربائي ،وينظم فرق الجهد في المكثف بالإضافة إلى تثبيط الخلخلات الموجودة في النظام .

في الفصل الخامس من البحث ،يتم اختبار كل من وحدات التحكم التي تم تصميمها على حدة ،ويتم تحليل كل منها بحسب معايير التحكم وذلك لمعرفة قدرة وحدة التحكم على الثبات بالرغم من وجود تغيرات طارئة في النظام .

ويخلص الفصل السادس و الأخير إلى النتائج التي تم الحصول عليها من المقارنة بين وحدات التحكم ،ويناقش نواحي و مكامن التطوير في هذا البحث.

جامعة البحرين
المكتبة
LIBRARY
University of Bahrain

جامعة البحرين

كلية الهندسة

قسم الهندسة الكهربائية والإلكترونية

تصميم المتحكم الذكي لموحد الطاقة الكهربائية باستخدام خوارزميات الحلول المثلى

أطروحة مقدمة كجزء من متطلبات الحصول على درجة الماجستير في
الهندسة الكهربائية و الالكترونية

إعـــداد

سيد أحمد علي مكي القلاف

الرقم الجامعي: 20037139

إشـــراف

الدكتور سيد علي الموسوي
أستاذ مشارك

الدكتور أنور حيدر
أستاذ مساعد

جامعة البحرين

مملكة البحرين

يناير 2015